Titre: Title:	Sonication of Cellulose Nanocrystals: From Fundamentals Towards Scale-Up
Auteur: Author:	Mélanie Girard
Date:	2022
Type:	Mémoire ou thèse / Dissertation or Thesis
Référence: Citation:	Girard, M. (2022). Sonication of Cellulose Nanocrystals: From Fundamentals Towards Scale-Up [Thèse de doctorat, Polytechnique Montréal]. PolyPublie. https://publications.polymtl.ca/10290/

POLYTECHNIQUE MONTRÉAL

affiliée à l'Université de Montréal

Sonication of cellulose nanocrystals: from fundamentals towards scale-up

MÉLANIE GIRARD

Département de génie chimique

Thèse présentée en vue de l'obtention du diplôme de *Philosophiæ Doctor*

Génie chimique

Avril 2022

POLYTECHNIQUE MONTRÉAL

affiliée à l'Université de Montréal

Cette thèse intitulée :

Sonication of cellulose nanocrystals: from fundamentals towards scale-up

présentée par **Mélanie GIRARD**

en vue de l'obtention du diplôme de Philosophiæ Doctor

a été dûment acceptée par le jury d'examen constitué de :

Basil FAVIS, président
Marie-Claude HEUZEY, membre et directrice de recherche
Jason Robert TAVARES, membre et codirecteur de recherche
François BERTRAND, membre et codirecteur de recherche
Daria Camilla BOFFITO, membre
Emily CRANSTON, membre externe

ACKNOWLEDGMENTS

This four-year PhD has been extremely beneficial for me, both professionally and personally. Despite the various obstacles encountered during its completion, I am very grateful to everyone listed below for having allowed me to live this enriching experience. I have gained a lot from my interactions with all of you, and I will definitely miss them.

First of all, I am very thankful to my supervisor and co-supervisors, Marie-Claude Heuzey, Jason R. Tavares and François Bertrand, who trusted me throughout my project. The autonomy you granted me helped me to gain confidence in myself during my work. Thanks to you, I had the opportunity to participate in several international conferences which led to interesting discussions. You also allowed me to do an internship at Université de Mons despite the unfavorable situation. François, even if I could not discuss as often with you due to your position, I was able to go further in many notions thanks to your help and your questions helped me to strengthen my thinking. Marie-Claude and Jason, I really appreciated your support, beyond the simple supervision, which allows me for instance to benefit from your advice for my future career. Jason, I thank you very much for listening to me during the doubtful moments. Thank you also for letting me be part of the WHS committee. Marie-Claude, thanks you very much to trust me and allow me to teach the lab sessions and some class lectures for the “Polymers” course.

I thank David Vidal for helping me on the first part of my project. You knew how to bring the field of modeling within my reach and our discussions were always very enriching. I also thank Daniel Pilon, as well as Maxime Beaudoin and Sébastien Chenard, without whom I would have lost my temper several times for my last experiments. I thank Bruno Blais and Nick Virgilio to share your knowledge with me.

I thank my rheology, PhotoSEL and URPEI research groups, to allow me to open my mind to other fascinating research projects. I thank more specifically Charles, who shared his deep knowledge on CNCs with me many times, leading to enriching discussions. I also thank David B. and Hamed for their help. I thank Charles, David, Hamed, Cristina, Salomé, Alessio, Pauline, Simon, Wendell and Matthieu for having easily integrated me in the team and for your friendship that accompanied me throughout my project. I thank Tiffany, for the interesting

discussions in the last months. I thank Lingyu, for the work we did together even if we could not go further. I thank Clémence and Chi who also made these years pleasant. I thank Anthony Tiffon, Ying Wen Wang and Alexia Guyomard for their internship with me, which helped me in my research. I also thank Claire, Narges, Zohreh, Amirhosein, for their shared friendship.

I would also like to thank my colleagues for the Next Gen CREPEC Committee and especially Carole Anne and Pablo to allow me to become its president. It has been a great opportunity for me to meet many professors and industrials I would not have met otherwise.

I also thank the Chemical Engineering department staff: Gino Robin, Martine Lamarche with whom I really enjoyed working, Anic Desforges for her pleasant collaboration in the "Polymers" labs, Brigitte Langevin with whom I quite liked discussing, and Alexandre Bréard.

Finally, I thank my family for the support despite distance. I thank my parents for letting me take part in such an adventure and for always encouraging me to surpass myself. I thank Cédric for his advice during my journey, and the example you gave me. I thank Xavier, Cerrie and their children for their loving support. I also thank Louise and Alain for their kindness. And I thank a lot Matthieu, for whom my words would never be enough. Thanks for trusting me and handling my mood swings due to doubt and stress. Your optimistic and cheerful mind was a great support.

RÉSUMÉ

Les nanocristaux de cellulose (CNCs) sont des nanoparticules biosourcées et biodégradables en forme de bâtonnets qui suscitent un intérêt croissant depuis quelques années. Leurs propriétés uniques, de nature mécanique, rhéologique ou optique, peuvent être exploitées dans une vaste gamme d'applications dans des domaines comme les plastiques et composites, l'alimentaire, les peintures et revêtements ou la construction. Dans ce contexte, des travaux approfondis sont menés par les chercheurs académiques et industriels pour tirer profit de ces matériaux à haute valeur ajoutée. L'une des spécificités intéressantes des CNCs, commune aux autres nanoparticules, est son aspect de forme, qui lui donne ces propriétés considérables, telles qu'une grande résistance mécanique ou un caractère iridescent. De plus, les nombreux groupes hydroxyle sur la surface des CNCs permettent une versatilité intéressante, via la modification de surface. Cependant, ces deux attributs sont aussi source de complications importantes lorsque leur dispersion en suspension est désirée. En effet, les CNCs ont tendance à former de solides agglomérats quand ils sont séchés après avoir été extraits de la source cellulosique.

Afin de pallier ce problème, induit par les forces de Van de Waals et les liaisons hydrogène entre les nanocristaux, il est nécessaire d'utiliser un outil suffisamment puissant, tel que l'ultrasonication. Ici, une uniformisation de cette approche est proposée. Un indice de dispersion est évalué, grâce à de la modélisation numérique validée par des analyses de conductivité et de rhéométrie. Cela permet de déterminer les paramètres à utiliser pour obtenir une suspension de CNCs bien dispersée. La sonde de sonication doit être placée de manière décentrée dans la partie haute du contenant. De plus, le volume doit être limité à ~60 mL (lorsque des béchers standards sont utilisés), car les zones de non-mélange (ou zones mortes) seraient prédominantes pour de plus grands volumes. Une énergie ~167 $kJ.g^{-1}.L^{-1}$ (par grammes de CNCs par litre de milieu de suspension) est nécessaire avec ce protocole pour atteindre un état de dispersion optimal.

L'état de dispersion doit être évalué rigoureusement pour s'assurer de l'efficacité du procédé. Les concepts de distribution et de dispersion sont ainsi étudiés de manière approfondie grâce à la rhéologie, afin de comprendre le comportement des CNCs pendant l'ultrasonication. L'homogénéité des suspensions est décrite par l'écart-type de la viscosité, tandis que la valeur de

la viscosité elle-même indique la présence ou non d'agglomérats. Ainsi, un faible écart-type et une viscosité minimale, par rapport à une suspension n'ayant pas été soumise à l'ultrasonication, sont le signe d'une suspension bien distribuée et bien dispersée. L'influence du volume d'échantillonnage est également mise en valeur. Une tendance à gélifier est observée pour une suspension plus concentrée, rendant l'analyse plus difficile. Cependant, il est possible d'obtenir un état de dispersion satisfaisant, en comparant avec une suspension de CNCs jamais séchés.

Enfin, cette étude est adaptée à de plus grandes quantités, jusqu'à 200 mL. Un montage semi-continu est recommandé afin de contourner la limitation du volume qui peut être traité par lots. Cela mène de plus à un gain d'efficacité, puisque l'énergie nécessaire est alors réduite de 64 %. Différentes concentrations en dessous du point de gélation sont ainsi préparées. Une méthode en ligne est exploitée pour valider l'état de dispersion, avec une simple mesure de la perte de charge le long de la conduite. La viscosité de procédé est calculée avec une approche plus complexe et peut être comparée à la valeur obtenue en rhéométrie rotationnelle. Ce montage a également été utilisé en ajoutant du polyéthylènimine (PEI), pour montrer les autres usages qu'il est possible d'en faire, tel que la modification de surface des CNCs.

ABSTRACT

Cellulose nanocrystals (CNCs) are biobased and biodegradable rod-like nanoparticles that have garnered a growing interest over the past few years. Their unique mechanical, rheological and optical properties may be exploited in a wide range of applications: in plastics and composites, food, paints and coatings, construction, among other major fields. In this context, both academics and industrials are carrying out extensive research works to exploit these high value-added materials. Of particular interest is the high aspect ratio of CNCs, a feature shared with many other nanoparticles, which provide them such valuable properties such as a high mechanical strength or iridescence. In addition, the numerous hydroxyl groups on the surface of CNCs confer upon them an interesting versatility as these can host surface modification. However, these two specificities are also an important source of complications when dealing with their dispersion in suspensions. Indeed, CNCs tend to form strong agglomerates when dried after their extraction from the cellulosic source.

Reversing this phenomenon, induced by van der Waals forces and hydrogen bonds, requires employing a powerful technique, such as ultrasonication. Herein, a standardization of this approach is suggested. Through numerical modeling validated by conductivity and rheometry analyses, a dispersion index is estimated. It allows to determine the optimal operating parameters needed to obtain a well-dispersed CNC suspension. The sonication probe should be placed off-centered in the upper part of the vessel. In addition, the volume should be limited to ~60 mL (using standard beaker geometry) as no-mixing (or dead) zones are predominant at a larger volume. Based on this protocol, an energy of ~167kJ.g^{-1}.L^{-1} (per grams of CNC per liter of suspending medium) is required to achieve an optimal dispersed state.

To ensure the proper efficiency of this process, the dispersion state must be properly evaluated. The concepts of distribution and dispersion are hence thoroughly discussed using rheology, helping to understand CNC behavior during ultrasonication. The homogeneity of the suspensions is described by the viscosity standard deviation, while the viscosity value demonstrates the presence of agglomerates. A well-distributed and well-dispersed suspension therefore induces a minimal viscosity standard deviation and minimum viscosity, compared to an unsonicated suspension. The sampling volume influence is also highlighted. A more concentrated

suspension displays a rheopexy behavior, troubling the analysis. However, a satisfactory dispersion state is obtained, by analogy with a never-dried suspension.

Eventually, all this study is adapted to larger quantities, up to 200 mL, aiming for industrial applications. A semi-continuous setup is recommended to alleviate the volume limitations implied with a batch system. It leads, furthermore, to an important gain in efficiency, requiring 64% less energy. Different concentrations, below the gelling concentration, are successfully prepared. An in-line method is used to assess the dispersion state, by simply measuring the pressure drop along the pipe. A more complete strategy allows the determination of the process viscosity that can be compared to the value obtained in rotational rheometry. This setup has then been employed while adding polyethylenimine (PEI) in a well-dispersed suspension, aiming to confirm further possible applications such as CNC surface modification.

TABLE OF CONTENTS

LIST OF TABLES

LIST OF FIGURES

LIST OF SYMBOLS AND ABBREVIATIONS

Symbols and variables

a	Bubble radius
A	Ultrasound amplitude
a_0	Acceleration
A_R	Aspect ratio
C	Concentration
c	Sound velocity
CC	Concentric cylinder geometry
C_m	Maximum packing concentration
c_p	Specific heat capacity
D	Diameter
DG	Couette double gap geometry
D_i	Dispersion index
d_p	Particle diameter
DX	Day X
E	Energy
F	Force
F	Resonance frequency (in Equation (4.1) only)
f_0	Ultrasound frequency
F_{adv}	Advective force
F_{el}	Electrostatic force
G'	Dynamic shear storage modulus

G''	Dynamic shear loss modulus
h	Probe depth immersed in the suspension
H	Suspension height in the beaker
I_0	Probe intensity
I_{cav}	Cavitation threshold intensity
I_i	Intensity at position i
K_p	Power constant for a Newtonian fluid
$K_{p(n)}$	Power constant for a power-law fluid
K_s	Geometry-dependent constant in Metzner and Otto concept
K_s'	Geometry-dependent constant in Metzner and Otto concept for an empty tube
L	Length
m	Consistency index (in Chapter 6)
m	Mass (in Chapter 4)
m_p	Particle mass
n	Flow index
N	Rotational speed
n_{cav}	Particle number in the cavitation zone
ND	Never-dried
N_p	Power number
n_{tot}	Total number of particles
P	Effective acoustic power
p	Fluid pressure
p_{acc}	Acoustic pressure
p_{cav}	Cavitation threshold pressure

p_e	External pressure
Pe	Peclet number
p_{gn}	Gas pressure in the bubble at rest
P_s	Set point power
p_{stat}	Static ambient pressure
p_v	Vapor pressure
Q	Flow rate
r	Axial position form the beaker center
R	Beaker radius
R_0	Sphere radius (for HSP theory)
r_0	Ultrasonication probe radius
R_a	Distance to assess chemical affinity
Re	Reynold number
Re_{PL}	Reynold number for a power-law fluid
S	Probe surface area
T	Temperature
t	time
T_m	Melting temperature
T_{onset}	Onset degradation temperature
t_R	Residence time in the semi-continuous setup
t_{R^*}	Residence time in batch
$\boldsymbol{u}$	Fluid velocity
u^*_{acci}	Complex conjugate of the acoustic velocity in coordinate i
u_{acc}	Acoustic velocity

v	particle velocity
$[\eta]$	Intrinsic viscosity
$[\eta]_{el}$	Electroviscous contribution
$[\eta]_0$	Rigid body contribution
α	Attenuation coefficient
$\dot{\gamma}$	Shear rate
δ_D	London dispersion force component
δ_H	Hydrogen bonding interaction component
δ_P	Dipole-dipole interaction component
ΔP	Pressure drop for Netwonian fluids
$\Delta P_{(n)}$	Pressure drop for Netwonian fluids
ΔP_e	Entry pressure
ΔP_{exp}	Experimental pressure drop
ΔP_m	Pressure drop obtained by modeling
δ_T	Total cohesion parameter
ε	Dielectric constant
η	Dynamic viscosity
η_0 or μ	Newtonian viscosity
η_r	Relative viscosity
μ_{pr}	Process viscosity
Π	Pressure acoustic field
ρ	Density
ρ_e	Real conjugate of the density perturbation

ρ_e*	Complex conjugate of the density perturbation
ρ_p	Particle density
σ	Conductivity
σ_w	Surface tension at the bubble wall
τ_w	Wall stress
φ	Volume fraction
ω	Angular wave frequency
ζ	Zeta potential

Abbreviations

AF_4	Asymmetrical flow field-flow fractionation
AFM	Atomic force microscopy
ASA	Alkenyl succinic anhydride
ATPR	Atom transfer radical polymerization
CFD	Computational fluid dynamics
ClO_2	Chlorine dioxide
CMC	Cellulose microcrystal
CMF	Cellulose microfibril
CNC	Cellulose nanocrystal
CNF	Cellulose nanofibril
DLS	Dynamic light scattering
DLVO	Derjaguin-Landau-Verwey-Overbeek
DMF	Dimethylformamide
DMSO	Dimethyl sulfoxide

FBRM	Focused beam reflectance measurement
Glyc	Glycerol
H_2O_2	Hydrogen peroxide
H_2SO_4	Sulfuric acid
HCl	Hydrochloric acid
HPH	High-pressure homogenization
HSP	Hansen solubility parameters
LC	Large beaker/Centered probe
Na_2S	Sodium sulfide
NaOH	Sodium hydroxide
OH	Hydroxyl
PAA	poly(acrylic acid)
PCL	Poly(caprolactone)
PDMAEMA	Poly(N,N-dimethylaminoethyl methacrylate)
PEG	Poly(ethylene glycol)
PEI	Polyethylenimine
PEO	Poly(ethylene oxide)
PLA	Poly(lactic acid)
PMMAZO	Poly(6-[4-(4-methoxyphenylazo) phenoxy] hexyl methacrylate)
PNiPAAm	Poly(N-isopropylacrylamide)
PS	Polystyrene
SALS	Small-angle light scattering
SAXS	Small angle X-ray scattering

SC	Small beaker/Centered probe
SDC	Small beaker/Deep centered probe
SOC	Small beaker/Off-centered probe
TEM	Transmission electron microscopy
TEMPO	2,2,6,6-tetramethylpiperidine-1-oxyl
UND	Ultrasonicated never-dried
USD	Ultrasonicated spray-dried
XPS	X-ray photoelectron spectroscopy
XTN	Xanthan

LIST OF APPENDICES

CHAPTER 1 INTRODUCTION

1.1 Background

Nanocellulose materials are a source of growing interest among researchers over the last decades. In Canada, while the pulp and paper industry declined at the end of the 1990s, nanocellulose gained in popularity [1, 2]. Indeed, this high value-added material presents at the same time the valuable properties of cellulose (high mechanical strength, hydrophilicity, ability for chemical modification), and of nanomaterials (large surface area, dispersibility) [3, 4]. Cellulose nanomaterials include cellulose nanocrystals or CNCs (width: 3-10 nm and aspect ratio A_R>5), cellulose nanofibrils or CNFs (width: 5-30 nm and A_R>50), cellulose microcrystals or CMCs (width: 10-15 μm and A_R<2) and cellulose microfibrils or CMFs (width: 10-100 μm and length: 0.5-50 μm). This term standardization (Standard Terms and Their Definition for Cellulose Nanomaterial WI 3021) was suggested by the Technical Association of the Pulp and Paper Industry (TAPPI) [5]. The sustainable, biocompatible, and renewable nature of nanocellulose makes it a promising candidate for various applications in polymers for mechanical reinforcement, in coatings for optimal rheological properties, in Pickering emulsions, adhesives [2, 6, 7]. It is therefore a rich avenue to explore for researchers and industries. The significant increasing number of publications in the last decade on cellulose nanomaterials illustrates this interest in fully exploiting these compounds [8].

In this context, in 2015, FPInnovations, an organization supporting Canada's forest competitiveness, launched six challenges among Canada to deepen the knowledge about cellulose nanocrystals and wood-based nanomaterials [9, 10]:

1. Dispersion of cellulose nanocrystals in aqueous media
2. Dispersion of cellulose nanocrystals in non-polar matrices
3. Reinforcement potential of nanomaterials derived from wood fibre
4. Characterization of nanomaterials derived from wood fibre
5. Compatibilization of nanomaterials derived from wood fibre
6. Thermal stability of nanomaterials derived from wood fibre

This work is part of the second challenge which aims to study the dispersion of CNCs in non-polar solvents and thermoplastics to develop a “dispersibility index” based on rheology and evaluated offline or inline and applicable in several manufacturing processes [11]. This led to pertinent discussions on CNC modification for hydrophobic compatibilization. This work is part of the second challenge which aims to study the dispersion of CNCs in non-polar solvents and thermoplastics to develop a “dispersibility index” based on rheology and evaluated offline or inline and applicable in several manufacturing processes [11]. However, it also highlighted the needs of more fundamentals works on CNC behavior in suspension, their surface properties, self-assembly and dispersion in any media [12-15].

Therefore, this dissertation aims to continue efforts on bringing such comprehension that can help handle the agglomeration tendency of CNCs. While non-polar based applications were the final objective of the challenge, it appears necessary to first master the complexity of the dispersion process in water. For this purpose, further understanding of the most common strategy used to prepare CNC suspensions, which is ultrasonication, is essential. This implies that CNC behavior during this process must be properly defined to determine what may affect the dispersion efficiency. A rigorous protocol must also be specified to evaluate the dispersion state, either offline or inline. Finally, this approach would have to be scalable at larger scale to target industrial applications.

1.2 Outline of the dissertation

Following this introduction, chapter 2 presents a review of the literature on CNCs and their dispersion. After the description of the CNC extraction process, behavior in suspensions and main properties, the dispersion issue is addressed. The sonication technique is explained along with the dispersion evaluation methods that are mostly used. A critical analysis of the main gaps concerning the subject will conclude this chapter. Responding to these identified gaps, chapter 3 introduces the objectives of this thesis. These points are tackled in chapters 4 to 6, which contain the main works carried out during this project, resulting in the corresponding articles. Then, complementary ideas are discussed in chapter 7, including approaches that did not lead to concluding outcomes. Finally, chapter 8 summarizes this work and its originality, and suggests several points for further study.

CHAPTER 2 CRITICAL LITERATURE REVIEW

To understand the different challenges regarding CNC dispersion in aqueous media, an overview of these nanoparticles is given in this chapter. First, the process to obtain and handle CNCs from the cellulose source is explained. Then, the behavior of CNC suspensions is described including properties pertinent to various applications in the next section of this chapter. Finally, to benefit from these properties, agglomeration, a too common issue with any nanoparticle, must be avoided. Different approaches for de-agglomeration are presented, along with techniques to evaluate the dispersion state. In this literature review, the focus is made on several gaps in knowledge concerning the fundamentals of redispersion and the limitations of current procedures.

2.1 From native cellulose to nanocrystals

2.1.1 Cellulose

Cellulose is found in abundance on Earth. Plants, tunicates, algae, and wood contain various amounts of this renewable and biodegradable compound. Cellulose is formed by repeat units composed of an anhydroglucose ($C_6H_{10}O_5$) ring covalently bonded by an oxygen atom. Its degree of polymerization varies according to its source, from 10 000 to 15 000 [16, 17]. During its biosynthesis, glucose chains form many (intra- and intermolecular) hydrogen bonds, aggregating to form microfibrils [18]. Each fibril contains both crystalline and amorphous regions [19]. They are surrounded by other components, including hemicellulose, lignin and impurities, forming fibers [18, 20] (Figure 2.1).

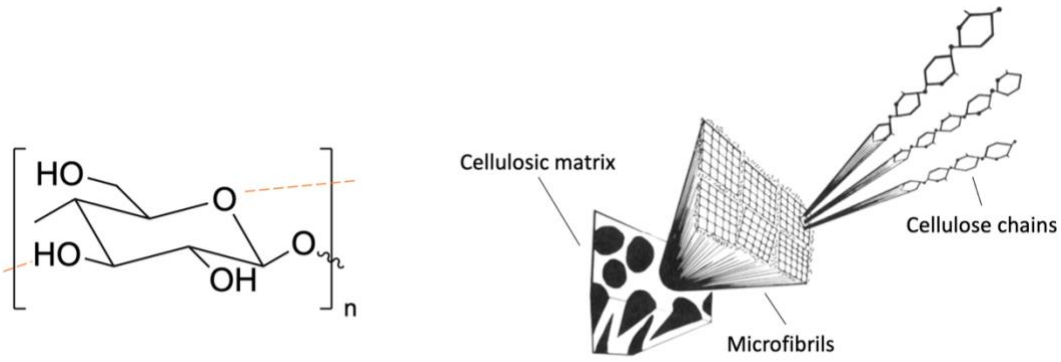

Figure 2.1: Cellulose chemical formula with possible intramolecular hydrogen bonds (adapted from [16]) and cellulosic material structure (adapted from [21])

The native form of cellulose is called cellulose I. Additional treatments can lead to cellulose II, III or IV, with cellulose II being the most thermodynamically stable form with a monoclinic crystal structure. Cellulose I may be found both with a triclinic (I_α) or monoclinic (I_β) crystalline structure, at a ratio depending on the cellulosic source [22, 23].

Cellulose materials present unique mechanical properties with the combination of crystalline (ordered) and amorphous (disordered) regions. While the disordered regions provide flexibility and plasticity, the ordered ones induce stiffness and elasticity. These properties depend, among other factors, on the source, as a higher cellulose content leads generally to a higher strength [18].

2.1.2 Extraction of CNCs

A purification step is needed to isolate cellulose from its matrix, via lignin, hemicellulose and impurity removal. For wood for example, kraft pulping – a treatment with heated sodium hydroxide (NaOH) and sodium sulfide (Na_2S) under pressure – and bleaching – using NaOH, chlorine dioxide (ClO_2) and hydrogen peroxide (H_2O_2) – are employed to depolymerize and solubilize lignin. The hemicellulose may also be solubilized in this process, while cellulose remains intact. Bleaching is usually applied when the aim is to achieve a high degree of crystallinity [24].

Afterwards, the microfibrillar and the crystalline parts of cellulose may be separated through either mechanical treatment, acid hydrolysis or enzymatic hydrolysis (though less

common). Microfibrillated cellulose (CMF) can be obtained for example from wood using high-pressure homogenization (HPH) or a grinder, leading after each pass through the system to smaller particles, but grinding leads to lower crystallinity [25, 26]. Nanofibrillated cellulose (CNF) is then obtained by additional chemical/mechanical treatments [27]. Acid hydrolysis is generally employed on bleached cellulose as it induces the destruction of the amorphous regions, while the crystalline parts are more acid-resistant, leading to rod-like CNCs [28, 29]. This step has a significant impact on the final nanocrystal properties. For example, a longer hydrolysis implies shorter CNCs [30]. Moreover, CNCs hydrolyzed with hydrochloric acid (HCl) are difficult to disperse, as they have a tendency to flocculate in water due to the lack of surface charge inducing electrostatic repulsive forces [31]. On the other hand, sulfuric acid (H_2SO_4) hydrolysis leads to the production of charged sulfate half-esters on the surface (-OH groups being partially converted to -OSO_3H), promoting suspension stability [32]. The resulting CNCs are generally smaller with a larger surface area (~400 $m^2.g^{-1}$) compared to those obtained with HCl. A higher degree of sulfation is linked to a greater dispersibility in water [33]. However, the presence of sulfate groups significantly decreases the onset degradation temperature T_{onset} for CNCs (~150˚C as compared to ~270˚C for CNCs hydrolyzed with HCl) [34-36]. This outcome is detrimental for applications in molten polymers (see Section 2.4.3) [37]. One way to improve the thermal stability is to neutralize the sulfate charges with counterions (Na^+, K^+, H^+, etc., increasing T_{onset} ~300˚C), which also plays a role on dispersion) [37]. One way to improve the thermal stability is to neutralize the sulfate charges with counterions (Na^+, K^+, H^+, etc., increasing T_{onset} ~300˚C), which also plays a role on dispersion [35, 38, 39] (Figure 2.2). Instead of a rod-like shape, a spherical morphology may be obtained by using both HCl and H_2SO_4 while sonicated. This helps slightly increasing the thermal stability (T_{onset} ~170˚C without neutralization) while promoting the suspension stability [40].). Instead of a rod-like shape, a spherical morphology may be obtained by using both HCl and H_2SO_4 while sonicated. This helps slightly increasing the thermal stability (T_{onset} ~170˚C without neutralization) while promoting the suspension stability [40].

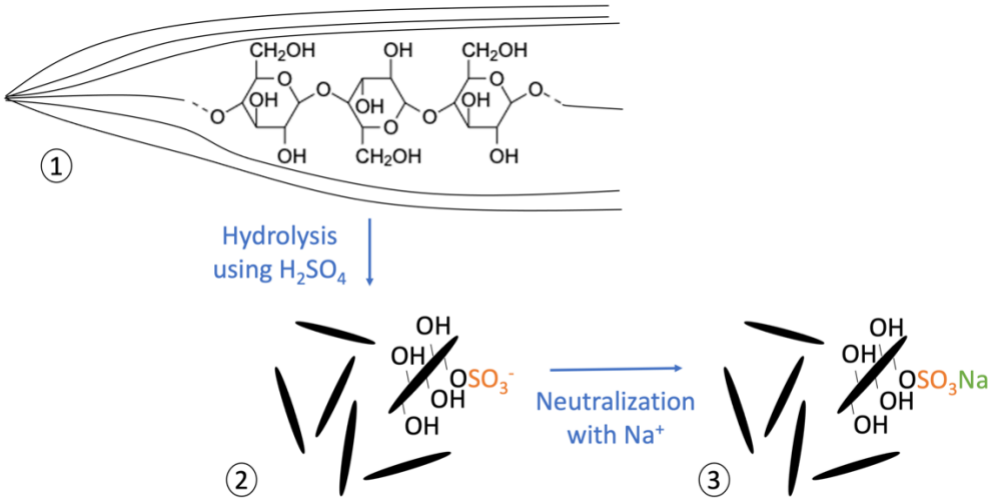

Figure 2.2: Acid hydrolysis using H_2SO_4: (1) Cellulose fibers, (2) Sulfated CNCs, (3) Neutralized sulfated CNCs

2.1.3 Drying

After extraction CNCs are generally dried for easier storage to be redispersed afterwards, as will be explained in Section 2.2. Several drying methods exist: spray-drying, freeze-drying, air drying, oven drying, supercritical drying or freeze-spray drying. Each approach impacts differently on the resulting powder morphology and thermal stability [41, 42]. Freeze-dried CNC appears as lamellar flakes whereas the spherical agglomerates obtained by spray-drying form a flour-like powder [43]. Spray-drying may be the best strategy to produce particle size in the nano-range. Air drying leads to microparticles, while freeze-drying and supercritical drying lead to a multi-scale material (nano and micro dimensions), but at added cost [42]. Spray drying additionally induces a better thermal stability and a higher crystallinity index that may be tailored with humidity and temperature conditions. Freeze-dried CNC appears as lamellar flakes whereas the spherical agglomerates obtained by spray-drying form a flour-like powder [43]. Air drying leads to microparticles, while freeze-drying and supercritical drying lead to a multi-scale material (nano and micro dimensions), but at added cost [42]. Spray drying additionally induces a better thermal stability and a higher crystallinity index that may be tailored with humidity and temperature conditions [41, 44, 45].

2.2 Redispersing CNCs in solvents

Dried CNCs may be challenging to redisperse due to the strong intermolecular hydrogen bonds and van der Waals forces (~10 kJ.mol^{-1}) formed while drying [12, 46, 47]. These interactions are stronger and more numerous for CNCs in the acid form (not neutralized) which limits redispersion, unless the moisture content has been kept above 4 wt% during drying [38, 43]. However, it is possible to obtain stable colloidal aqueous dispersion with neutralized CNCs using appropriate treatments [38, 43], the efficiency of which will be discussed in Section 2.5.

Electrostatic stabilization (predicted by the dielectric constant ε) and solvation-induced stabilization (related to the chemical affinity) are the two key mechanisms playing a role on the suspension stability [13]. CNC dispersion ability may be predicted using the Hansen solubility parameter (HSP) theory [14]. In this approach, each solvent and polymer may be defined by a triplet (δ_D; δ_P; δ_H) where δ_D is the component for the London dispersion forces, δ_P the component for the dipole-dipole interactions, and δ_H the component for the hydrogen bonding interactions [48]. This triplet represents the total cohesion parameter δ_T in MPa$^{1/2}$, defined such as:

$$\delta_T^2 = \delta_D^2 + \delta_P^2 + \delta_H^2 \tag{2.1}$$

To assess the chemical affinity between a solvent (1) and a polymer (2), a distance R_a in MPa$^{1/2}$ is then defined:

$$R_a^2 = 4\left(\delta_{D,1} - \delta_{D,2}\right)^2 + \left(\delta_{P,1} - \delta_{P,2}\right)^2 + \left(\delta_{P,1} - \delta_{P,2}\right)^2 \tag{2.2}$$

The solvent is considered as "good" for the polymer if $R_a \leq R_0$, R_0 being a sphere radius whose center is the polymer HSP. "Good" here mean that the polymer can at least swell in the solvent or is totally soluble, and this concept may be extended to dispersibility for non-soluble particles. Mixtures of solvents may also be defined the same way [48]. As CNC presents an amphiphilic behavior in suspension due to its anisotropy, two sets of HSP parameters may be defined. The main HSP sphere describing its polarity has a radius of 7.8 MPa$^{1/2}$ with a center (δ_D; δ_P; δ_H) = (18.1; 20.4; 15.3) ± (0.5; 0.5; 0.4) MPa$^{1/2}$. Then the non-polar sphere radius is much smaller (2.1 MPa$^{1/2}$) with its center at (17.4; 4.8; 6.5) ± (0.3; 0.5; 0.6) MPa$^{1/2}$ [14] (see Figure 2.3).

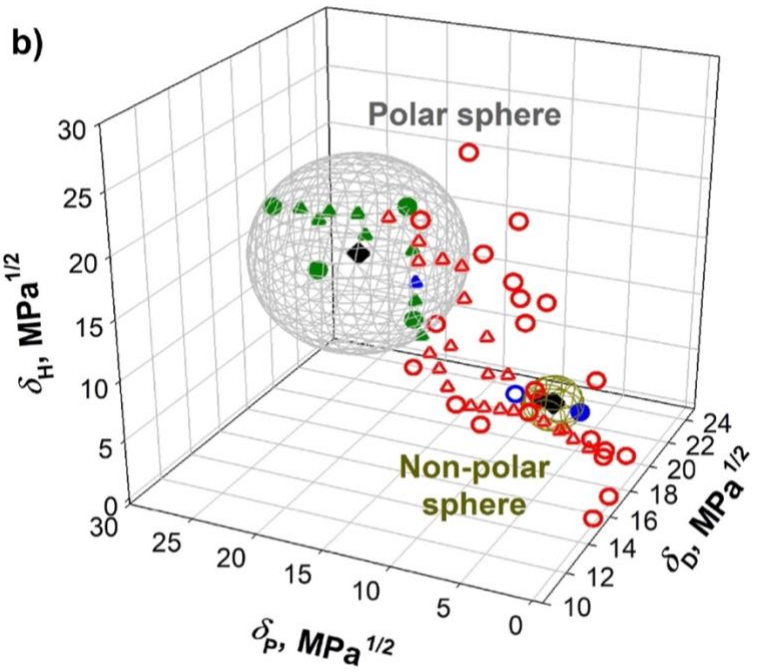

Figure 2.3: HSP graph of CNCs with solvents leading high (green), to medium (blue) and low (red) dispersibility. Reproduced with permission from [14]

Thus, suspending CNCs in polar organic media like dimethyl sulfoxide (DMSO) or dimethylformamide (DMF) may be accomplished, though a minor water content may be needed (<2 wt%) and some agglomeration is observed [49]. Dispersing CNC in non-polar media is also possible for a few solvents as predicted by the HSP theory [14]. However, to expand the range of possible solvents, solvent exchange may be employed, progressively exchanging to solvents with a lower polarity [50]. A surfactant or surface modification may also be used to overcome this problem [51-54].

2.3 CNC aqueous suspension behavior

2.3.1 Nanorod organization

The structure and the surface charge of the CNCs imply an ordering phenomenon [55]. The orientation of the nanorods is concentration-dependent. At low CNC content (below 3-4 wt% [56]), they do not adopt a favored orientation, resulting in an isotropic phase. At higher concentration, they form a chiral nematic phase with the optical properties of cholesteric liquid

crystal [57]. CNCs are arranged in parallel layers along one direction parallel to the layer plane. In addition, the main axis direction in each layer slightly rotates from the layer below, leading to a helicoidal distribution [58] (Figure 2.4). A transitional state is achieved at intermediate concentration with both isotropic and anisotropic phases [59]. Interestingly, only sulfated or phosphated CNCs display chiral nematic structure [33], and their corresponding films demonstrate iridescence properties. Eventually, higher concentrations (above 10-12 wt%) lead to a birefringent gel [56].

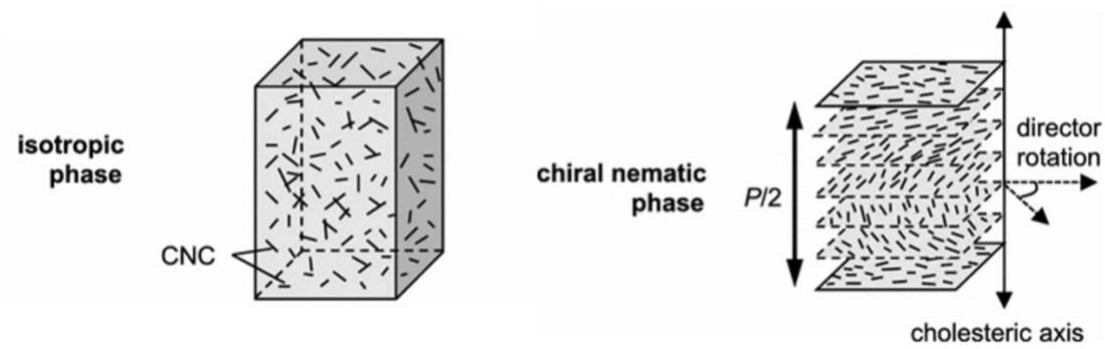

Figure 2.4: CNCs organization in the isotropic phase and in the chiral nematic phase, each chiral plane is composed of aligned nanorods, and their orientation slightly rotates from adjacent planes, P being the pitch of the obtained helix. Reproduced with permission from [60].

This self-organization ability depends on the balance between the attractive van der Waals forces and the repulsive steric and electrostatic forces [59]. Thus, the concentration limits discriminating each behavior are largely influenced by the surface charge [61]. Salt addition conducts to gel formation at much lower CNC concentration (1 wt%) as the ionic strength leads to a thinner electric double layer, reducing the electrostatic forces [62]. These notions are detailed in Section 2.5.1. The degree of sulfation affects the critical concentrations too, with higher limits for more sulfated CNCs [56]. Compared to H_2SO_4-hydrolyzed CNC suspensions, HCl-hydrolyzed CNC suspensions present a time-dependent rheological behavior. Indeed, as introduced in Section 2.1.2, HCl hydrolysis leads to a lower suspension stability, inducing agglomeration due to the lack of repulsive forces. When applying shear, these agglomerates may be broken, leading to a shear-thinning behavior [63].

2.3.2 Rheology

The three behaviors displayed by CNC suspensions, which are discussed above, namely the isotropic, chiral nematic and gel behaviors, present different rheological behavior in shear rate sweep studies. Thus, isotropic suspensions exhibit a Newtonian plateau at low and high shear rates (below 2.10^{-2} and above 10^{1} s^{-1}) and a shear thinning behavior at intermediate values. Lyotropic liquid crystal suspensions are also defined by a three-region viscosity profile, this time with shear-thinning at low ($<10^{-1}$-10^{1} s^{-1}) and high shear rate ($>10^{1}$-10^{2} s^{-1}), and a plateau at intermediate values. Finally, a typical behavior of a gel is shear-thinning over the entire range [64] (Figure 2.5).

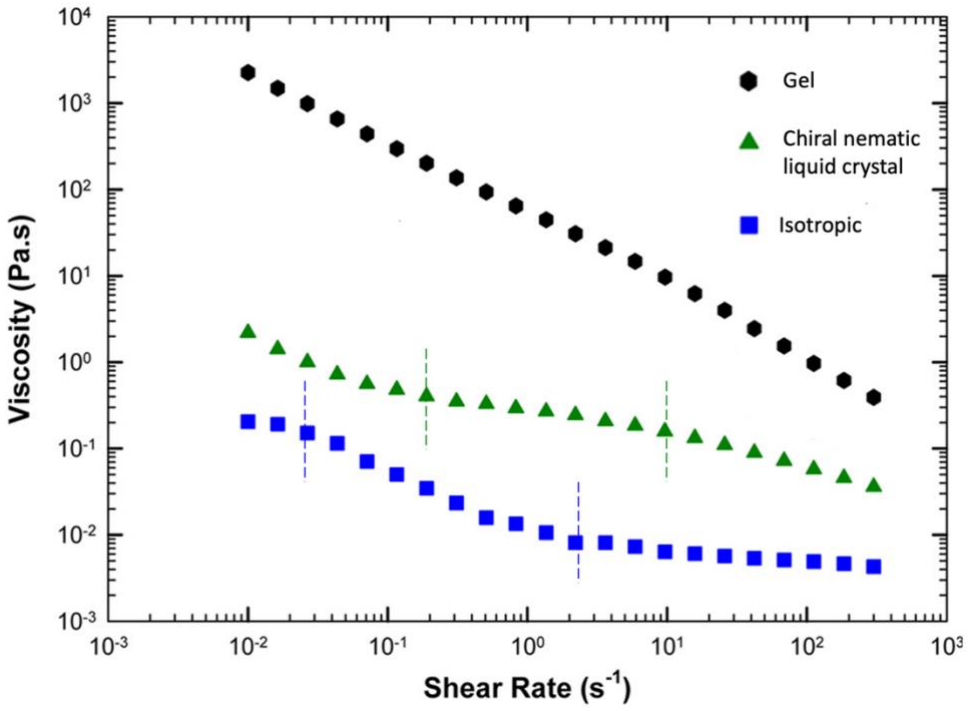

Figure 2.5: Viscosity as function of shear rate illustrating the three kinds of behaviors of CNC suspensions. Approximate limits between the different regions discussed in this section are indicated by vertical lines. Adapted from [64].

Combined with small-angle X-ray scattering (SAXS) and small-angle light scattering (SALS), Pignon et al. [65] successfully used rheology to understand the viscosity changes occurring for liquid crystalline suspensions of CNCs. The lowest shear rates disrupt large liquid crystalline domains into smaller tactoids (isotropic liquid crystalline microdomains), and the

helical axis of the cholesteric regions align perpendicular to the flow direction. Then, the tactoids keep the same orientation but they are broken into smaller entities, smaller than the pitch value. These units are finally completely broken at high shear rate and the nanocrystals remain oriented in the flow direction.

Different parameters may influence the suspension viscosity. A higher temperature leads to a decrease in the viscosity on the entire shear rate range for concentrations below 3 wt%. When there is more organization in the system, however, a small increase is observed for low shear rate, at 30-40 ˚C for concentration up to 7 wt%, or above 50˚C for concentration ~10 wt%. It suggests changes or rearrangement in the microstructure.

Salt content is a key parameter for the CNC aqueous suspension rheological behavior [66]. Xu et al [66] have for instance observed that for their type of CNC, the liquid phase below 3 wt% becomes a gel for salt concentration over 50 mM. At high CNC concentration (>10 wt%), a solid phase is observed where G'>G'' (G' and G'' being respectively dynamic shear storage and loss modulus). While the term "gel" is usually used in the literature, the term "glass" is suggested by the fact that the solid volume fraction is above glass transition (meaning that the high volume fraction does not allow rotational diffusion [67]). Thus, a repulsive glass is noticed at no/low salt content and an attractive glass for salt concentration above 20 mM, being dominated respectively by repulsive or attractive forces [68, 69]. Figure 2.6 reports all the different behavior described in this section.

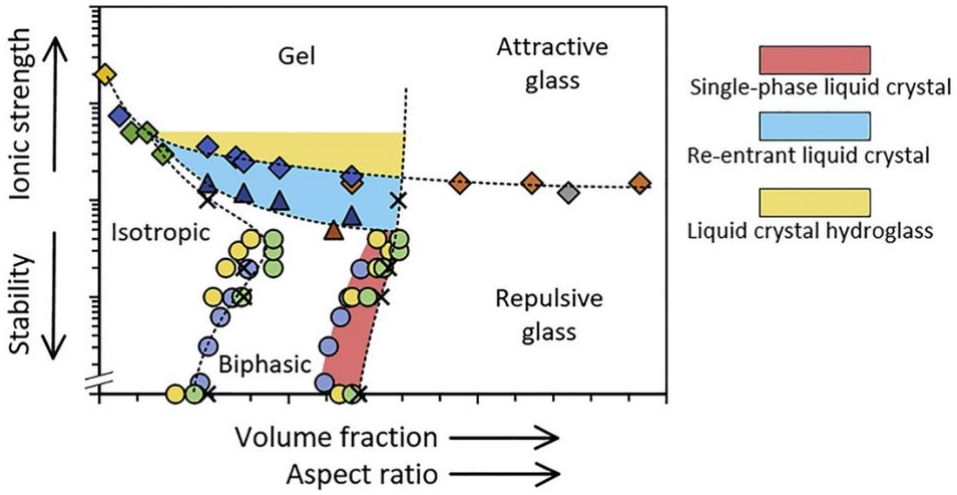

Figure 2.6: Phase diagram illustrating the different behaviors observed for CNC suspension. ("Re-entrant" means that an additional liquid crystal state is formed). Reproduced with permission from [67]

Fedors model, describing the viscosity of dilute and semi-dilute systems containing agglomerates, was successfully applied on CNC suspensions [12]. This model may be defined as [70]:

$$\frac{1}{2(\sqrt{\eta_r}-1)} = \frac{1}{C[\eta]} - \frac{1}{C_m[\eta]} \tag{2.3}$$

where the relative viscosity η_r is the ratio of the pseudo Newtonian plateau or Newtonian viscosity η_0, to that of water. $[\eta]$ is the intrinsic viscosity in volume/mass unit measuring the contribution of dispersed particles to the bulk viscosity [71]. $[\eta]$ is the sum of the rigid body $[\eta]_0$ and the electroviscous $[\eta]_{el}$ contributions, C_m is the maximum packing concentration and C is the concentration calculated by:

$$C = \frac{\varphi}{1-\varphi}\rho \tag{2.4}$$

with φ the volume fraction and ρ the solvent density. For spray-dried CNCs with a shape factor (or aspect ratio) A_R ~ 12.5, $[\eta]_0$ was estimated to 12 mL.g^{-1}. η_r and $[\eta]_{el}$ decrease for smaller particle size during dispersion in water. In addition, $[\eta]_0$ is function of the shape factor, such as, for CNCs [72, 73]:

$$[\eta]_0 = \frac{14}{15} + \frac{{A_R}^2}{15(\ln(2A_R) - 1.5)} + \frac{{A_R}^2}{5(\ln(2A_R) - 0.5)} \quad (2.5)$$

Thus, as the aspect ratio accordingly decreases, a larger $[\eta]_0$ is also expected. In addition, C_m is decreasing upon dispersion (up to a maximum value ~ 0.11), displaying agglomerate breakage [12]. Hence, this model demonstrates the great potential of rheology for describing colloidal suspensions.

2.4 A brief overview of CNC applications

2.4.1 Main properties

CNC's unique properties make them valuable for a wide range of applications. With a high crystallinity and a low density (~ 1.6 $g.cm^{-3}$), their specific Young's modulus is competitive with that of Kevlar (~ 42 $J.g^{-1}$) and higher than that of glass fibers (~ 29 $J.g^{-1}$) [18, 74].

The liquid crystallinity of the CNCs leads to optical properties that may be tuned by controlling the orientation of the nanorods in the matrix. The wavelength of the reflective light is influenced by the pitch of the helix controlled by CNC concentration, its surface charge, or the ionic strength. The pitch can also be changed by ultrasonic treatment, by changing the evaporation temperature or by further surface modification [58, 60, 75].

CNCs may demonstrate swelling properties as nanocrystals are arranged such that water can penetrate between them [76, 77]. For the same reason, a high diffusion coefficient and gas permeability is also observed [78]. CNCs hydrolyzed by H_2SO_4 display permselective properties because of their surface charge, absorbing only positively-charged species [79].

2.4.2 Surface modification

CNCs may be incorporated to polymers to enhance the properties of the native matrix. One limitation for this to fully benefit from these properties is their polarity. To compatibilize CNCs with non-polar polymer matrices, CNCs must usually be modified by taking advantage of the numerous reactive OH groups present on the nanorod surface. Different methods exist and are briefly stated in this section (Figure 2.7).

Substitutions of OH groups using small molecules (in orange in Figure 2.7) has been extensively studied in the literature. 2,2,6,6-tetramethylpiperidine-1-oxyl (TEMPO) is used to oxidize the CNCs to favor polymer grafting or promote suspension stability [53, 80].

Polymer grafting may be performed by attaching polymer chains onto OH groups (grafting-onto) with a coupling agent (in blue in Figure 2.7) or by polymerization on CNC (grafting from) through ring opening polymerization, atom transfer radical polymerization (ATPR) using an initiator or single-electron transfer living radical polymerization (in green in Figure 2.7) [32, 81]. Acetylation can provide a hydrophobic behavior to the CNCs [82]. Interestingly, a single-step process combined with the hydrolysis step (see Section 2.1.2) was developed. The Fischer esterification allows at the same time acetylation and extraction of the crystalline part [83]. The same method can by apply with esters [84]. Silylation also leads to hydrophobic modified CNCs but a high degree of substitution (>1) leads to a loss of the original crystal morphology [51].

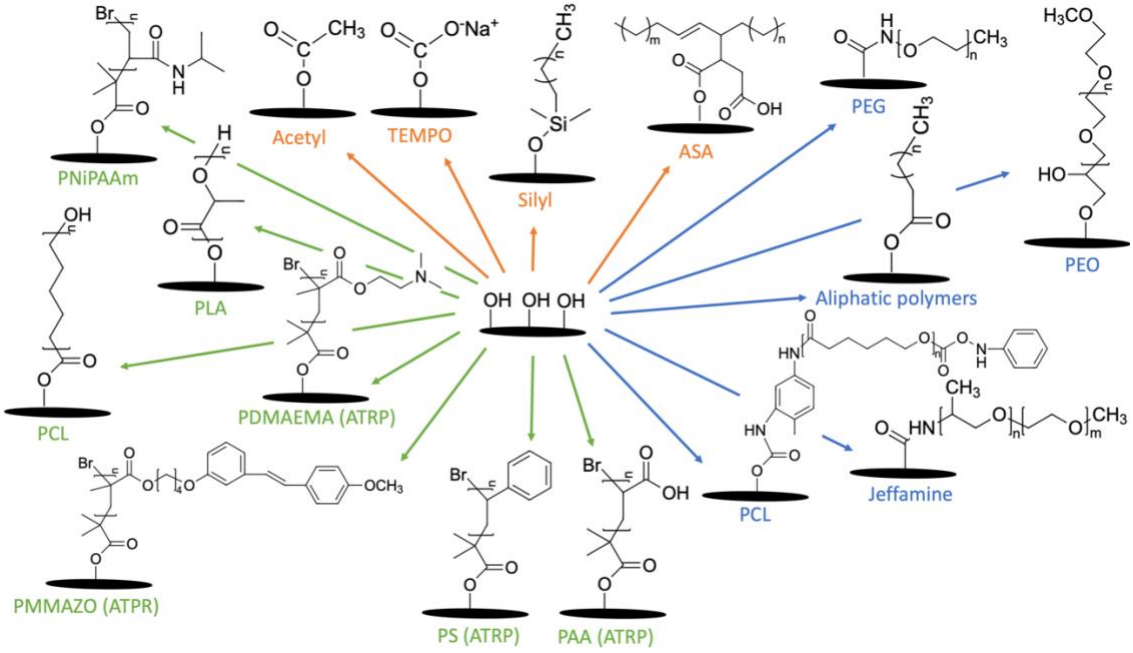

Figure 2.7: Common CNC surface modification strategies [PEG: poly(ethylene glycol); PEO: poly(ethylene oxide); PLA: poly(lactic acid); PCL: poly(caprolactone); PAA: poly(acrylic acid); PS: polystyrene; PNiPAAm: poly(N-isopropylacrylamide); PMMAZO: poly(6-[4-(4-

methoxyphenylazo) phenoxy] hexyl methacrylate); PDMAEMA: poly(N,N-dimethylaminoethyl methacrylate); ASA: alkenyl succinic anhydride]. Adapted from [81]

Non-covalent methods allow modification with a low environmental impact, without any coupling agent or purification step. This approach is based on electrostatic interactions, for instance between a surfactant and the CNCs [85-87]. Cationic surfactants are usually favored as it is better adsorbed by the negatively charged CNC [88]. Many polymers (charged and uncharged) as well as precipitated sugars may also be used. The drawback of this method is that a large amount of surfactant is generally required because of the high specific area of CNCs [87].

2.4.3 CNC addition in polymers

The objective of CNC addition in polymers may vary. Mechanical properties are often targeted due to the high mechanical strength of CNCs [89, 90]. Although significant mechanical improvement has been achieved (e.g., an elastic modulus 10 times higher than the neat matrix at the rubbery plateau [91]), many parameters may inhibit the desired properties such as the percolation threshold and the filler dispersion [18, 91, 92]. However, other properties may be enhanced when adding CNC in a polymer such as the flow behavior for 3D printing applications [93, 94], piezoelectricity [95-98], tunable optical properties for photonic materials [99-101], etc.

CNCs (modified or not) are most commonly incorporated into polymers by solvent-casting or melt compounding approaches. Solvent-casting relies on preliminary dispersion of CNCs in a solvent that is miscible with the polymer solution, or that can solubilize the targeted polymer. The resulting blend is dried before being used for the desired application (extrusion, compression molding) [16]. In addition to being time-consuming, the downside of this approach is that finding a suitable medium may be complex [16, 102]. HSP theory (introduced in Section 2.2) may overcome this problem [14, 48]. In addition, the evaporation step is critical leading either to destabilization-induced self-assembly or evaporation-induced self-assembly. The second phenomenon, occurring either alone when $\varepsilon<11$ and $R_a>7.8\text{MPa}^{1/2}$ or combined with solvation-induced stabilization when $\varepsilon<11$ and $R_a<7.8\text{MPa}^{1/2}$, needs to dominate to form continuous thin film [13].

A more straightforward technique consists in mixing the CNCs in the molten polymer before extruding or compression molding [16]. A masterbatch may be employed beforehand to favor the compatibilization between CNCs and the matrix, with either the same polymer or a compatibilizer [103-105]. In all cases however, it is essential that the processing temperature (close to the matrix melting temperature T_m) remains largely below the thermal degradation point of CNCs. For instance, sulfated CNCs must be neutralized to be added in PLA (T_m ~ 173-178˚C) or polyhydroxybutyrate (PHB, T_m ~ 177˚C) [106] (as detailed in Section 2.1.2, T_{onset} ~ 150˚C for sulfated CNCs while T_{onset} ~ 300˚C after neutralization).

2.5 Dispersion challenges

2.5.1 Agglomeration and dispersion theory

An optimal dispersion state, along with colloidal stability, is usually desirable for many applications, with any nanoparticles such as CNCs [107-109]. The colloidal stability is described by the Derjaguin-Landau-Verwey-Overbeek (DLVO) theory, combining attractive van der Waals forces and repulsive electrostatic forces [110]. Zeta potential is usually a good indicator of the suspension stability as it gives information on the surface charge density [111]. This parameter is the potential at the slipping plane: a charged particle is surrounded by a double layer, composed of an inner layer or Stern layer of ions with opposite charge to that of the particle, and a diffusion layer with both charges. The slipping plane is then the interface with the medium. By measuring the electrophoretic mobility under an applied electric field, it is possible to deduce the zeta potential with Hückel or Smoluchowski approximations. A zeta potential absolute value above 30 mV implies attractive forces weaker than repulsive forces, leading to suspension stability. However, lower values may be sufficient if the van der Waals forces are weak [112].

A distinction may be made between an “aggregate” and an “agglomerate”, despite these terms are often being used interchangeably in the literature. When nanoparticles are held by van der Waals forces, they form an agglomerate. “Aggregate” is generally used for stronger chemical or sintering bonds (“hard” bonds) [110, 113]. In other words, when the repulsive forces of the primary particles are too weak, this results in agglomeration. These forces are a function of the surface charge, electrostatic, and steric forces. The electrostatic forces influence the zeta potential

and the electric double layer thickness, as explained above. The first parameter is influenced by the pH while the second depends on the medium ionic strength. Indeed, when the particle net surface charge is zero, this is called the isolectric point. pH values lower or higher than the value at this point leads to a higher zeta potential. Thus, stronger repulsive forces are obtained further from the isoelectric point, leading to a better stability. Moreover, a higher ionic strength induces the compression of the electrical double layer. This eventually triggers agglomeration [110].

2.5.2 Ultrasonication

While used for several applications such as emulsion preparation [114] or chemical reactions [115], ultrasonication is often employed for solid particle dispersion [43, 111, 116]. Two types of ultrasonication are usually employed: probe (or horn) and bath sonication (Figure 2.8). Whereas the two methods are based on the same phenomenon, defined in this section, only probe sonication is addressed here. Indeed, bath sonication is an indirect technique providing lower amount of energy because of a lower intensity and non-uniform process (20-40 $W.L^{-1}$ compared to 20 000 $W.L^{-1}$ for a probe device) [117, 118]. This approach is thus less efficient regarding agglomerate breakage [110].

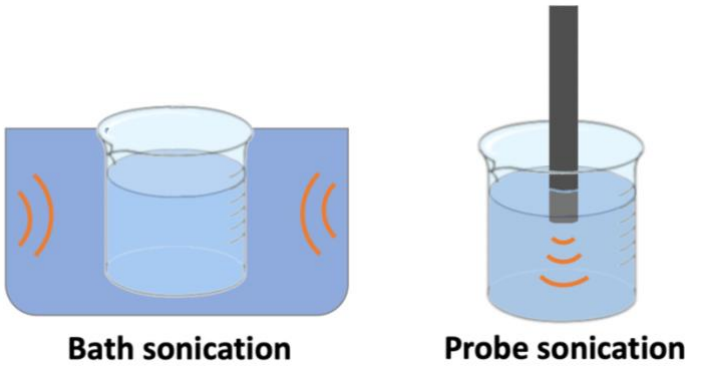

Figure 2.8: Bath and probe sonication configuration

This process is based on acoustic cavitation (Figure 2.9). Sinusoidal waves are generated by piezoelectricity at high frequency (> 20 kHz), leading to alternating positive and negative pressures. This creates vacuum bubbles, immediately filled with vapor, in the liquid medium. Subject to the pressure changes, these bubbles grow until a critical size (ex. 170 µm at 20 kHz) [119]. At this point, an implosion occurs releasing a very high amount of energy stored during

bubble growth, resulting in local temperature and pressure over 5 000 K and 100 bars. In addition, a "microjet" approaching 400 km/h is observed when the implosion occurs near a solid boundary [119, 120]. With these intense conditions, a very brief light emission (~10^{-10} s) may be noticed [121]. Moreover, it can lead to thermal dissociation of the vapor, or solvent decomposition in case of non-aqueous solutions. Sonication forms free radicals or radical products, which are exploited in sonochemical reactions [122, 123].

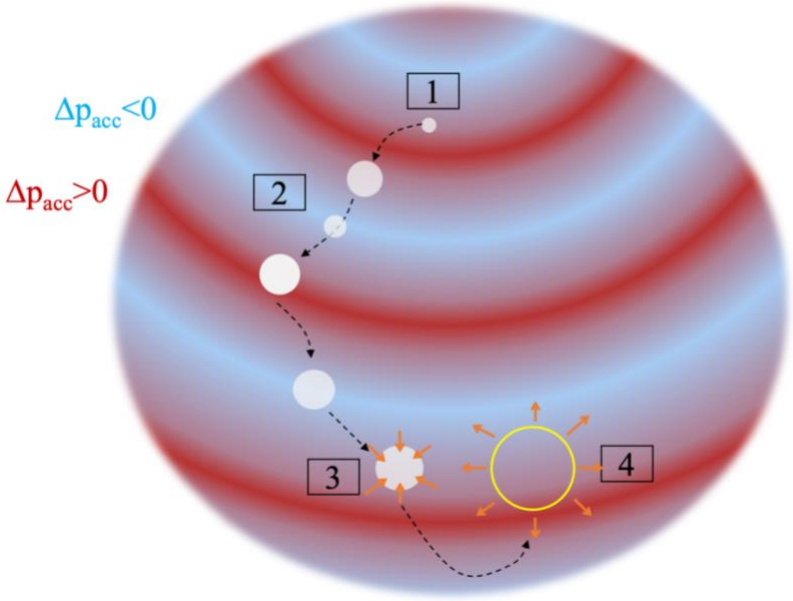

Figure 2.9: Cavitation theory: (1) A cavitation bubble is formed due to the pressure changing (positive and negative acoustic pressure fields Δp_{acc} are respectively illustrated in red and blue). (2) Its size is affected by the pressure and grows until a critical size (3) that triggers implosion and (4) releasing high amount of energy (yellow circle). (Note that positions (3) and (4) are only differentiated for the readability of the figure).

For the cavity (or vapor bubble) to be formed, a specific pressure must be achieved: the acoustic cavitation threshold, depending on the static pressure, the acoustic frequency, the medium and its temperature. It has been measured to be between ~0.8 and ~3 bars at 20 kHz [121].

The Rayleigh-Plesset equation accurately models the behavior of a single bubble [121]:

$$\rho R\ddot{R} + \frac{3}{2}\rho\dot{R}^2 = p_i - p_e = p_{gn}\left(\frac{R_n}{R}\right)^{3\kappa} + p_v - p_{stat} - \frac{2\sigma_w}{R} - \frac{4\mu}{R}\dot{R} - p(t) \qquad (2.6)$$

where R and R_n are respectively the actual bubble radius and the radius at rest, ρ the fluid density, μ the fluid dynamic viscosity, p_i the internal pressure, p_e the external pressure, κ is the polytropic exponent of the internal gas. p_v and p_{stat} are respectively the vapor and the static ambient pressure, σ_w is the surface tension between liquid and vapor phases at the bubble wall, and p_{gn}, the gas pressure in the bubble at rest, which is defined by:

$$p_{gn} = \frac{2\sigma}{R_n} + p_{stat} - p_v \tag{2.7}$$

The multi-bubble dynamics have also been well described. Clusters, streamers or double layers can be formed, depending on the forces governing their motion [121]. Tzanakis et al. [124] successfully demonstrated the effect of different liquids on the pattern cavitation bubbles form. Whereas a cone-like structure is observed for water, a circulating formation is visible for more viscous fluids like glycerol, and less viscous liquids like ethanol do not lead to any organization (Figure 2.10). The cone-like structure in water was also highlighted by Moussatov et al. [125] who additionally proved that smaller probe diameters lead to more turbulent flow. The acoustic intensity is indeed inversely proportional to the horn surface.

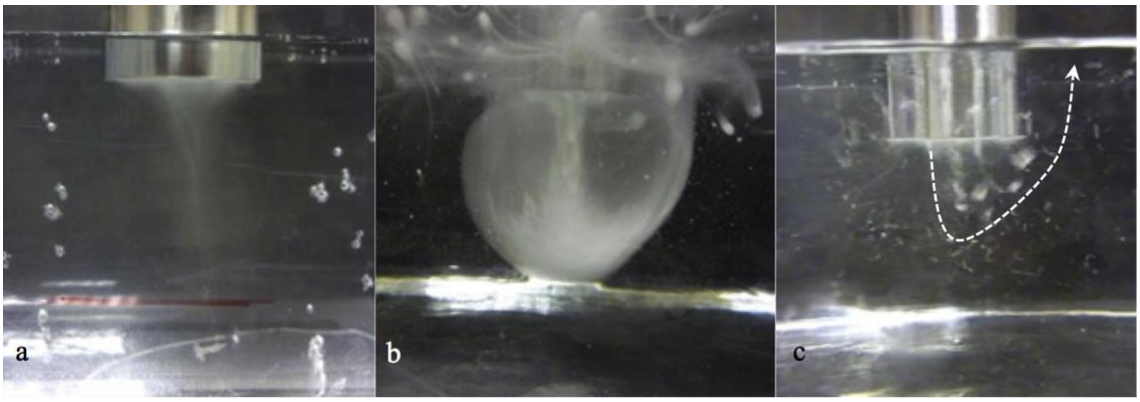

Figure 2.10: Different cavitation bubble structures forming under the probe: a) conical shape in water, b) circulating formation in glycerol and (c) random structure in ethanol. Reproduced with permission from [124]

To further understand the ultrasonication process, several modeling works have been carried out. Based on the bubble dynamics theory presented above, Louisnard et al. [126, 127] modeled the cavitation model structure and defined an “active zone” where cavitation occurs. Schanz et al. [128] were able to predict the sonochemiluminescence of a cavitation bubble. They

used a hard sphere model for the species inside the bubble, and the Rayleight-Plesset equations were applied for the surrounding medium. Moreover, the fluid dynamics induced by the acoustic streaming force was simulated by Rubinetti et al. using laminar approximation [129, 130]. The acoustic equations were coupled with the laminar fluid flow equations with the following body force $\boldsymbol{F}$:

$$\boldsymbol{F} = {}^{1}/_{2}\, Re[\rho_e^* \omega \boldsymbol{u_{acc}}] + {}^{1}/_{2}\, \rho_e \left(Re\left[u_x^{*}\, {}^{\partial \boldsymbol{u_{acc}}}/_{\partial x}\right] + Re\left[u_y^{*}\, {}^{\partial \boldsymbol{u_{acc}}}/_{\partial y}\right] + Re\left[u_z^{*}\, {}^{\partial \boldsymbol{u_{acc}}}/_{\partial z}\right]\right) \tag{2.8}$$

where u_{accx}^{*}, u_{accy}^{*}, u_{accz}^{*}, the complex conjugates of velocity components in Cartesian coordinates at a specific location and only the real portion of each term is considered. ρ_e and ρ_e^* are real and complex conjugate of density perturbation and scalar ρ_e is obtained from the Helmholtz equation such as:

$$\rho_e = {}^{p_{acc}}/_{c^2} \tag{2.9}$$

with p_{acc} the acoustic pressure and c the velocity of sound in the medium. However, in all numerical models, the experimental conditions of ultrasonication were rarely discussed, except for the probe diameter and power influence in aluminum dispersion [131].

The cavitation phenomenon is known to be efficient enough to erode and break agglomerates [117, 132]. The maximum energy released by cavitation (~ 100 kJ.mol^{-1}) is larger than the binding energy of hydrogen and van der Waals forces (~ 10 kJ.mol^{-1}) [12]. Erosion is favored for low energy settings, and more important for agglomerates with a larger specific surface area [133, 134]. Fracture requires a higher energy. This implies that the particle residence time in the region where cavitation occurs (active zone) must be long enough for the cavitation forces to be significant [134]. In addition, erosion is independent of the input acoustic power [133]. It must be noted nonetheless that ultrasonication may not be efficient enough to break the hard bonds holding the aggregates [110].

Several parameters affecting ultrasonication efficiency have been discussed in the literature. Firstly, the frequency value impacts the size of the collapsing bubble. A too small bubble will imply a weak cavitation phenomenon as the released energy is proportional to the cavity size. However, a too large bubble induces less frequent collapsing events. Accordingly, the

frequency value must be chosen properly to find a balance between both phenomena. This is especially important in chemical reactions to increase the radical production rate [135]. The time needed for dispersion reported in the literature varies largely. Beck et al. [58] suggested that sonicating longer than 5 minutes does not imply a better dispersion. On the contrary, others described an improved dispersion state at longer times up to 60 min, when re-agglomeration occurs [109, 136]. Longer treatment would also induce significant probe erosion [137]. Nevertheless, even longer times (up to 150 min) were reported as optimal in the literature [107, 108]. This discrepancy highlights the lack of knowledge about this technique and may imply that the process cannot be generalized whatever the experimental conditions.

Similar contradictions arise when studying temperature effects on ultrasonication efficiency. Dumée et al. [138] observed for instance a weaker diffusion at lower temperature, leading to enhanced suspension stability, and improved dispersibility. Conversely, Li et al. [136] demonstrated that higher temperature favors a faster dispersion by reducing the attractive forces. Ultrasonication may be performed either in a continuous or in a pulsed mode. The pulsed mode was sometimes suggested to avoid overheating [12] but no gain in efficiency has been proven [139]. The energy needed to obtain well-dispersed suspension has also been discussed. While Beck et al. [43] proposed 5000 $J.g^{-1}$ at most for this purpose, Beuguel et al. [12] recommended a value of 10000 $J.g^{-1}$. In both cases, recommendations made do not account for container geometry or suspension volume. It must also be highlighted that concentration is sometimes mentioned as a limiting factor and high CNC concentrations (>3 wt%) should rather be obtained by evaporating more dilute suspensions [43, 111].

The cavitation phenomenon also depends on the medium properties. The intensity I_x varies with the distance from the probe surface x, following the equation:

$$I_x = I_0 e^{-2\alpha x} \tag{2.10}$$

where I_0 is the initial acoustic intensity and α is the attenuation coefficient, defined by:

$$\alpha \propto \frac{2\mu f^2}{3\rho} \tag{2.11}$$

with f the acoustic frequency [140]. Thus, the acoustic waves are more attenuated for more viscous fluids, inducing a lower efficiency.

While details about the experimental conditions used for ultrasonication are rarely presented in articles, a few works have been carried out on sonication parameters' influence. Recently, sonochemiluminescence, calorimetry and potassium iodide dosimetry techniques were employed to define optimal conditions based on the sonochemical activity. It was found that a probe placed 10 mm from the bottom of the vessel (500 mL), centered, with a liquid height of 70 mm and a high power were giving the best results [141]. It must be pointed out though that this study was only carried out in water, implying generally a lower density and viscosity than suspensions, with the latter impacting the acoustic wave propagation. Moreover, the conditions would not be necessarily adapted for dispersion as the challenges are not the same (mixing is needed in addition to cavitation). Indeed, the opposite recommendation (placing the probe near the surface) has been recommended to ensure better foamability of Pickering emulsions [142]. Concerning dispersion, Taurozzi et al. [117] suggests immersing the horn to 2-5 cm, keeping at least 1 cm from the bottom of the beaker. In addition, the acoustic wave exposition may be maximized for smaller containers. However, the authors do not present any justifications for these guidelines. Nevertheless, the volume limitation has been reported elsewhere in the literature. Kusters et al. [133] have experimentally proven that the fragmentation rate of the agglomerates is inversely proportional to the total suspension volume.

This limitation constrains the scalability of ultrasonication. Because the acoustic intensity is inversely proportional to the probe area, a larger probe that one would be tempted using to increase the cavitation zone diameter, is in fact less efficient. A continuous flow system has infrequently been employed for other applications than nanoparticle dispersion (especially in food industry). A recirculation is allowed between a tank containing a large volume and a small flow cell where ultrasonication is applied (Figure 2.11). This showed interesting gain in energy and time [143, 144]. More expensive approaches are suggested such as to use several probes in series, a flow cell with multiple transducers working at different frequencies, or a barbell horn to achieve higher sound amplitude, employed either in batch or continuous flow modes [145-147]. However, whereas this last method should effectively allow to provide higher acoustic wave amplitude due to the probe shape, there are not much details about the overall efficiency (energy consumption, etc.). In addition, these scaled-up systems do not allow any inline validation which seems critical to assess when the nanoparticle dispersion process is achieved at an industrial

scale. Note that no reports specifically on CNC dispersion have been identified in the literature for such scaled-up systems.

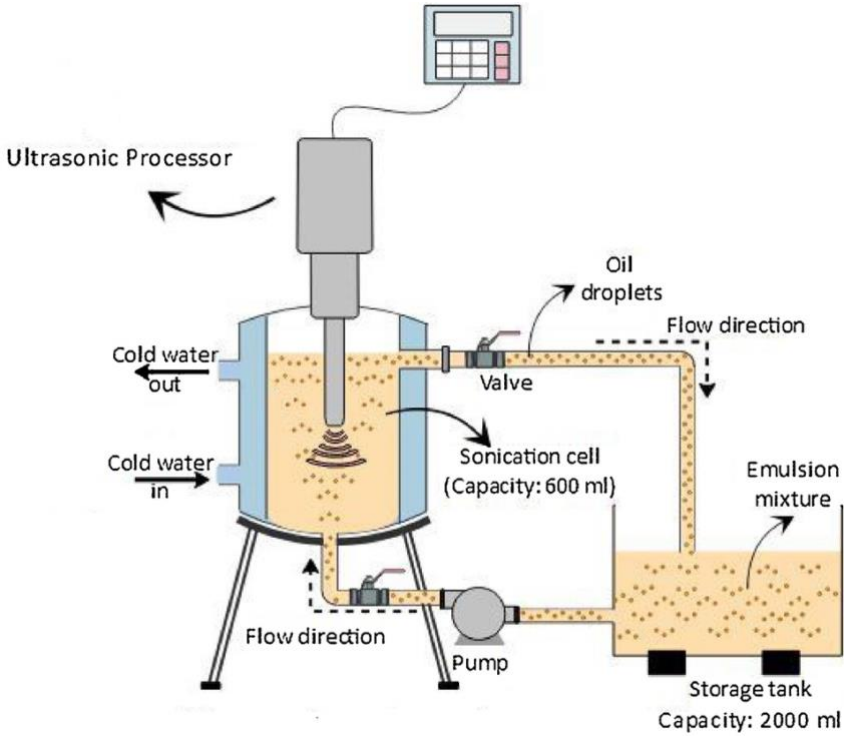

Figure 2.11: Recirculating flow ultrasonication for emulsion. Reproduced with permission from [143]

2.5.3 High-pressure homogenization

Another way to break agglomerates apart and obtain a well-dispersed CNC suspension is to use HPH. This technique forces a liquid through narrow nozzles at high-pressure (around $1.6.10^8$ Pa), inducing high-shear and cavitation [148]. This process has been widely exploited for cellulose extraction [25, 149-151] and emulsion preparation [152]. To the best of our knowledge, however, only a few research works have been led on nanoparticle dispersion with HPH [153-155]. This may be due to its infrastructure cost or energy consumption [156, 157]. Azoubel et al. [158] compared this technique with ultrasonication concluding that HPH was a more efficient method, being less time-consuming (10 min compared to 1h for 100 mL of a 0.5 wt% carbon nanotube suspension). While the process offers indeed an easy scale-up suitability, Azoubel's findings may highlight again the lack of knowledge needed to use the ultrasonication approach

optimally. Unfortunately, they do not report the ultrasonication energy to make a relevant comparison with the one applied in HPH (estimated ~16 $MJ.g^{-1}$).

2.5.4 Dispersion state validation

Several qualitative and quantitative methods may be applied to assess the dispersion state of CNC suspension.

Dynamic light scattering (DLS) gives information on the hydrodynamic apparent particle size of the CNCs. This technique measured the light intensity scattered by the particles affected by Brownian motion, which is proportional to their size via Stokes-Einstein relation [112]. However, it must be assumed that the CNCs are spherical. This limitation may be avoided using a multi-scattering device. With a polarizer and based on the rotational and translational coefficients, it is possible to estimate the length and diameter of the nanoparticle [159]. In “standard” DLS analysis, because of their orientation and high aspect ratio, neither the “real” particle size nor the particle size distribution can be quantified at the risk of overestimation. addition, the polydispersity of CNC suspensions is difficult to handle as the light scattered from smaller particles are screened by the larger ones [160]. Nevertheless, the apparent particle size allows characterizing qualitatively the dispersion state. To be reliable, the measurements must be carried out on suspensions at 0.025 wt%-0.05 wt% as lower or higher concentrations false the analysis [111].

Atomic force microscopy (AFM) or transmission electron microscopy (TEM) can provide quantitative information on CNC size and morphology. Recently, Campano et al. [161] defined rigorously different types of clusters according to their morphology with TEM. This helped them prove that with increasing ultrasonication time, the largest agglomerate types are fewer, while more clusters with shorter non-branched particles are obtained. Based on their work, the same conclusion was reported by Metzger et al. [162] who observed a decrease of the mean particle length and a narrower particle length distribution. Yet, these imaging techniques require the suspension to be dried, which may affect the original state [163]. It may be possible to perform TEM in a wet-cell, intended for fluid characterization, but this sample holder is not widely available [164].

UV-vis spectroscopy or turbidity measurements may also help define the dispersion state as long as the same protocol is used to compare different samples [165-167]. A higher transmitted intensity would be obtained for better dispersed suspension, though this must be compared with the pure solvent to ensure the absence of complete sedimentation. However, turbidity is also linked to other parameters than agglomeration. Thus, the results must be exploited cautiously and completed with another technique [111].

Asymmetrical flow field-flow fractionation (AF_4) coupled with multi-angle light scattering is a promising method that can overcome the limitation of the previous approaches. It allows defining the particle size distribution directly from the suspension [162, 163]. Similarly, Raman et al. [168] used an *in situ* focused beam reflectance measurement (FBRM) probe in a continuous flow apparatus to monitor particle size distribution. It may also give information on the particle texture. The FBRM probe emits a light whose reflected intensity is measured. The recording signal may then be processed to give the chord length measurements (time for the beam to cross the particle, divided by the beam's rotation speed), which may subsequently be linked to the particle size [169, 170].

The dispersion state plays an important role in the rheological behavior of a suspension. Compared to microscopy or DLS, rheometry presents the asset of requiring no dilution or drying, ensuring that the results are only owed to the suspension preparation method and the properties of the material itself. A better dispersion leads to a smaller hydrodynamic diameter, along with a smaller interparticle distance resulting in a lower viscosity [12, 65, 136, 171]. However, for highly concentrated suspensions (12 wt%), the viscosity increases again at rest over time. This may be due to a reorganization of the cholesteric domains [172]. In addition, a gel behavior is obtained for suspension containing agglomerates whereas the same concentration gives a three-region viscosity curve specific to a chiral nematic liquid crystal phase (see section 2.3.2) for a well-dispersed suspension [64].

Sulfated CNC dispersion state may also be characterized by their conductivity due to the charged surface. It was proposed that during hydrolysis, some ions remain trapped in the CNC agglomerates. When applying ultrasonication, the trapped ions may be released in the suspension, leading to a thinner electrical double layer and a higher conductivity [12, 58]. This ion release

theory was however refuted later, suggesting rather that the conductivity increases was due to faster diffusion of smaller particles and the availability of surface charges [162].

However, it must be noted that apart from the FBRM technique, which requires nonetheless some post-processing work, all these approaches imply a dispersion state evaluation performed separately from the suspension preparation. In other words, these are not in-line measurements.

2.6 Summary

Several important points have been highlighted in this literature review:

- To aim for industrial applications of CNCs, the whole process (dispersion and characterization) must be applicable at large scale and easy to perform. Only a few examples employing ultrasonication for higher scale may be found in the literature and are not used to disperse nanoparticles.
- While being widely exploited for nanoparticle dispersion, the key parameters of the ultrasonication technique are not fully understood. The numerous differences observed in the protocols applied in the literature have certainly important loss in terms of efficiency.
- Though rheometry is a powerful method to qualitatively assess CNC suspensions and their dispersion state without any post-treatment (-ultrasonication) modification, no work has been done on the homogeneity of the suspension. Using other strategies for this purpose that need either to dry or dilute the suspension may change its state. Furthermore, it conducts to particle size distribution rather than giving information on the suspension homogeneity.
- All dispersion state evaluation techniques require an additional step, either for the measurement itself or for post-processing. This may not be efficient for industrial applications.

CHAPTER 3 RESEARCH OBJECTIVES AND COHERENCE OF THE ARTICLES

3.1 Identification of the problem

CNCs are typically obtained from cellulose through sulfuric acid hydrolysis [28, 32]. They are then generally dried for subsequent use [41]. However, significant agglomeration is induced from this drying step, strong hydrogen bonds being formed between particles accompanied by important van der Waals forces [46, 47]. Before considering any applications with CNCs, their proper dispersion must be ensured. Ultrasonication is mostly used for this purpose. Based on cavitation, it provides enough energy to break agglomerates [12, 117]. Yet, important contradictions and information gaps regarding the operating parameters of this technique were highlighted in Chapter 2. However, a study on the influence of different sonication parameters requires a proper evaluation of the dispersion state. Several approaches have been identified in Section 2.5.4, such as microscopy, light scattering, or spectroscopy [111, 161, 166]. While qualitative analyses may be performed with these tools, their reliability is questioned [111, 160]. Most of them rely on dilution or require drying the dispersion prior to its characterization, which undoubtedly changes the dispersion state. On the other hand, rheometry is capable of providing valuable information about the CNC suspension [12, 64, 65]. Thus, this method must be fully exploited for a well-founded dispersion state evaluation. This understanding is also necessary to adapt the optimized sonication process beyond laboratory conditions. Indeed, to consider any application at industrial scale, the loss of ultrasonication efficiency for larger volumes must be circumvented [117, 133]. A continuous flow setup would be an interesting solution [143, 144], but one must know when the targeted dispersion state is reached. Keeping the idea of industrial application in mind, it is necessary to implement a measurement method that does not require any external tool or complex post-processing.

3.2 Research objectives

The main objective of this work is to obtain reproducible and validated well-dispersed CNC suspensions with ultrasonication at various scales. To answer this challenge, the following points must be addressed:

1. Understand the influence of the ultrasonication operating parameters on CNC dispersion to optimize its use for lab scale.
2. Evaluate the “true” dispersion state of CNCs suspension (with no drying or dilution steps).
3. Adapt ultrasonication for larger volumes with inline validation to aim for industrial applications.

3.3 Coherence of the articles

The first article, entitled “*Evidence-based guidelines for the ultrasonic dispersion of cellulose nanocrystals*”, published in Ultrasonics Sonochemistry [173] (Chapter 4), determines the optimal parameters that must be used to disperse CNCs. This work was entirely carried out in water, to facilitate the study. By combining numerical modeling, rheology and conductivity measurements, a dispersion index has been defined. It allows to find out the required energy, as well as the ultrasonication probe positioning to ensure a good dispersion in small volumes. This article aligns with specific objective 1.

The volume limitation of ultrasonication was also evidenced in this first article, but a preliminary study was needed to address this point. Thus, the second article named “*Rheological insights on the evolution of sonicated cellulose nanocrystal dispersions*” published in Ultrasonics Sonochemistry [174] (Chapter 5), aims to better understand the behavior of CNC suspensions during ultrasonication. Both liquid-like and gel-like behaviors were studied with different CNC concentrations. Rheology was the main tool used for this purpose. This article aligns with specific objective 2.

Finally, the third article, entitled “*A technique for the ultrasonic dispersion of larger quantities of cellulose nanocrystals with in-line validation*”, submitted to Chemical Journal Engineering (Chapter 6), proposes a semi-continuous setup that allows applying all results obtained from the previous articles while dispersing larger quantities of CNCs at larger volumes. Moreover, an inline measurement approach is employed, providing direct dispersion state validation. This article thus aligns with specific objective 3.

CHAPTER 4 ARTICLE 1: EVIDENCE-BASED GUIDELINES FOR THE ULTRASONIC DISPERSION OF CELLULOSE NANOCRYSTALS

Mélanie Girard, David Vidal, François Bertrand, Jason R. Tavares, Marie-Claude Heuzey. Evidence-base guidelines for the ultrasonic dispersion of cellulose nanocrystals. *Ultrasonics Sonochemistry*, 71 (2021), 105378. Submitted on 9 July 2020 and published online on 28 October 2020.

Abstract

Nanoparticles possess unique, size-driven properties. However, they can be challenging to use as they easily agglomerate - their high surface area-to-volume ratio induces strong interparticle forces, generating agglomerates that are difficult to break. This issue prevails in organic particles as well, such as cellulose nanocrystals (CNCs); when in their dried form, strong hydrogen bonding enhances agglomeration. Ultrasonication is widely applied to prepare CNC suspensions, but the methodology employed is non-standardized and typically under-reported, and process efficiency is unknown. This limits the ability to adapt dispersion protocols at industrial scales. Herein, numerical simulations are used in conjunction with validation experiments to define and optimize key parameters for ultrasonic dispersion of CNCs, allowing an operating window to be inferred.

Keywords: Ultrasonication; CFD; Multiphysics modeling; Dispersion; Suspensions; Cellulose nanocrystals

4.1 Introduction

Cellulose nanocrystals (CNCs) are bio-based rod-like nanoparticles with high mechanical strength, making them promising candidates for polymer reinforcement amongst other applications (e.g. barrier or optical films, coatings [175]). From a mechanical perspective, a wide range of values for their longitudinal modulus has been reported in the literature [18], averaged around 130 GPa. With a density of 1.6 $g.cm^{-3}$, their specific Young's modulus is around 85 $J.g^{-1}$, much higher than for steel or glass fibers (around 25 $J.g^{-1}$) and close to Kevlar [176]. When added to polymer matrices, CNC could form a stiff percolating network allowing the transfer of these unique mechanical properties. Moreover, the interfacial behavior between CNCs and the matrix

are playing and important role because of the reactivity of the CNC surface and its specific area [177]. However, such a network requires homogeneous dispersion. One reason for this is the higher aspect ratio obtained from well-dispersed particles, leading to higher percolating stiffness, because of stronger hydrogen bonding [178] and van der Waals forces [179, 180].

Usually, CNCs are extracted from purified cellulose fibers with sulfuric or hydrochloric acid (H_2SO_4 or HCl) to hydrolyze the amorphous part. Whereas HCl tends to lower dispersion ability on account of the lack of surface charges, the charged sulfate esters introduced during H_2SO_4 hydrolysis improve the dispersion of CNCs in water [31]. However, higher acid sulfate groups content will lead to a weaker thermal stability[39]. Zeta potential (ζ) measurements carried out by Yu et al. [181] confirm this behavior with ζ = -22.4 mV for CNCs extracted with H_2SO_4, compared to ζ = -12.2 mV with HCl, as a larger ζ value leads to a more stable suspension. Typically, a suspension in water is considered stable when $\zeta > \pm 30$ mV and partially stable when $\pm 10 < \zeta < \pm 30$ mV [182, 183]. However, the ζ measurement is only reliable for clear and diluted suspensions [112]. In addition, it may be more challenging compared to other nanoparticles to use usual models (ex: Smoluchowski's equation) because of the double layer relaxation and end effect of CNC [184]. Beyond surface charge, hydrolysis conditions (temperature, time, concentration) also impact the particle size [16, 185, 186]. CNCs are then neutralized and the counterion nature is impacting on the suspension (critical concentration for ordered phase, stability, redispersion ability, etc.) [38, 111].

For handling purposes, CNCs are typically dried through either freeze- or spray-drying. Whereas a loosely packed aerogel or a flake structure is obtained by freeze-drying (respectively at lower – below 3 wt% – or higher concentration [111]) with thicknesses in the nanometer range, spray-drying leads to spherical agglomerates. On top of having lower energy requirements, spray-dried CNCs are usually preferred for storage reasons; they also exhibit higher crystallinity and thermal stability [12, 41].

As CNCs are nanoparticles, their high surface area (~150-400 $m^2.g^{-1}$ [33, 87]) induces strong interparticle forces with an agglomerate strength around 10^4-10^9 Pa depending on primary particle size [46]. This agglomeration problem is shared with all nanoparticles because of their high surface area-to-volume ratio [187]. Due to these forces, dry powder forms strong

agglomerates that need an energetic process such as ultrasonication to allow homogeneous suspension in a medium. Ultrasonication has been widely used in the literature for dispersion, because it provides enough energy to break interparticle bonds (with an energy density of 10^6-10^8 Pa [188]). Compared to high-pressure homogenizers, which have also demonstrated efficiency for nanoparticle dispersion, ultrasonication is typically favored for smaller volumes [148], and thus is more common at the lab scale. Different configurations exist: ultrasonic baths or cup-horn sonicators offer indirect sonication (and hence lower effective energy levels), compared to ultrasonic probes [117] which are the ones used herein. Magnetic stirring is subsequently a very inefficient method for CNC dispersion [148]. However ultrasonication may also affect the CNC crystallinity, stressing the importance of a controlled protocol [189].

Ultrasonication is based on acoustic cavitation. Using the piezoelectric effect, electric current is converted to mechanical vibration, which generates a sinusoidal pressure wave. This leads to a series of compression (positive pressure) and rarefaction (negative pressure) regions in the medium. Vacuum bubbles are created by this mechanism, their size varying with the pressure: cavities are formed and grow under low pressure and are compressed at high pressure, absorbing a small amount of energy at each cycle. For low intensities, the bubbles oscillate according to the pressure cycle (without causing cavitation) [119]. At higher intensities, once a cavity has reached a critical size (170 μm in diameter at 20 kHz in water [119]), it can absorb a significantly higher energy amount during growth in a single cycle before imploding. Implosion occurs when the acoustic resonance frequency of the bubble matches the ultrasound frequency, defined by the Minnaert equation [190]:

$$Fa \approx 3 \qquad (4.1)$$

where F is the resonance frequency and a is the bubble radius. This process is called cavitation, leading to localized, very high energy release with temperatures and pressures exceeding 5000 K and 100 bars, respectively. De-agglomeration can be induced by two mechanisms: shock waves or “microjets”. Indeed, the shock waves generated by cavitation [119] are leading either to erosion or fracture of the agglomerates. Moreover, the localized implosion leads to “microjets” when the cavitation bubble collapses near a solid boundary [119, 120]. This second phenomenon can be detrimental for the material integrity of a wall or vessel but can improve mixing or particle

de-agglomeration. However, it cannot damage individual particles as entities smaller than 200 μm cannot be affected by the jet [120]. Thus, for smaller entities only the first mechanism is occurring.

While ultrasonic probes are efficient and widely used tools to break CNC or other nanoparticle agglomerates, it remains difficult to find clear protocols to achieve a uniform dispersion consistently. Currently, very few details are given in articles when authors describe their methodology for dispersion (e.g. [52, 191, 192]). Beuguel et. al [12] investigated the impact of energy and power applied to CNC suspensions to identify the most pertinent operating values. They concluded that an energy threshold of 10,000 $J.g^{-1}$ at a power of 90 W will lead to good dispersion without any agglomerates. However, this neglects any geometric or volume effects. Indeed, depending on the volume of fluid one is trying to homogenize, the guidelines they provide do not always lead to the expected result. Figure 4.1 illustrates two cases obtained with ultrasonication at 90 W using 10 $kJ.g^{-1}$: a 20 mL suspension and a 200 mL suspension, both containing water with 3 wt% CNC. In the smaller beaker, this energy dose is sufficient to form a translucent suspension with a blueish tone, whereas the larger volume still contains agglomerates. Thus, ultrasonication time and power are not the only parameters to consider. The mixing system configuration (beaker size, probe position) as well as the medium specification (concentration, volume, temperature, density, viscosity, etc.) must also be taken into account to achieve a homogeneous and reproducible dispersion.

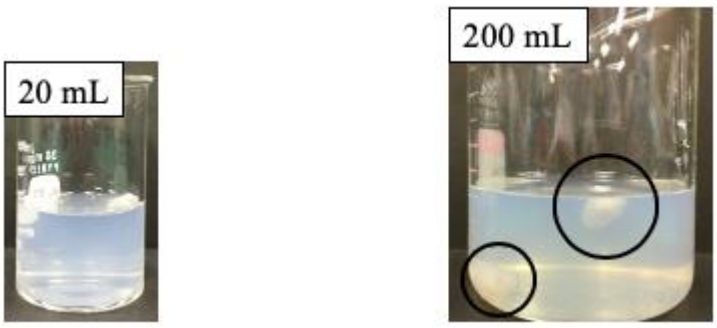

Figure 4.1: 3 wt% CNC suspension in water ultrasonicated using 10 $kJ.g^{-1}$ at 90 W in 20 mL (left) and 200 mL (right). The encircled areas highlight remaining CNC agglomerates.

Herein, we develop an evidence-based approach to efficiently use ultrasonication for nanomaterial dispersion, using a combination of experiments and simulations. To our knowledge,

no study has been carried out regarding the optimized use of an ultrasonic probe, considering all experimental conditions (set-up, medium and probe). This gap in knowledge is one of the key factors that limit the use of ultrasonication to the dispersion of small, lab-scale volumes. Additionally, industries would need to adapt laboratory protocols by trial and error, which is prohibitively time-consuming and costly. It is our hope that this methodical approach to dispersion could be generalized to all nanoparticle types to prevent agglomeration and facilitate industrial uptake.

The numerical simulations carried out in this work, with the objective of modeling the ultrasonication probe's effect on mixing, are built upon the foundational work of previous authors. Ayar et al. [131] visualized the influence of the tip diameter and power applied in a liquid aluminum dispersion and compared it with a water dispersion. Rubinetti et al. [129, 130] numerically solved the acoustics and fluid dynamics coupled together in a beaker, with experimental validation for further studies with several fluids. Louisnard [126, 127] also modeled the cavitation bubble structure relying on bubble dynamic equations. However, a common feature of all this simulation work is that it does not seek to optimize dispersion or mixing but only focuses on fundamental understanding without any direct applications.

In the present work, the ultrasonication modeling methodology, leaning on the solution of a coupled problem between a steady state form of the wave equation and the Navier-Stokes equations, is detailed (Section 4.2), along with the experimental strategy used for numerical validation. Several cases using different ultrasonication parameters are compared both numerically and experimentally (Section 4.3). The dispersion state is studied through the calculation of the medium velocity field and the resulting nanoparticle motion trajectories, and is confirmed by conductivity and viscosity measurements, allowing the formulation of a sonication protocol and operating windows (Section 4.4).

4.2 Methodology

All simulations and experiments performed were based on a 12.7 mm probe (VCX500, Sonics & Materials) operating at 20 kHz. To identify the parameters that play a significant role in CNC dispersion, this work focused on modeling a simplified ultrasonication system using the

finite element COMSOL Multiphysics solver (version 5.4). This was then validated by employing conductivity, particle size and viscosity analyses.

4.2.1 Numerical modeling

The reference ultrasonication set-up was modeled in 3D using a cylindrical domain to represent the whole beaker volume (60 mL), in which a smaller solid cylinder was introduced from the top to account for the submerged ultrasonic probe (Figure 4.2A). For the purpose of the study, dimensions of the beaker and probe position (axial and depth) were varied. The different configurations studied in this work are illustrated in Figure 4.2, with Case A being the reference configuration, and are characterized by the following ratios of characteristic lengths:

- *h/H*, where *h* is the probe depth immersed in the suspension and *H* the suspension height in the beaker;
- r_0/R, where r_0 and *R* refer respectively to the probe and the beaker radii;
- *(R-r)/R*, where *r* is the axial position from the beaker center.

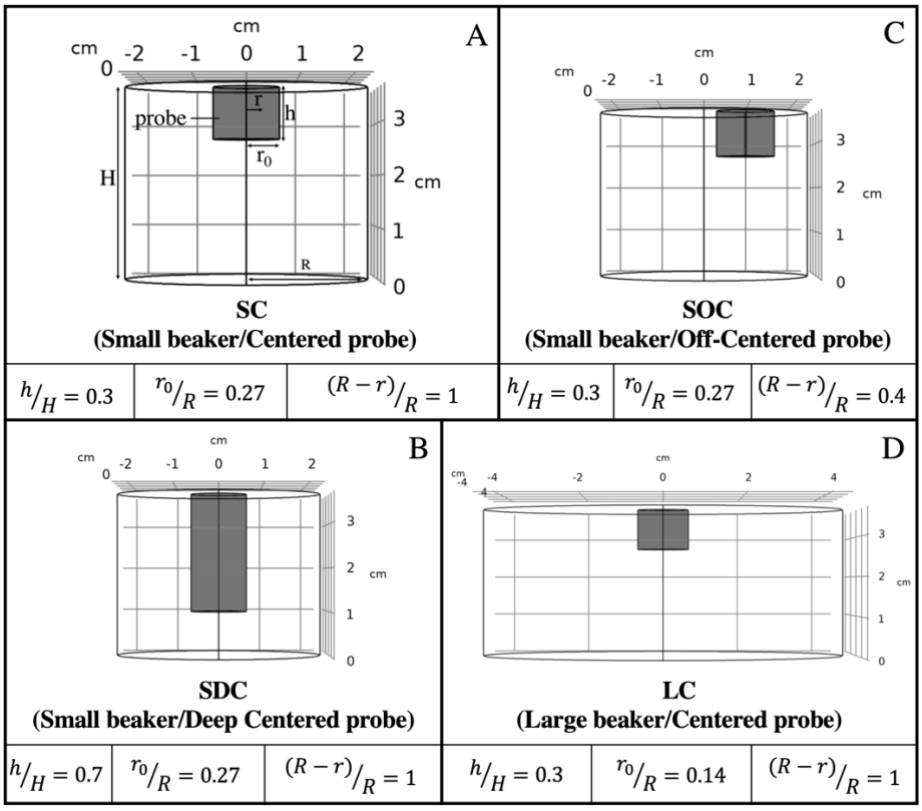

Figure 4.2: 3D domains modeling the different studied configurations of the ultrasonication probe in a beaker (A: Small beaker/Centered probe, B: Small beaker/Deep Centered probe, C: Small beaker/Off-Centered probe, D: Large beaker/Centered probe)

Acoustic wave propagation and the resulting fluid flow was modeled through the solution of a one-way coupled problem involving the Helmholtz and Navier–Stokes equations using respectively the acoustic and fluid flow modules of COMSOL. The different steps of the numerical modeling along with the link between each step are reported in Figure 4.3 and detailed in the following paragraphs.

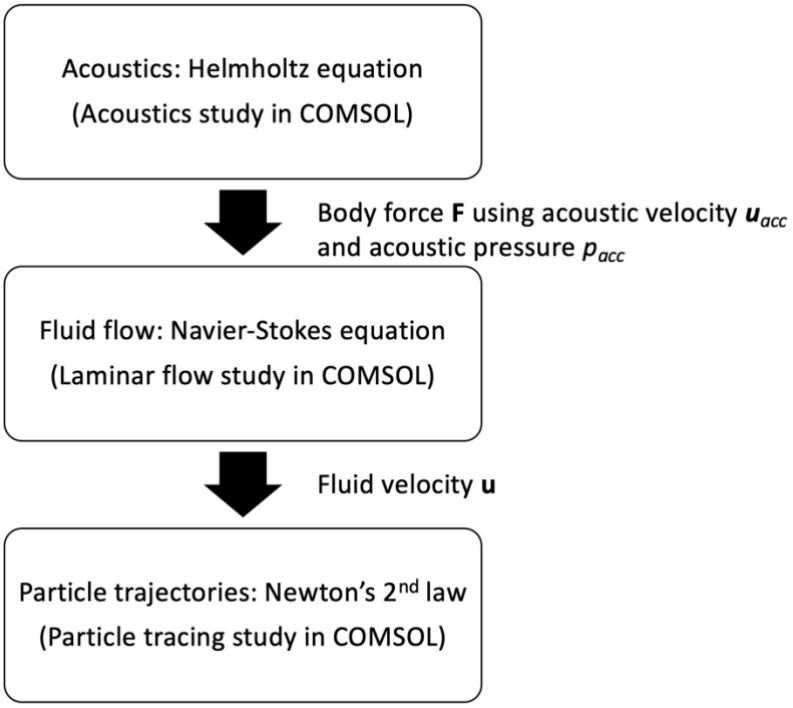

Figure 4.3: Modeling steps.

4.2.1.1 Fluid properties

The aim of the simulation was to model CNC suspension in water. Thus, for every modeling case, the suspension fluid was approximated as a Newtonian fluid, the properties of which were taken as those of water (density, sound velocity) except for the viscosity. Indeed, a higher viscosity was used to account for CNC addition [12, 64]. For a given concentration, the viscosity was determined by combining rheology measurements and numerical modeling. From a simulation with water only, an average shear rate in the active zone was determined. Subsequently, the corresponding viscosity for the suspension was measured at the identified shear rate with a rheometer (Anton-Paar, MCR502). This approximation is possible as a plateau is observed in the considered shear rate range in function of the viscosity. These results are reported in Section 4.3.3.3 giving 10 mPa.s for a 3 wt% CNC suspension. The studied concentration was low enough to keep the density the same as water, despite the change in viscosity. Moreover, the flow was assumed to be isothermal as the beaker temperature was kept more or less constant by means of an ice bath during the corresponding lab experiments.

4.2.1.2 Helmholtz equation

First, the Helmholtz equation was solved to obtain the pressure field in the medium. This equation, a steady state form of the wave equation, is defined as follows:

$$\nabla^2 \mathbf{\Pi} + k^2 \mathbf{\Pi} = \boldsymbol{a_0} \tag{4.2}$$

where $\mathbf{\Pi}$ is the pressure field (static pressure) defined by $\mathbf{\Pi} = p_{acc}\boldsymbol{I}$ and k may be formulated as:

$$k^2 = (\omega/c - i\alpha)^2 \tag{4.3}$$

with ω the angular wave frequency, c the sound velocity in the medium and α the attenuation coefficient. In addition, a_0 in Eq. (4.2) is an acceleration applied as an external source term at the surface of the probe to generate an acoustic wave at this boundary given by:

$$a_{0z} = -4\pi^2 {f_0}^2 A \tag{4.4}$$

where a_{0z} is the acceleration in the z-axis, f_0 and A are respectively the ultrasound frequency and amplitude (here $f_0 = 20$ kHz as it corresponds to the frequency of the ultrasonication device in our experiments), and A may be calculated through the following equation [193]:

$$P = \frac{1}{2}\rho c A^2 S (2\pi f_0)^2 \tag{4.5}$$

where P is the effective acoustic power, ρ is the medium density and S is the probe surface area.

The sound wave attenuation is defined by:

$$I_z = I_0 e^{-2\alpha z} \tag{4.6}$$

where z is the distance from the probe, I_z is the corresponding intensity at position z and I_0 is the probe intensity given by:

$$I_0 = P/S \tag{4.7}$$

and α is the attenuation coefficient given by:

$$\alpha = {(2\mu\omega^2)}/{(3\rho c^3)} \tag{4.8}$$

in which μ is the medium viscosity.

4.2.1.3 Navier-Stokes equations

Then, Navier-Stokes equations were solved for a Newtonian medium at steady state to model the corresponding laminar flow (with the Reynold number lower than 100) for an incompressible medium. Knowing that the continuity equation may be defined by:

$$(\nabla . \boldsymbol{u}) = 0 \tag{4.9}$$

where $\boldsymbol{u}$ is the fluid velocity, the Navier-Stokes equation may then be formulated by:

$$\rho(\boldsymbol{u} \cdot \nabla)\boldsymbol{u} = \nabla[-2p\mathrm{I} + \mu((\nabla \boldsymbol{u}) + (\nabla \boldsymbol{u})^{\mathrm{T}})] + \boldsymbol{F} \tag{4.10}$$

where p is the fluid pressure (static and dynamic) and $\boldsymbol{F}$ is a body force (source term applied on the whole domain), coupling in a one-way manner the Navier-Stokes and Helmholtz equations [130], and which may be calculated as:

$$\boldsymbol{F} = {}^1\!/_2\, Re[\rho_e^* \omega \boldsymbol{u_{acc}}] + {}^1\!/_2\, \rho_e \left(Re\left[u_x^* {\partial \boldsymbol{u_{acc}}}/{\partial x}\right] + Re\left[u_y^* {\partial \boldsymbol{u_{acc}}}/{\partial y}\right] + Re\left[u_z^* {\partial \boldsymbol{u_{acc}}}/{\partial z}\right]\right) \tag{4.11}$$

where ρ_e and ρ_e^* are real and complex conjugate of density perturbation and u_{accx}^*, u_{accy}^*, u_{accz}^*, the complex conjugates of velocity components in Cartesian coordinates at a specific location and only the real portion of each term is considered. Scalar ρ_e is being calculated from the Helmholtz equation and may be obtained by:

$$\rho_e = {p_{acc}}/{c^2} \tag{4.12}$$

4.2.1.4 Effective power

The effective acoustic power *P* takes into account the power transmitted to the fluid, as opposed to the power set point shown on the ultrasonication device that convolutes electrical,

mechanical and heat losses. The power effectively transmitted to the medium was determined using a calorimetric method suggested by Taurozzi et al. [117], in which the temperature increase of the ultrasonicated medium was measured using a temperature probe leading to the effective acoustic power P given by:

$$P = m\, c_p \frac{dT}{dt} \tag{4.13}$$

where m is the mass of the medium, c_p its specific heat capacity, T the temperature and t the time.

Calorimetric experiments were conducted in an adiabatic beaker to avoid heat losses (contrary to the dispersion experiments where the beaker is cooled with an ice bath) and the medium used was water. Different power set points were tested, and the results can be found in Figure A.1. It is worth mentioning that approximately only a small amount of the set point power is effectively transmitted to the fluid. Experimental and simulation work herein was conducted at an amplitude of 3.10^{-6} m and a set point power of 65 W, corresponding to an effective power P of 15 W. This power was chosen to obtain a balance between ultrasonication time and transmission efficiency. In any case, for a constant energy, changing the power would not affect the suspension state as presented in Figure A.2.

4.2.1.5 Mesh

The mesh size was automatically generated by the Fluid Flow module from COMSOL using linear elements, and a mesh refinement sensitivity analysis was carried out to verify the resulting model convergence. For the conditions presented in Figure 4.2A, the model was solved with finer and finer meshes until the solution did not change by more than 1%, and the finest mesh was retained for the entire study. Moreover, the maximum element size was set to ensure that there are at least 5 elements per wavelength λ (at 20 kHz, $\lambda = 7.5$ cm).

Based on this methodology, velocity fields were calculated and compared for each configuration presented in Figure 4.2 using the Fluid Flow module for a viscosity of 10 mPa.s. Then, tracer trajectories were computed (with the density of the tracer $\rho_p = 1540$ kg.m^{-3}) and used to estimate dispersion state. To study the influence of viscosity, a higher viscosity of 20 mPa.s was also tested for the best configuration. These results are presented in Section 4.3.1.

4.2.1.6 Boundary conditions (Figure 4.4)

The boundary conditions used at the air-liquid interface at the top of the beaker were a sound soft boundary condition, meaning that the acoustic pressure was zero, and combined with a zero normal stress condition for the fluid flow. For every other domain boundary, a combination of sound hard (normal derivative of the pressure is zero) and no-slip (velocity is zero) boundary conditions were used, and a zero normal component of the acceleration was assumed.

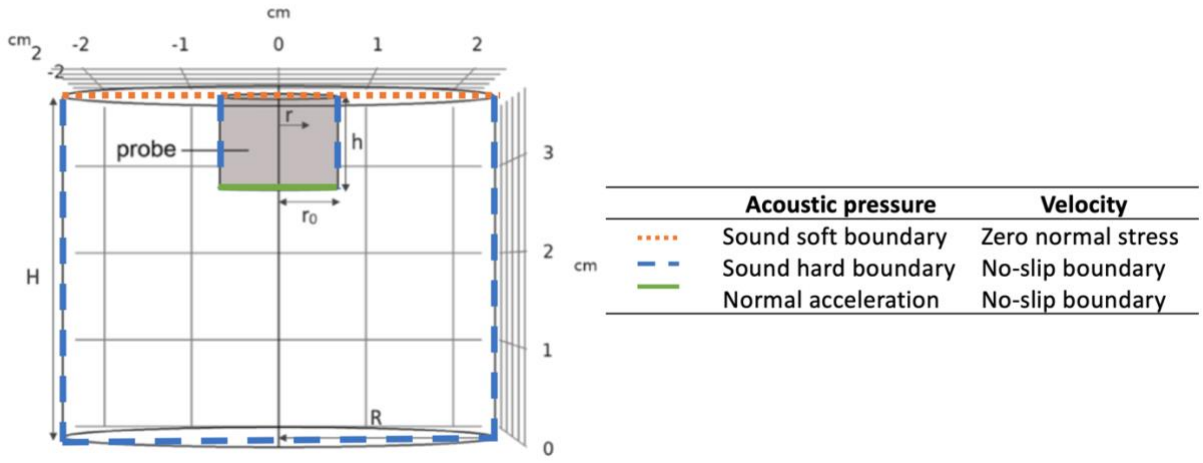

Figure 4.4: Boundary conditions

4.2.1.7 Tracers

Finally, from the steady-state flow pattern, tracer trajectories were computed to visualize nanoparticle pathways over time by calculating the drag force due to the fluid flow such as:

$$\boldsymbol{F} = {}^{18\mu}\Big/_{\rho_p d_p^2}\, m_p(\boldsymbol{u} - \boldsymbol{v}) \qquad (4.14)$$

where m_p, ρ_p and d_p are respectively the particle mass and $\boldsymbol{v}$ is the particle velocity (which is zero a t=0). Tracers presented a density of 1540 kg.m^{-3} and a radius of 26 nm, close to the properties of CNC [12] (using a spherical shape approximation, with an equivalent volume to the CNC value). They were initially released homogeneously in the beaker (except for the validation of the suspension preparation in Section 4.3.2) and assumed to be solely affected by gravity and drag forces. The number of tracers remained approximately constant and arbitrarily fixed at 890 ± 10 % for the 60 mL volume, for every case (the uncertainty is due to geometrical

constraints). One may reasonably assume that Brownian diffusion and electrostatic effects were negligible with respect to the flow motion. Indeed, the Peclet number, , $Pe = {uL}/{D} \gg 1$, where u is the flow velocity, L is the characteristic length and D is the diffusion coefficient (in the order of 10^{-12} $m^2.s^{-1}$ [159, 194]), and $F_{el} \ll F_{adv}$, where F_{el} is the electrostatic force and F_{adv} is the force due to advection.

4.2.1.8 Active zone

An active cavitation zone in which the energy is high enough for breakage of nanoparticle agglomerates by cavitation was defined manually to determine the process efficiency. Lauterborn et al. [121] have defined a cavitation threshold pressure for water between 0.8 and 3 bar at 20 kHz so it is possible to calculate the corresponding intensity using the following equation:

$$I_{cav} = {|p_{cav}|^2}/{(2\rho c)} \quad (4.15)$$

where I_{cav} and p_{cav} are respectively the cavitation threshold intensity and pressure. Knowing the sound attenuation, one can deduce a zone where $I_x > I_{cav}$, which defines the active cavitation zone, probe and fluid-dependent only. The bubble zone has been previously described by Moussatov et al. [125] as conical, but here, for the sake of simplicity, it was approximated by a cylindrical zone having the same diameter as the probe. This assumption has a minimal effect on the following findings presented herein. To avoid any overestimation of the cavitation zone depth, the threshold pressure was set to its maximum value, i.e. $|\Pi_{cav}|$ = 3 bar. This cavitation zone is an approximation, since the collapse of the cavitation bubbles generates turbulence and shock waves capable of breaking agglomerates; this was not directly accounted for in our simulations because of the inherent complexity of the phenomenon.

In the numerical simulations, the tracers in this corresponding cylindrical active zone at a given time were counted. A dispersion index D_i could then be deduced through the following equation:

$$D_i = {n_{cav}}/{n_{tot}} \quad (4.16)$$

where n_{cav} is the particle number in the cavitation zone and $n_{tot}$is the total number of particles launched. This ratio describes the dispersion efficiency of the process for a given set of

parameters and is intended to be maximized. It normally increases over time and thus, for every case, it was evaluated over the same time period (i.e. 200 s) required by the actual ultrasonication experiments to transfer 7 $kJ.g^{-1}$ of energy to the suspension at a 15 W effective power (65 W setpoint power) for the small beaker (60 mL).

4.2.2 Experiments

CNCs used in this work were supplied by Celluforce. They are sulfated CNCs neutralized by sodium hydroxide, with 3.4 sulfate half ester groups per 100 anhydroglucose rings corresponding to a sulfur over carbon S/C atomic ratio around 0.0057 [12] and a final crystallinity around 80 % [35]. Sulfate half ester groups result from the hydrolysis step used to extract CNC from cellulose fiber and from removing lignin, hemicellulose and impurities. The CNCs have subsequently been spray-dried. They were used in this work as-received in powder form, with a density of 1540 $kg.m^{-3}$. Ultrasonication is not employed by the supplier (Celluforce) during CNC production.

A rigorous protocol was implemented for suspension preparation to ensure reproducibility. CNC dispersions in milli-Q water (conductivity σ = 2 $\mu S.cm^{-1}$) were prepared by adding half of the water amount, the prescribed amount of CNC and then the remaining water, in this order. This methodology is justified from a modeling point of view, as will be seen in results reported in Section 4.3.2. This preliminary suspension was then pre-mixed for 30 s with a vortexer (Mini Roto S56 – Fischer Scientific – 2800 rpm). These steps prevent local gelation. The dispersion was ultrasonicated for a specific time in an ice bath as heating may desulfate the CNCs [195], avoiding any manual shaking. If needed, ice was added to the bath during ultrasonication to avoid any temperature fluctuation or beaker displacement due to ice melt. One may note that continuous sonication has been applied to avoid any additional effects imparted by pulsed operation (a method often used to prevent the probe from overheating). The time between ultrasonication and the subsequent analyses was also recorded and kept constant and carried out in the next four hours.

The same cases as those presented in Figure 4.2 were studied experimentally: the small beaker/Centered probe case (SC), the small beaker/deep centered probe case (SDC) and the small beaker/off-centered probe (SOC). The CNC concentration was 3 wt% (1.95 vol%) unless

mentioned otherwise. The large beaker case (LC) was dropped for lab experiments, as it was identified as the worst-case scenario in the simulations (Section 4.3.1).

The dispersion state was assessed by electrical conductivity measurements, particle size analyses and rheology study.

CNCs present ionic charges on their surface because of the sulfate half ester groups. When CNCs agglomerate, these charges are mostly hidden or trapped. However, they are released during sonication as the flocs break down into individual particles, as explained by Beck et al. [58]. This behavior generates a proportional increase in the conductivity value, which can be used to evaluate the dispersion state. Thus, the electrical conductivity of the suspension was measured directly after ultrasonication using a conductivity meter from Hanna Instruments (HI98303). As demonstrated by Beuguel et al. [12], E = 10,000 J.g^{-1} and P_s = 90 W are required to obtain a homogeneous CNC dispersion in a 20 mL beaker. Under these "best case" conditions and using numerical modeling results to position the probe optimally, several CNC suspensions containing different concentrations (1.5 wt%, 3.2 wt% and 5 wt%) were ultrasonicated and conductivity was measured to create a calibration curve. These resulting conductivity values were then assumed to be the target for any other experimental conditions at a given concentration for complete CNC dispersion.

The particle size distribution was measured using a laser particle sizer (EyeTech, Ankersmid). Indeed, while conductivity is a simple way to evaluate the dispersion state of a suspension, a more precise technique was required to confirm that CNCs are individualized. Contrary to electron microscopy (SEM, TEM), which would require extensive sample preparation including drying the sample, or DLS (dynamic light scattering) where the sample is diluted, the EyeTech laser technique could be used directly with a raw suspension. The rotating beam could deduce the particle size by measuring the duration of obscuration, without the need for physical or optical data, or knowledge of particle shape. The drawback is that this technique is not sensitive to particle diameters smaller than 0.1 μm. Thus, it is not possible to observe individual CNCs but it is relevant to highlight ultrasonication parameter influence. To support this technique, DLS measurement have been carried out on 0.2 wt% suspensions (obtained by diluting every suspension) at 25 °C using a Malvern Zetasizer Nano-ZS (DTS1070 cell). The refractive and absorption indices were set to 1.59 and 0.01, respectively (based on [12] and

following the recommendations of the instrument manual). All measurements were obtained using an average of 3 successive measurements of 15 runs each. However, the DLS technique was used as a second analysis as it may not be accurate for a polydisperse non-spherical nanoparticle distribution (according to the manufacturer and [196]).

Rheology was also used to characterize the dispersion efficiency. A double Couette flow geometry was used for this purpose on an Anton-Paar rheometer (MCR502). Sampling was carried out using a syringe, thereby excluding large agglomerates (greater than 2 mm). This sampling method allowed us to measure viscosity locally, considering that the local viscosity of a well-dispersed suspension is the same no matter the sampling position (refer to Section 4.3.3.3). Samples were pre-sheared for 100 s at 10 s^{-1} before every test, to remove air bubbles in the sample, followed by a 180 s rest time. The viscosity as a function of shear rate was measured going from high to low shear rates. To highlight the fact that a bad dispersion leads to fluctuations in the viscosity values, the relative standard deviation, which is the standard deviation of three samples divided by the average viscosity value, was also calculated.

Validating both conductivity and rheology results with a separate, never-before used probe, no discernable effects from possible metal particles coming from the probe during ultrasonication were observed. Indeed, the conductivity of a 3 wt% CNC suspension is 332 ± 10 $\mu S.cm^{-1}$ with the probe mainly used in this work compared to 441 ± 10 $\mu S.cm^{-1}$ with a never-before used probe. The rheology results are reported in Figure A.3.

4.3 Results and discussion

The results obtained with the methodology presented in the previous part are reported in this section. The numerical results are first discussed for all the cases introduced in Section 4.2. After confirming that the suspension preparation was optimal, they are validated against experimental data. These results altogether lead to an operation window that provides guidelines for the homogenization of CNC dispersions in water.

4.3.1 Numerical modeling

The velocity field obtained for each of the cases illustrated in Figure 4.2 are shown in Figure 4.5. The homogeneity can be assessed by the velocity values and the corresponding color

fringes. The dark blue hatched areas indicate very low velocities (velocity magnitude lower than 2 $mm.s^{-1}$). Agglomerates originally in these areas have a low probability of transit towards the cavitation zone where they can be broken; these areas behave as dead zones. If the volume of these dead zones is large, the homogeneity is low. In addition, in these zones, the shear is lower leading to a less efficient agglomerate breakage. The dispersion index, as defined by Equation (4.16) and calculated with a precision of 1 %, serves as an indication of mixing efficiency (these two quantities are reported in Table 4.1). The precision has been determined by slightly changing the initial position of the particles four times and calculating the standard deviation of the resulting dispersion index. The dispersion index over time is plotted in Figure A.4. The reference case (SC, 60 mL, Figure 4.5) was composed of 51 % dead zones and yielded a dispersion index of 75 %.

Instinctively, one might think that placing the probe deeper in the beaker would increase the mixing efficiency due to more powerful reflected sound waves. Indeed, the area receiving higher velocity values is broadened in width (SDC, Figure 4.5). However, the mixing efficiency is lower due to the occurrence of dead zones between the beaker wall and the probe, as sound waves are fading therein. The volume ratio of these dead zones increased to 65%, despite a similar dispersion index (77%). This can be explained by the fact that particles are not motionless in dead zones, yet they move very slowly. Also, the dispersion index D_i is indicated after 200s, although it increased more slowly for the SDC case than for the SC case.

Another parameter of interest is the axial position of the probe. It is indeed common practice to off-center impellers to improve efficiency in unbaffled systems provided with radial or axial flow impellers [197]. Figure 4.5 (SOC) confirms this behavior results in more efficient mixing (only 20 % of dead zones) than the reference case, with a globally higher velocity. Accordingly, the dispersion index increases up to 95 %. Moreover, the fluid accelerates near the beaker side wall close to the probe, which this may be explained by the occurrence of sound waves reflecting on this wall, implying more efficient mixing in this area.

The larger beaker (LC, Figure 4.5) had a proportion of dead zones (51 %) similar to the reference case, but these are less well distributed in the total volume of the beaker. Thus, the dispersion index is much lower (29 %). The beaker size was indeed previously shown in Figure 4.5 to be a critical parameter for a 3 wt % CNC suspension. The higher velocity values observed

below the probe are attributed to the fact that the flow is less affected by the no-slip viscous boundary layer than a narrower beaker.

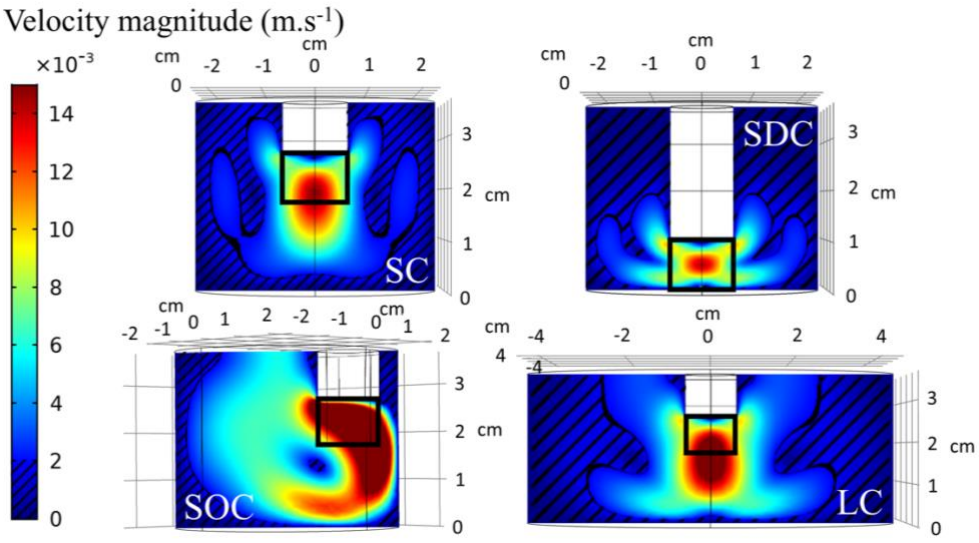

Figure 4.5: Velocity field comparison of different beaker-probe configurations for a simulated CNC suspension (i.e. water with η = 10 mPa.s) obtained by numerical simulation: SC, SDC, SOC, LC. The rectangle below each probe pictures the active zone as defined in Section 4.3.1. Hatched areas represent dead zones where the velocity is lower than 2.10^{-3} m.s^{-1}.

Table 4.1: Dead zone volume ratio and dispersion index calculated from Equation (4.16) for each case. (See Section 4.2.1 for active zone definition)

Case at 10 mPa.s	**Dead zone volume ratio (%)**	**D_i (% $\pm$1%)(active zone depth: 0.96 cm)**
Reference (SC) (60 mL)	51	75
Deep probe (SDC) (60 mL)	65	77
Off-centered probe (SOC) (60 mL)	20	95
Large beaker (LC) (200 mL)	51	29
Case at 20 mPa.s		(active zone depth: 0.48 cm)
Off-centered probe (SOC)	33	66

Given the sensitivity of suspension viscosity to CNC concentration, it is pertinent to study the effect of the viscosity for the best configuration (SOC, Figure 4.6). Doubling the viscosity

(i.e. 20 mPa.s in Figure 4.6 - right) leads to much lower velocity values than in the 10 mPa.s case (Figure 4.6 - left). This is due to severe attenuation of the impact of sound waves on the flow field as a result of viscous dissipation. Consequently, the dead zone volume ratio increased from 20 % to 33 % and the dispersion index decreased from 95 % to 66 % (Table 4.1). Note that the cavitation zone is also reduced at higher viscosity due to more important sound attenuation (Equations (4.6) and (4.8)) This indicates that the mixing efficiency of CNC suspension would decrease with increasing concentration. This will be emphasized by the gelling phenomenon which can be observed above 5 wt%[64].

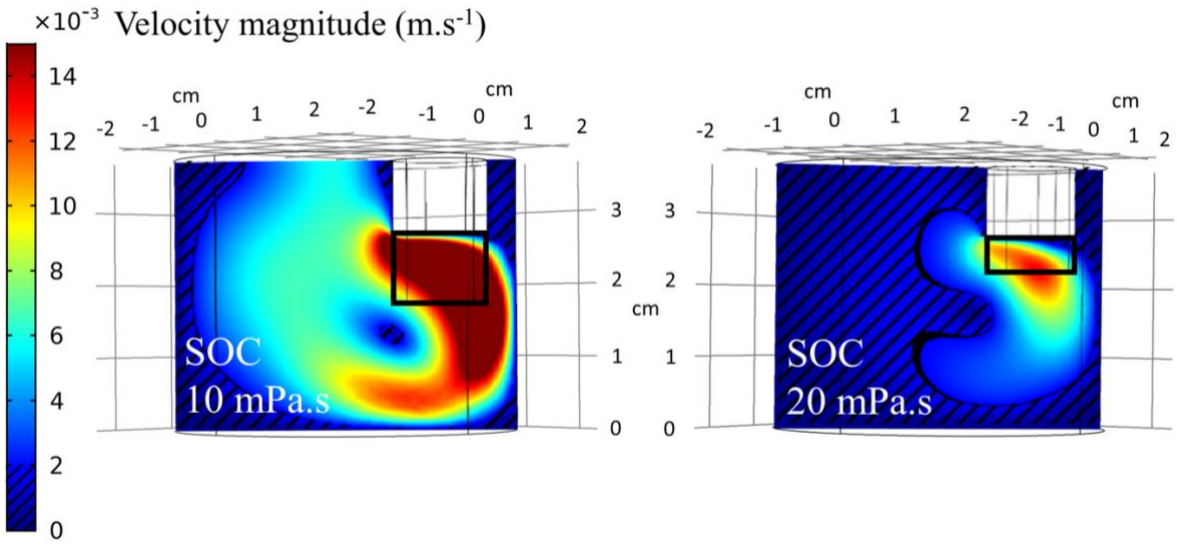

Figure 4.6: Velocity field comparison for a simulated CNC suspension of different viscosity for the SOC configuration obtained by numerical simulation: (left) η=10 mPa.s, (right) η=20 mPa.s. The rectangle below each probe pictures the active zone as defined in Section 4.3.1. Hatched areas represent dead zones where the velocity is lower than 2.10^{-3} $m.s^{-1}$.

4.3.2 Suspension preparation validation

Before assessing the numerical results with the experimental data, it is important to confirm that the rigorous protocol used to prepare the CNC suspensions as introduced in Section 4.2.2 is optimal. For this purpose, three common preparation cases were compared numerically using the tools developed in Section 4.3.1. The aim is to study the influence of the initial positions of the nanoparticles, which depends on how water and nanoparticles are

introduced. The locations of the nanoparticles along with the underlying preparation steps are presented in Table 4.2. Case II corresponds to the protocol used to prepare all suspensions. The dispersion index was calculated in all cases for a 10 mPa.s corresponding to a 3 wt% CNC suspension. We must keep in mind that when CNC concentration is higher than 5 wt%, a gel is obtained [64]. This might happen locally before dispersion occurs. When CNC particles collide with the beaker wall, they may easily stick to it. The numerical model does not account for this gelling phenomenon, meaning that D_i for case I was overestimated. One can notice that Case II exhibits the best D_i.

Table 4.2: Preparation procedure (D_i calculated for a 10 mPa.s suspension)

Case	Location of the nanoparticles in the beaker	Step 1	Step 2	Step 3	D_i (%)
I	At the bottom	Nanoparticles	Water	-	86
II	In the middle	½ water	Nanoparticles	½ water	99
III	On top	Water	Nanoparticles	-	96

4.3.3 Experimental validation

Probe position, beaker size and fluid viscosity were highlighted as important parameters through numerical simulations (Section 4.3.1). The modeled cases were accordingly reproduced experimentally at different CNC concentrations in water, to assess dispersion homogeneity. The ultrasonication power depended on the experiment, and the effective value is specified herein along with the set point value in brackets. It should be noted that expressing the energy in $J.g^{-1}$ may not be appropriate as it was shown in Section 4.3 that the volume also influences ultrasonication efficiency. Therefore, the normalized energy density will be subsequently expressed in $kJ.g^{-1}.L^{-1}$ (normalizing the energy per gram of CNC and liter of solvent).

4.3.3.1 Conductivity

To build a calibration curve under the best-case conditions, based on simulation results (Section 4.3.1), the probe was placed at h/H = 0.3 and r = 0 (the beaker being too small to allow for off-centering). Under these conditions, three CNC concentrations were ultrasonicated for E = 500 $kJ.g^{-1}.L^{-1}$ (10 $kJ.g^{-1}$ in 20 mL [12]) and conductivity was measured (Figure 4.7). As an

optimized dispersion state is assumed in these conditions, this curve was used to provide target values for other experimental conditions.

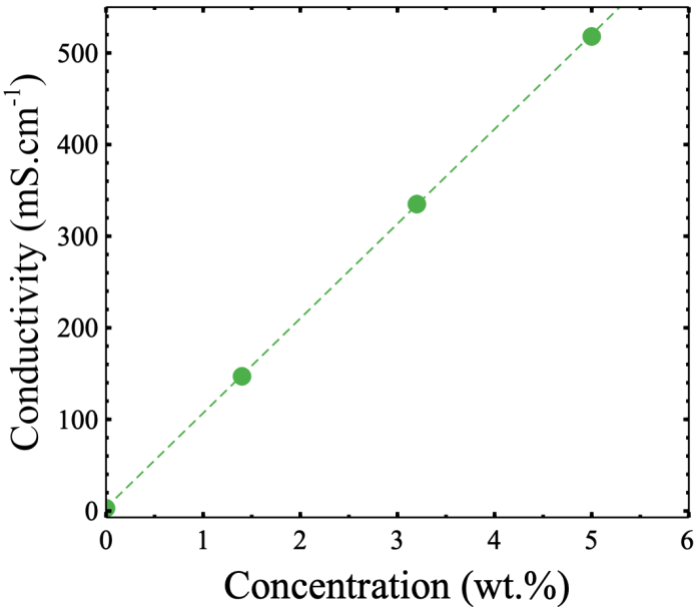

Figure 4.7: Conductivity of CNC ultrasonicated suspensions at different concentrations (V = 20 mL, h/H = 0.3, E = 500 $kJ.g^{-1}.L^{-1}$, P = 33 (90) W, (R-r)/R = 1). (The standard deviation is ± 10 $mS.cm^{-1}$).

Figure 4.8 plots the measured conductivity (σ) as a function of the normalized energy density (or ultrasonication time) in a 3 wt% CNC suspension, for three probe positions (SC, SDC, SOC). As a reference, a conductivity target of 334 ± 10 $mS.cm^{-1}$ was obtained from Figure 4.7. The visible agglomerate threshold, the limit at which the suspension becomes visibly clear, is also indicated. Visible agglomerates disappear sooner around 117 $kJ.g^{-1}.L^{-1}$ in the off-centered case (SOC), compared to 250 $kJ.g^{-1}.L^{-1}$ for a high-centered (SC) probe. The target conductivity is also reached earlier, around 175 $kJ.g^{-1}.L^{-1}$ for SOC, compared to 260 $kJ.g^{-1}.L^{-1}$ for SC. This confirms that an off-centered probe (SOC) provides a more efficient dispersion, as expected from the numerical simulations. Concerning the deep centered probe (SDC), there are still visible agglomerates after applying 330 $kJ.g^{-1}.L^{-1}$ for 10 minutes and the targeted value has not been reached yet.

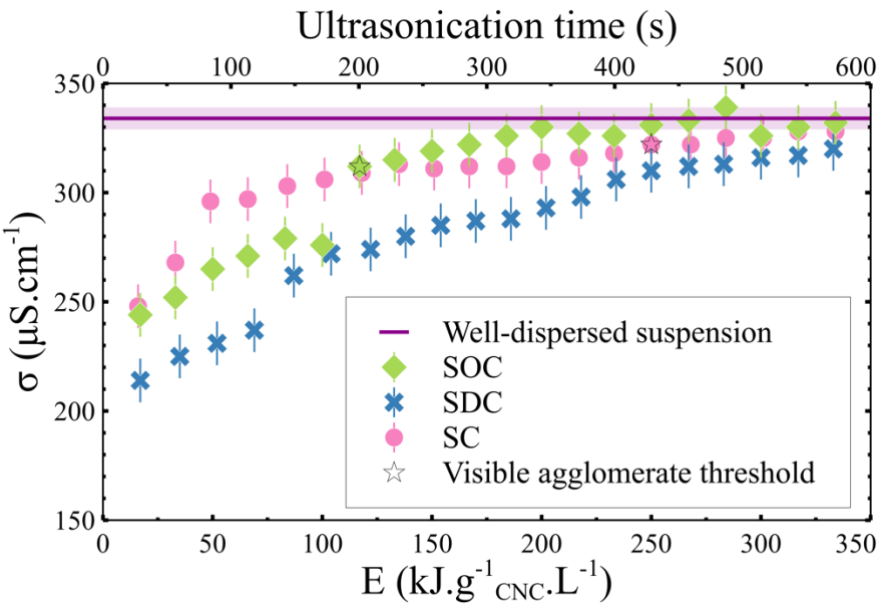

Figure 4.8: Conductivity of 3 wt% CNC ultrasonicated suspensions (V = 60 mL, P = 15 (65) W) obtained either with an off-centered probe high in the beaker (SOC), a centered probe (SC) or a deep centered probe (SDC). The light purple area represents the average standard deviation. The vertical lines correspond to the standard deviation for each experiment.

4.3.3.2 Particle size

The particle size distribution was obtained for all three cases analyzed via conductivity measurements (Section 4.3.3.1), to confirm the extent to which conductivity is representative of de-agglomeration of CNC particles (Figure 4.9). The minimum particle size attained is approximately the same for each case (approximately 0.4 µm, i.e. close to the resolution limit of the measuring device). However, the off-centered probe (SOC) case leads to more de-agglomerated particles, with 20% of the agglomerates measuring 0.7 µm whereas SDC and SC contain only 4% of agglomerates of this size and fractions for all other sizes are larger. In addition, a more uniform size distribution is observed for SDC. These data are consistent with conductivity measurements and thus validate the approach. Even so, the smallest sizes that are observed here are still above the primary particle size (around 0.1 µm), meaning that the agglomerates have not been fully broken. Figure 4.9 presents the distribution in volume, while distribution in number can be found in Figure A.6 and Figure A.7. To confirm this trend, this analysis has been duplicated using a DLS method. It shows that individual particle sizes are

obtained with SOC, close to the results obtained by the 3 wt% calibration case presented in Section 4.3.3.1 (Figure A.8). The target values for other concentrations are reported in Figure A.9.

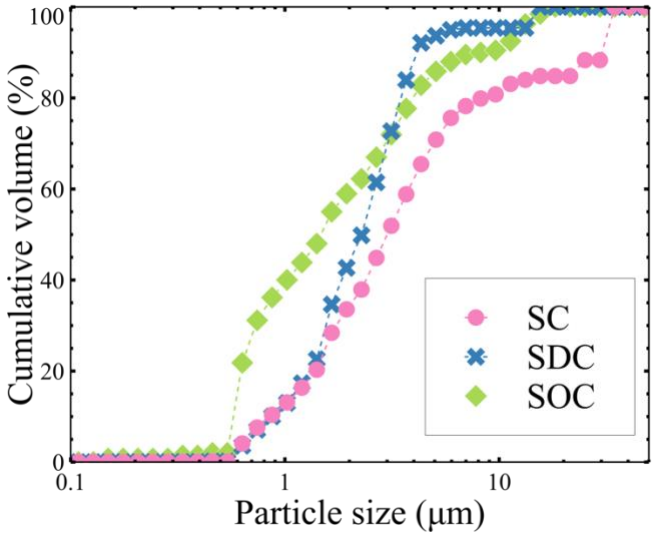

Figure 4.9: Particle size in cumulative volume of 3 wt% CNC ultrasonicated suspensions (V = 60 mL, P = 15 (65) W, E = 167 $kJ.g^{-1}.L^{-1}$) obtained either with an off-centered probe high in the beaker (SOC), a centered probe (SC) or a deep centered probe (SDC).

4.3.3.3 Viscosity

In addition to the conductivity and particle size analyses, a rheology study was also carried out to support the previous conclusions. Figure 4.10 illustrates the viscosity of the three cases studied (SC, SOC, SDC) for a shear rate test from 10 s^{-1} to 10^3 s^{-1}. For comparison purpose, the 3 wt% calibration case viscosity presented in Section 4.3.3.1 has also been reported. The target values for other concentrations are reported in Figure A.10). A classic behavior is observed for a 3 wt% CNC suspension: a plateau is obtained at low to medium shear rates followed by shear-thinning behavior [64]. Indeed, CNC networks are broken during the test when applying higher shear rates. When the SOC case is compared to the other two cases (SC and SDC), one can see that the viscosity is 1.3-1.5 times higher at 10 s^{-1}. The value for the SOC configuration corresponds to the one measured by Beuguel et al. for a well-dispersed 3 wt% CNC suspension [12]. SC and SDC both still contain agglomerates, so the samples present a distributed particle concentration lower than expected, leading to a lower measured viscosity.

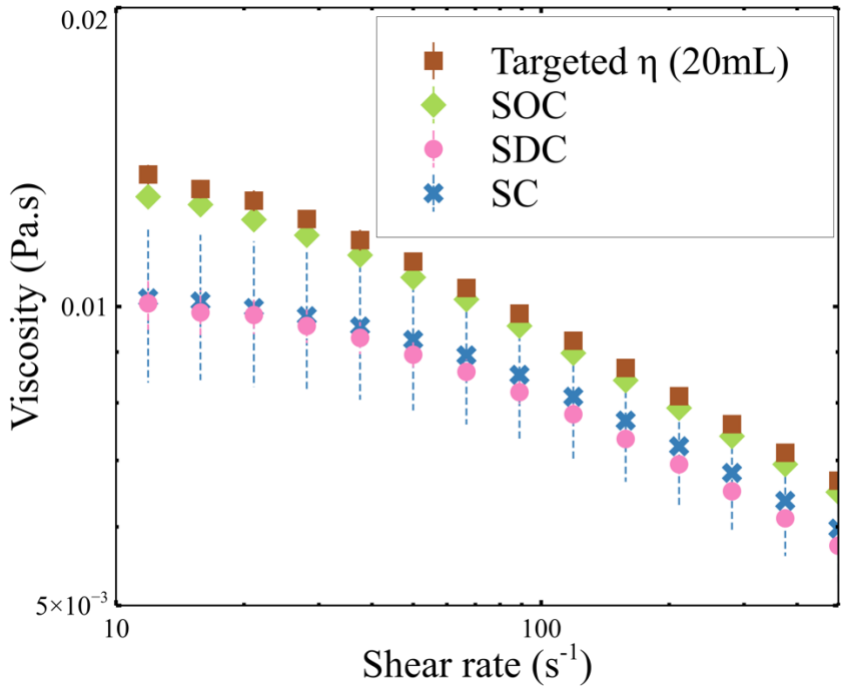

Figure 4.10: Viscosity of 3 wt% CNC ultrasonicated suspensions as function of shear rate (V = 60 mL, P = 15 (65) W, E = 167 kJ.g^{-1}.L^{-1}) obtained either with an off-centered probe high in the beaker (SOC), a centered probe (SC) or a deep centered probe (SDC). The targeted viscosity (η) corresponds to the reference case presented in Section 4.3.3.1 at 3 wt% (V = 20 mL, h/H = 0.3, E = 500 kJ.g^{-1}.L^{-1}, P = 33 (90) W, (R-r)/R = 1).The vertical lines correspond to the standard deviation.

The relative standard deviation of the viscosity is reported in Figure 4.11 to confirm the link between the inhomogeneity in the viscosity values and the bad dispersion state. The relative standard deviation is almost 10 times lower for the SOC case, which agrees with the previous statement, indicating the CNC homogeneity in the suspension.

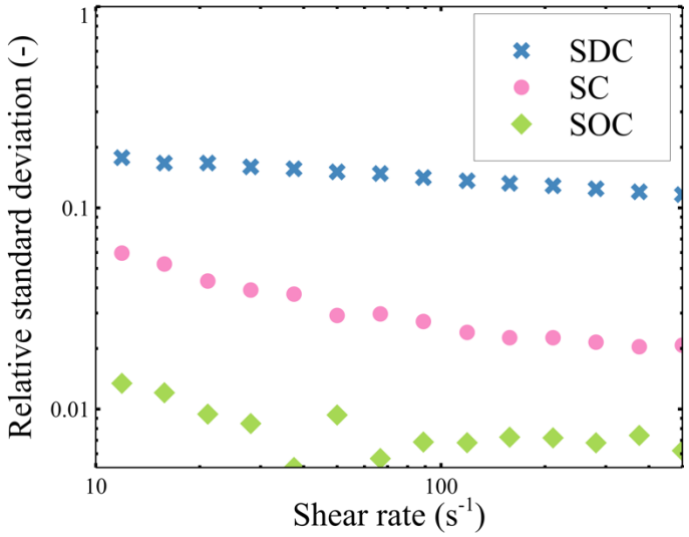

Figure 4.11: Relative standard deviation of 3 wt% CNC ultrasonicated suspensions as function of shear rate (V = 60 mL, P = 15 (65) W, E = 167 $kJ.g^{-1}.L^{-1}$) obtained either with an off-centered probe high in the beaker (SOC), a centered probe (SC) or a deep centered probe (SDC).

4.3.4 Operating window

Numerical studies have identified the geometric and volumetric parameters that affect dispersion, on top of the previously identified energy thresholds. These were validated with experimental studies, and thus allowed us to define an operating window to guide users for CNC dispersion. This could further serve as a starting point for the dispersion of other nanomaterials.

As only one probe was considered in this work, r_0/R is only depending on the beaker size which directly affects the volume processed by ultrasonication. Thus as the energy unit is $kJ.g^{-1}.L^{-1}$, r_0/R is an underlying parameter of the energy. Unfortunately, this work cannot be generalized for all probe types as these are expected to exhibit different efficiencies in terms of delivered power. For different probe geometries, the reader may use the analyses provide in Section 4.2.2 as a guideline for other probes.

Probe depth and axial position play major roles, and for each parameter the two previously discussed cases were considered: h/H = 0.3 or 0.7 and (R-r)/R = 1 or 0.4 for a 60 mL beaker. Additional intermediate cases are also presented: h/H=0.5 and (R-r)/R = 0.7.

Thus, an operating window based on these parameters can be derived from the dispersion index calculation in Section 4.3. The probe depth influence is illustrated in Figure 4.12 and the centering effect in Figure 4.13 for η = 10 mPa.s.

As expected from the previous results, the dispersion index D_i is higher when the probe is placed off-centered (SOC). Probe depth is a more complex parameter to study, as it depends on the centering position. For a centered probe (Figure 4.12A), the process is more efficient when the probe is halfway up, at higher energy density. Interestingly, this is not a case that was studied initially with our numerical model; its efficiency may be explained because the acoustic waves are powerful enough to be reflected by the bottom of the beaker to be effective over the whole volume when centered. However, it is better to place the probe in the upper or lower parts of the beaker when it is off-centered (Figure 4.12B), though this is only apparent at higher energy densities. Between these two cases, the probe placed in the upper part is preferred, as a higher D_i is obtained at lower energy. However, when the probe is off-centered, the reflection from the side becomes predominant. Increasing the energy generally increases D_i but one has to be aware that a high amount of energy requires a longer time for a larger beaker. Thus, 30 $kJ.g^{-1}.L^{-1}$ corresponds to 200 s in a 200 mL beaker, but only 54 s in a 60 mL system.

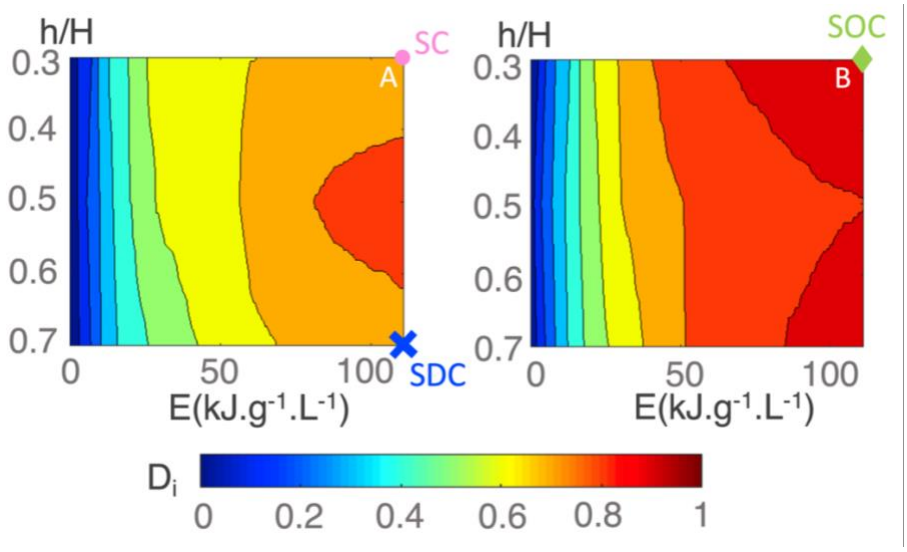

Figure 4.12: Operating window showing the dispersion index D_i for η = 10 mPas.s as a function of h/H and E for (A): (R-r)/R = 1 and (B): (R-r)/R = 0.4. The three points SC, SDC and SOC correspond to the conditions used in the experiments.

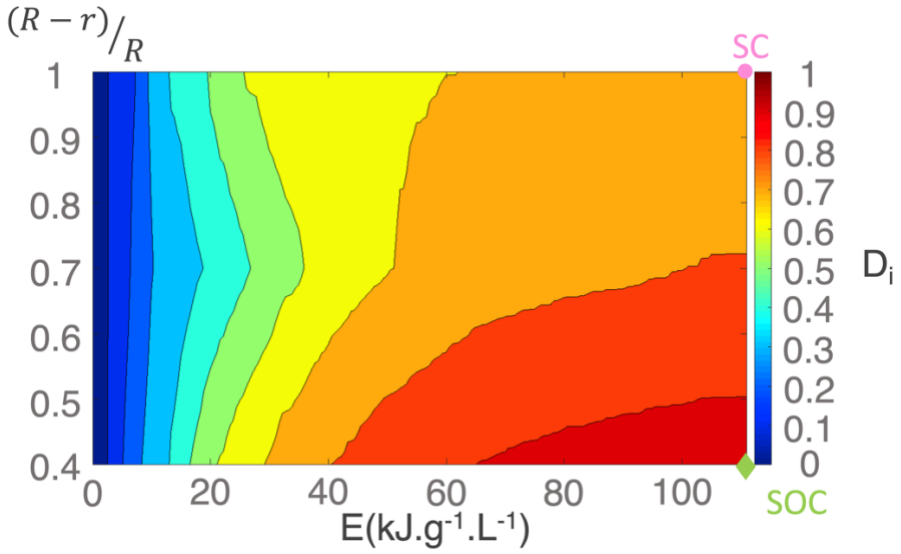

Figure 4.13: Operating window showing dispersion index D_i for η = 10 mPas.s as a function of centering (R-r)/R and sonication energy density E for a probe depth of h/H=0.3. The two points SC and SOC correspond to the conditions used in the experiments.

4.4 Conclusion and further recommendations

Using numerical modeling, several key parameters were identified to obtain a well-dispersed CNC suspension: the beaker geometry and the probe position, and more specifically depth and centering. Thus, the best dispersion is obtained with a small beaker placing the probe off-centered and halfway up, considering that the lowest amount of energy is needed. Because the dispersion is energy-dependent, reducing the volume reduces the time needed to apply the same amount of energy and would thus be more efficient.

These numerically-obtained guidelines were validated experimentally using simple characterization techniques such as electrical conductivity measurements and rheometry, with further validation through size distribution measurements. Whereas the conductivity method can be only applied on charged nanoparticle suspension, the rheology protocol can be extended to any nanoparticle type.

This standardized method requiring to work in small volumes are not practical for industry. However, at larger scale, we suggest working with an inline continuous process: the suspension would be treated gradually, and a loop could be implemented for online

conductivity/viscosity measurements to check the dispersion state. Moreover, this could help to increase the dispersion efficiency for small volumes. Additional mixing tools in combination with sonication could be pertinent as well. These elements are the focus of on-going research in our team.

Declaration of Competing Interest

The authors declare that they have no known competing financial interests or personal relationships that could have appeared to influence the work reported in this paper.

Acknowledgments

The authors thank the National Science and Engineering Research Council of Canada (NSERC), namely its CRD and CREATE programs, Prima Québec and FPInnovations for the financial support. Celluforce is acknowledged for providing the cellulose nanocrystals. Additionally, we would like to thank CREPEC for the expertise and infrastructure access and the Simulation-based Engineering Science (Génie Par la Simulation) group for scholarship and resource support. The authors are also grateful to Dr. H. Nasri for the particle size analysis, Pr. N. Virgilio for the ultrasonic probe, D. Pilon for the technical support for the calorimetry study, M. Gauthier for the help on post-processing and A. Tiffon for preliminary investigation work.

CHAPTER 5 ARTICLE 2: RHEOLOGICAL INSIGHTS ON THE EVOLUTION OF SONICATED CELLULOSE NANOCRYSTAL DISPERSIONS

Mélanie Girard, François Bertrand, Jason R. Tavares, Marie-Claude Heuzey. Rheological insights on the evolution of sonicated cellulose nanocrystal dispersions. *Ultrasonics Sonochemistry*. 78 (2021), 105747. Submitted on 8 July 2021 and published online on 7 September 2021.

Connecting statement

In Section 4.3.3.3, the standard deviation obtained for the viscosity values is quite important for the cases where the probe is not optimally placed (SC and SDC), leading to unexpected lower viscosity. As introduced in the corresponding section, this highlights a problem of homogeneity in the suspension. The sampling method which was used leads to unreliable measurements. This chapter aims to answer this issue by studying the effect of the sampling method and the evolution of the standard deviation at low sonication energy.

Abstract

Cellulose nanocrystals (CNCs) are promising biomaterials, but their tendency to agglomerate when dried limits their use in several applications. Ultrasonication is commonly used to disperse CNCs in water, bringing enough energy to the suspension to break agglomerates. While the optimized parameters for sonication are now well defined for small volumes of low concentration CNC suspensions, a deeper understanding of the influence of the dispersing process is needed to work with larger volumes, at higher concentrations. Herein, rheology is used to define the distribution and dispersion states upon ultrasonication of a 3.2 wt% CNC suspension. After considering the importance of the measurement sampling volume, the behavior of a more concentrated suspension (6.4 wt%) is examined and compared with a never-dried suspension of the same concentration to validate the dispersion state.

Keywords: ultrasonication, distribution, dispersion, suspensions, cellulose nanocrystals

5.1 Introduction

Cellulose nanocrystals (CNCs) are bio-sourced nanoparticles that can be used in various applications such as polymer reinforcement, barrier films or biomedicine [175, 176, 198]. Their

size and shape, along with their surface chemistry confer upon them beneficial properties for these sectors. For instance, they present a high longitudinal modulus (around 130 GPa) [18], iridescence [58], and barrier properties [199].

These nanorods are extracted from purified cellulose fibers through acid hydrolysis, either with hydrochloric or sulfuric acid (HCl and H_2SO_4). Amorphous portions are thus removed, leaving only the crystalline part. H_2SO_4 is particularly useful, as it introduces charged sulfate half-ester groups on the CNC surface, facilitating their dispersion in water (contrary to HCl) [31]. However, thermal stability is affected by a high sulfate half-ester group content [39]. The hydrolysis conditions may additionally affect the particle size [16, 185, 186].

Following hydrolysis, CNCs are generally neutralized. The choice of the counterion influences the stability or the dispersion ability [38, 111]. CNCs may then be dried using either freeze- or spray-drying approaches. Spray-drying is usually favored for industrial synthesis, as it requires less energy. In addition, spray-dried CNCs present higher crystallinity and thermal stability because of a higher cellulose II content than their freeze-dried counterparts, and lead to a more compact powder [12, 41]. However, CNCs tend to agglomerate during drying, either as spherical aggregates when spray-dried or as flakes when freeze-dried. Agglomeration hinders the exploitation of CNC's desirable properties. With the application of appropriate mechanical energy on agglomerated CNC suspensions, it is possible to obtain the same properties and behavior for spray- or freeze-dried systems than for never-dried CNC suspensions [43].

Breaking the agglomerates formed upon drying requires high energy input. Indeed, due to the high surface area of the CNCs (around 150-400 $m^2.g^{-1}$ [33, 87]), the agglomerate strength may reach 10^4 to 10^9 Pa depending on the initial particle size [46]. Ultrasonication is typically used in the literature for CNC dispersion, as it can provide energy densities from 10^6 to 10^8 Pa. An alternate solution is to use a high-pressure homogenizer, also based on cavitation generation; this process may be interesting as it makes the suspension flow at high velocities [200], preventing the formation of dead zones identified when using ultrasonication. Due to infrastructure cost, high-pressure homogenization remains rarely used at the lab scale for CNC dispersion.

Ultrasonication probes generate a sinusoidal pressure wave in the medium thanks to piezoelectricity. This induces compression and rarefaction cycles (respectively of negative and positive pressure), creating vacuum bubbles. Bubble sizes are influenced by these pressure variations by growing and absorbing energy under low pressure and contracting at high pressure. These cycles are repeated until the cavities reach a critical size (~170 μm in diameter at 20 kHz in water), which leads to their implosion at high frequency [119]. This phenomenon called cavitation releases a high amount of energy. However, the active zone in which cavitation takes place is limited to the near-probe region, the size of which is largely dependent on the viscosity of the medium. This limits dispersion in highly concentrated (and therefore viscous) suspensions or in large volumes [173].

Rheology is a powerful tool to characterize CNC suspensions [111], especially given the fact that their behavior is concentration dependent. Suspensions go from isotropic at low concentration (below 2 to 4 wt%), to liquid crystal at medium concentration (between 4 wt% to 5 wt%) and finally to a gel at high concentration by forming a percolating network [69] (over 5 and up to 12 wt%) [56, 64, 201, 202]. A glassy state has also been defined for high concentrations (over 8 wt%) and very low ionic strength (less than 10^{-2} mol.L^{-1}), with the addition of salt increasing this concentration threshold [69]. In the glassy state, the solid-like behavior is governed by repulsive interactions [68]. The concentration thresholds delimiting the suspension states are not strictly defined as they may depend on the sulfatation degree, ionic strength of the suspending medium and on the CNC aspect ratio [55, 56]. Isotropic suspensions exhibit a plateau at low shear rate, shear thinning at intermediate shear rate and another plateau at high shear rate. On the other hand, liquid crystal suspensions lead to a three-region behavior for viscosity in shear rate sweep tests: shear-thinning, plateau, and shear-thinning, respectively for low, intermediate, and high shear rates. For the gel state however, only shear-thinning is observed [64]. CNC gels present a yield stress resulting from the competition between microstructure build-up and destruction. Thus, applying a low shear stress (below the yield stress) results in viscosity build-up over time, or ageing. Conversely, applying a high shear stress (above the yield stress) leads to a viscosity decrease over time, or “rejuvenation” [203, 204]. This must be kept in mind for rheological characterization as it induces change in the behavior one is trying to observe.

Rheology can also be used to assess the CNC dispersion state [12, 173]. Studies on ultrasonication parameter influence have revealed a decrease in viscosity as the particles become dispersed, i.e. as the agglomerates are broken down due to a thinner electrostatic double layer because of the Na^+ counterion release [12, 56]. Moreover, for highly concentrated suspensions, the gel behavior can be disrupted to reach a liquid behavior through ultrasonication. The recovery of the initial state, i.e a stable gel, may take more than 6 months [172].

Even if ultrasonication is widely used in the literature, many challenges remain, and a deeper understanding is needed to fully benefit from this processing method. In our previous work, a rigorous protocol involving probe position and key metrics accounting for container volume were defined to disperse CNCs efficiently in water [173]. However, that study, as well as most literature articles, focuses almost exclusively on the end-point of dispersion - parameters that lead to a well-distributed and well-dispersed suspension - but neglect the path to achieve this final state. Understanding the sequence of events leading to dispersion may help work around the current limitations of ultrasonication.

Thus, the objective of this paper is to characterize the behavior of CNC liquid-like and gel-like suspension during ultrasonication. In this study, we carefully differentiate distribution and dispersion: while the first refers to the homogeneity of the suspension, the latter qualifies the particle state in the suspension (individual or agglomerated). This paper focuses on the rheology of the CNC suspension during ultrasonication. The effect of the sampling method for rheology measurements is first analyzed. Then, by focusing on sonication at low energy levels (below the previously identified thresholds for dispersion [173]) on a 3.2 wt% CNC suspension (liquid-like behavior), it is possible to better understand the sequence of events to reach a good dispersion state through ultrasonication. Additionally, the comparison of the results given by two rheometer flow geometries further highlights the effect of the sampling volume. Finally, the behavior of a 6.4 wt% CNC suspension (gel-like behavior) is investigated to confront the previous outcomes to concentrated media.

5.2 Methodology

5.2.1 Material

The CNCs used in this work were provided by Celluforce. They present sulfate half ester groups on their surface that result from the hydrolysis step after extracting CNCs from cellulose fiber and removing lignin, hemicellulose, and impurities. There are approximately 3.4 sulfate half ester groups per 100 anhydroglucose rings, giving a sulfur over carbon S/C atomic ratio around 0.0057 [12] or 211 $mmol.kg^{-1}$. These CNCs were neutralized using sodium hydroxide before either being spray-dried (particle size ~ 127 nm when resuspended, as specified by the manufacturer), or kept in suspension at 6.4 wt% (never-dried, particle size ~ 90 nm). Note however that both particle size measurements have been carried out by the supplier with 2 wt% suspensions and the results may hide dispersion problems. In both cases, the final crystallinity ratio is around 80 % [35] and the density 1540 $kg.m^{-3}$. The dried CNCs were used as-received in powder form and have never been sonicated prior to this work.

5.2.2 CNC suspension preparation

Starting from dried CNCs, suspension preparation followed the same rigorous protocol presented in our previous work [173]. Briefly, 60 mL of either a 3.2 wt% (2.08 vol%) or a 6.4 wt% (4.16 vol%) CNC suspension were prepared by adding half of the water amount, the required CNC amount (respectively 1.91 g or 3.84 g) and the remaining water, in this specific order, to facilitate CNC incorporation, in a 100 mL beaker. A vortexer (Mini Roto S56 – Fischer Scientific – 2800 rpm) was then applied for 30 s to avoid gelation.

This pre-mixed suspension was then sonicated for a specific time at power P = 65 W, placing the probe off-center near the liquid surface. This power level has been chosen to find a balance between ultrasonication efficiency and time needed to achieve dispersion. This value is the one shown on the device and correspond to an actual delivered power of 15 W [173]. The beaker was put in an ice bath to avoid overheating. Under these conditions, the required sonication energy is around 167 $kJ.g^{-1}.L^{-1}$ to achieve a well-dispersed suspension (refers to kilojoules per gram of CNCs and liter of suspension) [173]. We will refer to this value as “optimal energy level” henceforth in the text. Ultrasonication was used at different energy levels,

ranging from very low (2 $kJ.g^{-1}.L^{-1}$ or ~ 3 s of ultrasonication for a 3.2 wt% suspension), low (15 $kJ.g^{-1}.L^{-1}$ or ~ 10 s at 3.2 wt%) or optimal (167 $kJ.g^{-1}.L^{-1}$ or ~ 320 s at 3.2 wt%).

The never-dried CNC suspension was either characterized as received, or after applying the equivalent optimal energy level (167 $kJ.g^{-1}.L^{-1}$ or ~ 640 s), following the same protocols outlined above. This energy level leads to a minimum viscosity and longer ultrasonication does not decrease the viscosity any further (Figure B.1).

5.2.3 Rheology

Rheology measurements were carried out using an Anton-Paar rotational rheometer (MCR501). Either a concentric cylinder (CC) or a Couette double gap (DG) flow geometry was used. The required volume for each geometry (20 mL for CC or 8 mL for DG) was sampled using a syringe unless specified otherwise. Shear rate sweep tests were carried out from 1000 s^{-1} to 1 s^{-1} (high to low shear rate, unless specified otherwise). These tests were preceded by a pre-shear at 10 s^{-1} for 120 s to prevent the presence of air in the sample and ensure of a similar starting microstructure, followed by a 180 s rest time. All tests were performed at 25 ˚C.

5.2.4 Particle size analysis

Particle sizes were determined using a laser obscuration time technique (EyeTech, Ankersmid). This method was chosen as no dilution is needed prior to analysis, avoiding any change in the particle dispersion. It can measure particles as small as 0.1 μm.

5.2.5 UV-vis spectroscopy

One way to evaluate the dispersion state is by analyzing suspension turbidity. This was carried out with UV-vis spectroscopy (USB4000-XR1-ES, Ocean Insight). The absorbance was measured between 200 and 850 nm using 1-cm quartz cell. However, results must be interpreted carefully as other physical phenomena could influence the optical properties.

5.2.6 Ageing tests

The behavior of a never-dried CNC suspension was compared to that of a suspension of the same concentration, i.e 6.4 wt%, prepared with spray-dried CNCs. Shear rate sweeps from

1000 s^{-1} to 1 s^{-1} (high to low) were done on those suspensions within 5 min following ultrasonication and were then repeated after a specific time to follow the evolution (ageing) over time. This specific time, specified in the corresponding discussion as DX for “day X”, was the same for every suspension. Meanwhile, the suspensions were stored at room temperature.

Because of the fast-evolving behavior over time, a repeatability study was carried out by analyzing one sample of three suspensions obtained with the same parameters, instead of several samples of the same suspension. This allowed us to keep the study time constant.

5.3 Results and discussion

5.3.1 Sampling method

As explained in Section 5.2.3, suspensions are usually sampled with a syringe. However, this may filter out the largest agglomerates (larger than 2 mm) and bias the rheological assessments. Thus, two additional sampling methods were compared to study their effect: a truncated syringe allowing agglomerates up to 15 mm to be sampled, and pouring the sample directly from the beaker into the flow geometry.

To highlight the effect of the sampling method, the applied ultrasonication energy was 2 $kJ.g^{-1}.L^{-1}$, as inhomogeneity in the distribution and poor dispersion are expected at this very low energy level. The DG flow geometry was used to carry out a shear rate sweep study. The three sampling methods were compared by analyzing six to seven samples for each, and repeated three times. Then, the standard deviation normalized by the average viscosity value was calculated for all samples and averaged for all three repetitions to compare the variation caused by each sampling method (Figure 5.1).

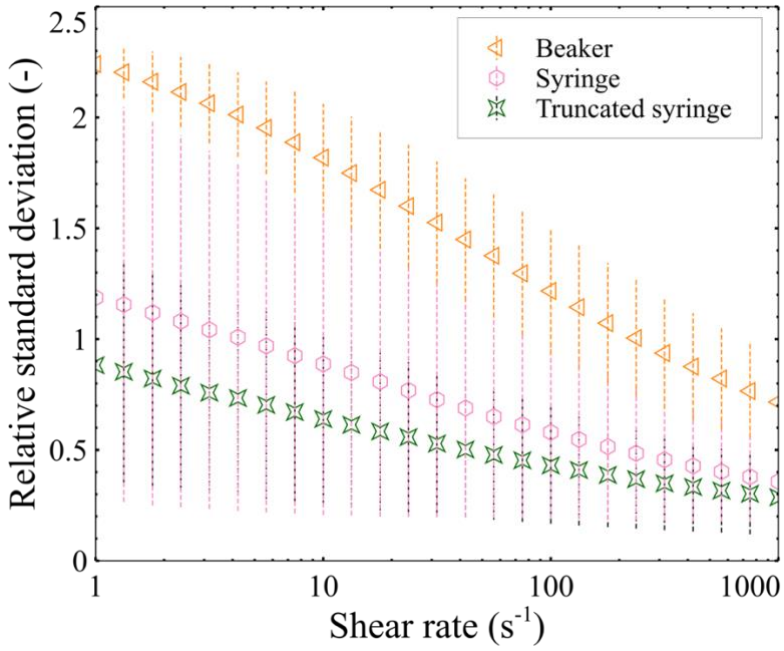

Figure 5.1: Relative standard deviation of 3.2 wt% CNC ultrasonicated suspensions as function of shear rate (V = 60 mL, P = 65 W, E = 2 $kJ.g^{-1}.L^{-1}$) using either the syringe, the truncated syringe or the beaker sampling method

Note that, at this energy level, the initial state influences the measured viscosity. Indeed, even if the suspension preparation protocol was rigorously followed, a great deal of variability was introduced by the very low-energy dispersion approach. Agglomerates were formed randomly, and the ultrasonic probe could not be placed at the same position relative to each of them, leading to variations between each repetition.

This variation between samples obtained with the same sampling method is significant, showing that the initial state influence prevails over the effect of the sampling method itself. Indeed, by considering this variation, the value of the standard deviation is approximately the same whatever the method. The higher values observed for the beaker sampling method are inherent to the fact that all agglomerates are considered with this method whereas only a few agglomerates are collected with both syringe sampling methods. It also confirms that despite the rigorous preparation protocol meant to avoid manipulation error, there is some variability that cannot be controlled.

For the following analyses, the syringe sampling method was retained, and the whole suspension was analyzed unless stated otherwise. While the truncated syringe is moderately better (Figure 5.1), the plain syringe approach is much easier to implement.

5.3.2 Ultrasonication mechanism over time

The suspension must be well-distributed and well-dispersed to give optimal results. To understand how these conditions can be reached, the ultrasonication process was decomposed into several steps and the suspensions were then analyzed using rheology. The DG flow geometry was used again for this study. Starting from an initial state consisting of an inhomogeneous medium with many large agglomerates, ultrasonication was applied either at 2 $kJ.g^{-1}.L^{-1}$ (purple data in Figure 5.2), 20 $kJ.g^{-1}.L^{-1}$ (green data) or 167 $kJ.g^{-1}.L^{-1}$ (red data).

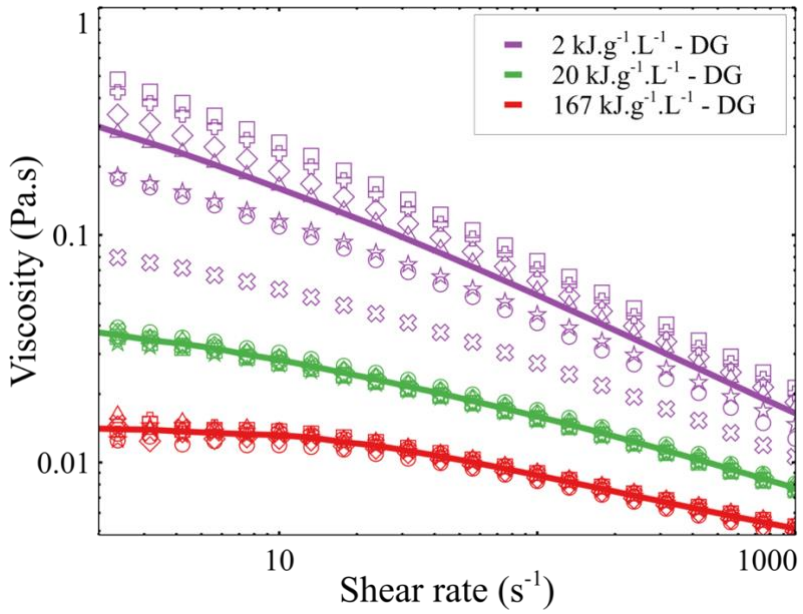

Figure 5.2: Viscosities of 3.2 wt% CNC ultrasonicated suspensions obtained for E = 2, 20 or 167 $kJ.g^{-1}.L^{-1}$ as function of shear rate (V = 60 mL, P = 65 W, DG flow geometry). Solid lines represent the average values of all corresponding measurements.

Applying the lowest amount of energy led to large variations between samples. Although the average of the measurements may indicate that a fair dispersion was achieved, the overall variations show that the suspensions were in fact inhomogeneous. This confirms that, at this very low energy level, the distribution and the dispersion are both unsatisfactory.

Increasing the sonication energy to 20 $kJ.g^{-1}.L^{-1}$ resulted in a significant reduction of the data spread: all samples have similar viscosity values, meaning that a good distribution state must have been reached (i.e. all samples measured are similar, and thus there is better homogeneity). However, when these values are compared to those of a well-dispersed suspension (Figure 5.2) at 167 $kJ.g^{-1}.L^{-1}$, it becomes clear that the dispersion had not yet reached its optimal state (as the viscosity values at 20 $kJ.g^{-1}.L^{-1}$ are significantly higher).

In summary, three states can be observed during ultrasonication, as illustrated in Figure 5.3. Upon increasing the energy level, the suspension goes from a not-well distributed and not-well dispersed state to a distributed but not well-dispersed state before finally reaching a well-distributed and well-dispersed state. Indeed, by increasing the time of ultrasonication, more mixing cycles may be achieved, increasing the process efficiency. This confirms the findings from numerical simulations presented in our previous work [173]. Photos taken right after ultrasonication validate this sequence. While photos on the left show the suspension as is, increasing the contrast and decreasing the brightness (photos on the right) helps to better visualize the presence of agglomerates at $t = 0$ and t_1. In addition, an opaquer suspension is observed for t_2 compared to t_f, confirming a worse dispersion. This last point has also been proved using UV-Vis spectroscopy (Figure B.2).

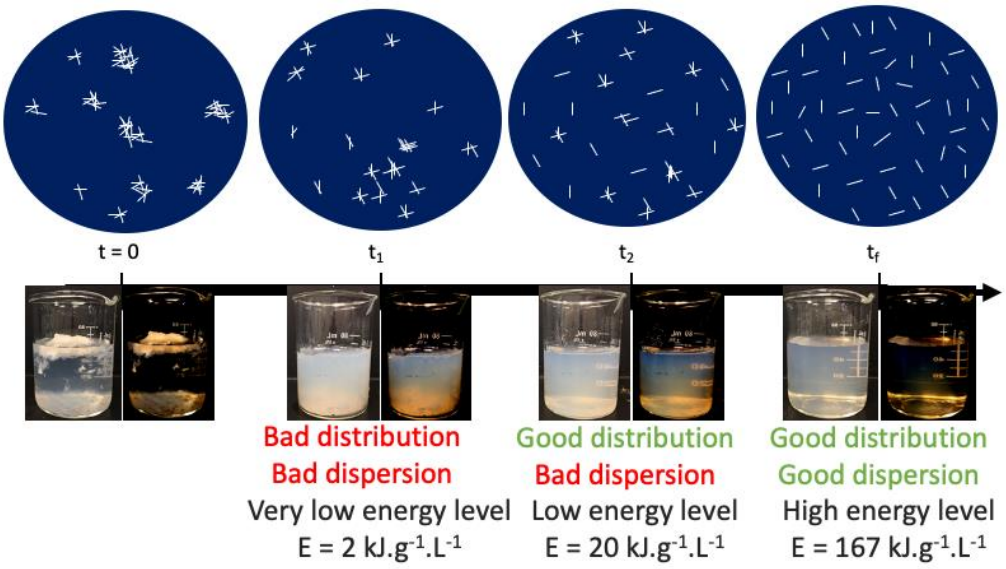

Figure 5.3: Suggested ultrasonication mechanism over time. Original (left) and modified (right) photos are shown for each time (ultrasonication energy being directly proportional to sonication time). The same image post-processing modifications have been applied for every case.

5.3.3 Geometry comparison and sampling volume

The previous section has underlined that variations in the viscosity values provide information on a suspension's distribution state. This suggests that the sampling volume is critical when analyzing a suspension. To validate this hypothesis, the concentric cylinder (CC) and the Couette double gap (DG) flow geometries were compared as these require sample sizes of either 20 mL or 8 mL, respectively. Several levels of energy were studied: either 2, 10, 15 or 20 $kJ.g^{-1}.L^{-1}$ to reach progressively the well-distributed state (minimum of 20 $kJ.g^{-1}.L^{-1}$).

To account for variations between samples, the standard deviation may be more relevant than the viscosity value itself. As discussed in Section 5.3.1, the average obtained from all the samples analyzed with the same geometry may differ from a suspension to another because of a different initial state (CNC agglomerates being formed in an uncontrolled manner in the beaker). Thus, the standard deviation is normalized by the average viscosity for each sample, giving a relative standard deviation, to minimize the effect of the initial state. Figure 5.4 present thus the relative standard deviation as a function of the shear rate for the different energy levels, for the DG case (empty symbols) and the CC case (filled symbols). The relative standard deviation is

larger for the DG case than the CC case at all energy levels. The DG flow geometry volume being smaller, the distribution effect is more visible. As the ultrasonication energy increases, the difference between the two geometries is reduced. This indicates that the sampling volume is less influential. In addition, as the distribution state improves when increasing the ultrasonication energy, the relative standard deviation decreases. Both points imply an improving distribution state.

Thus, relative standard deviation of the viscosity value serves as an indicator for distribution. However, the absolute value of viscosity needs to be considered to assess the dispersion state as explained in Section 5.3.2.

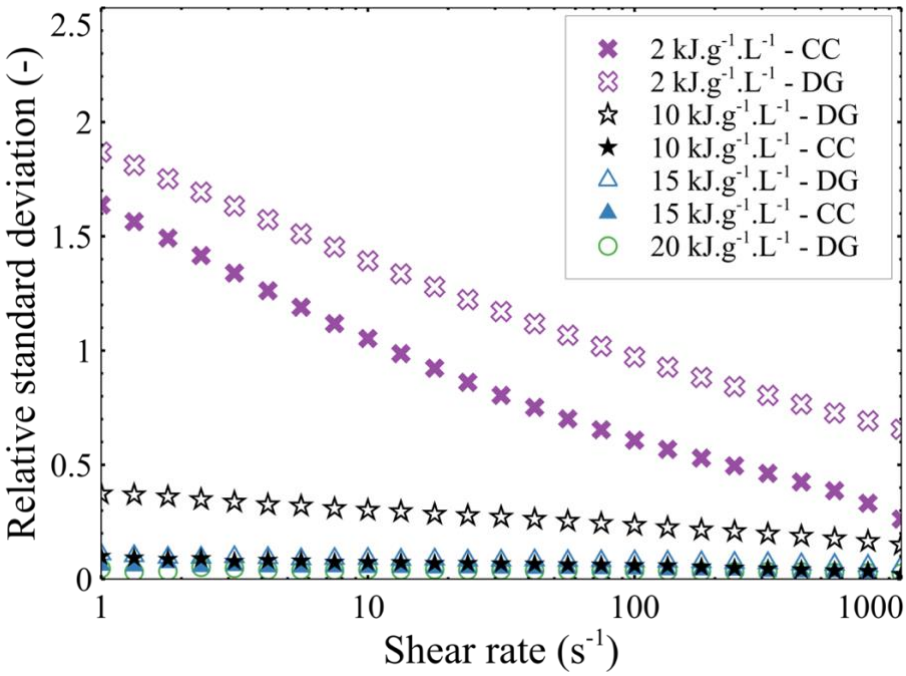

Figure 5.4: Relative standard deviation of 3.2 wt% CNC ultrasonicated suspensions obtained either with a concentric cylinder (CC – filled symbols) or a double gap (DG – empty symbols) geometry for E = 2, 10, 15 or 20 kJ.g-1.L-1 as function of shear rate (V = 60 mL, P = 65 W).

5.3.4 Challenges at higher concentrations

At higher concentration, CNC suspensions present a gel-like behavior. In this case, the previous conclusions may not be easily extrapolated, which warrants studying a 6.4 wt% CNC suspension.

One of the main concerns at higher concentration is to validate that a good dispersion can still be achieved as the formed agglomerates present a much higher local concentration than those of the suspension, multiplying the interparticle interactions. Thus, an ultrasonicated never-dried CNC suspension (UND) was compared with a spray-dried CNC suspension (USD) at the same 6.4 wt% concentration. Both have been ultrasonicated by applying the same energy level (167 $kJ.g^{-1}.L^{-1}$) to study the viscosity buildup after ultrasonication. Figure 5.5 depicts the viscosity values of each suspension as functions of shear rate followed over time after ultrasonication. The unsonicated, never-dried CNC suspension (ND) behavior is reported as a reference. ND and UND suspensions are supposed to present a well-dispersed state, as the CNC agglomeration is mainly induced from the drying process. At day 0 (D0), the viscosity measurements are essentially the same for USD and UND suspensions. This suggests that the dispersion state of the USD suspension is the same as the UND suspension, meaning that CNCs have been well-dispersed and well-distributed. The usual gel behavior at high concentration is replaced by a two-region curve: a shear-thinning behavior below 100 s^{-1} and a zone with a higher slope at higher shear rate. Though we do not observe a plateau at intermediate shear rates, a similar behavior has been reported in the literature [64] and a shear thinning region with a high slope is expected at lower shear rate: this is a liquid crystal behavior. To ease the comparison, the viscosity value at 5.62 s^{-1} is followed over time (Table 5.1). This value has been chosen to be in the mid-range of the lower shear rate values, where the interparticle contribution is visible [205]. After 11 days (D11), the final state seems to have been reached, as there is no significant difference with the behavior at day 20 (D20). The original ND values (1.4 Pa.s ± 0.1 at 5.62 s^{-1}) have been reached for the D20 USD suspension, but the D20 UND suspension remains at a lower viscosity level. However, the behavior for all suspensions is similar for shear rates above 40 s^{-1}. Indeed, only the hydrodynamic contribution plays a role on viscosity values at high shear rate [205]. The absence of complete recovery of the viscosity for the UND suspension has already been reported for ultrasonicated commercial concentrated suspension, even over longer time scales [172]. Two zones can be distinguished on the viscosity curve, which may suggest a biphasic structure with isotropic and anisotropic regions. This observation is also valid for the USD suspension even if this is much slighter.

To complement this study, a shear rate sweep has been carried out from low to high shear rates (Figure 5.6A). In this case, both UND and USD suspensions behave the same as the ND suspension. In addition, the comparison between both tests for the ND suspension (Figure 5.6B) shows a hysteresis phenomenon below 10 s^{-1}. This behavior has been already observed in the literature for thixotropic yielding materials [203], implying different dynamic and static particle network structures [206]. Thus, as differences from USD/UND and ND are visible only from high to low shear rates, it implies that the dynamic particle network structure is not the same. This point was confirmed by measuring a larger light absorbance for USD and UND compared to ND suspensions aged by 1 and 8 days, increasing with time (Figure B.3). The ultrasonication step allows CNCs to re-arrange themselves while the gelation phenomenon is not instantaneous. It has been reported that CNC suspensions present a larger anisotropic volume fraction with increasing ultrasonication time [207], which would lead to a larger absorbance.

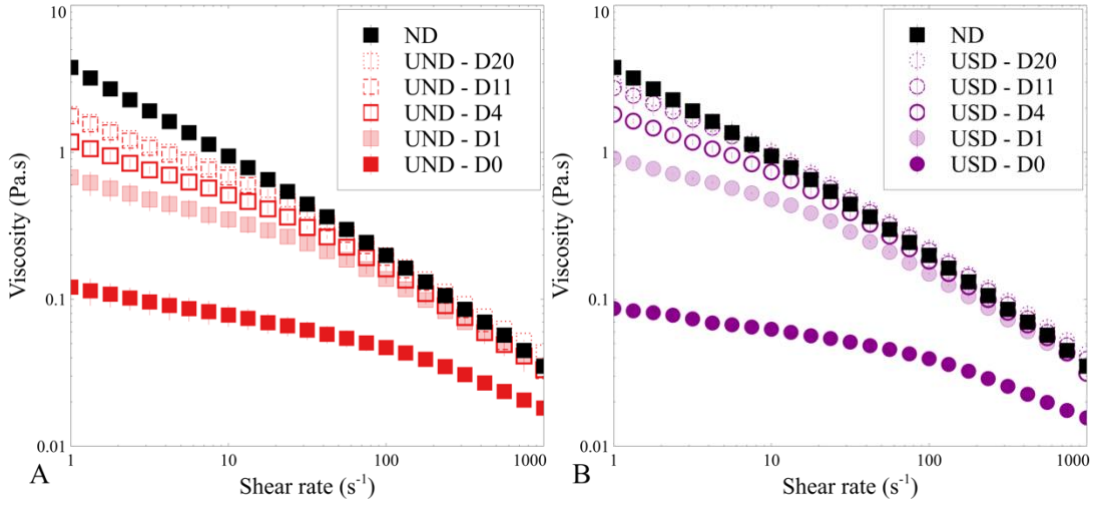

Figure 5.5 : Sample viscosities of 6.4 wt% never-dried (A) or spray-dried (B) CNC ultrasonicated suspensions, respectively noted UND or USD (E = 167 $kJ.g^{-1}.L^{-1}$,V = 60 mL, P = 65 W) after 0, 1, 4, 11 and 20 days (D0, D1, D4, D11, D20) compared with a 6.4 wt% never-dried CNC suspension, noted ND (no ultrasonication) as function of shear rate (high to low).

Table 5.1: Sample viscosity values at 5.62 s^{-1} of 6.4 wt% never-dried (A) or spray-dried (B) CNC ultrasonicated suspensions, respectively noted UND or USD (E = 167 $kJ.g^{-1}.L^{-1}$,V = 60 mL,

P = 65 W) after 0, 1, 4 11 and 20 days (D0, D1, D4, D11, D20). The value for the 6.4 wt% never-dried CNC suspension is indicated as a reference.

	D0 (Pa.s)	D1 (Pa.s)	D4 (Pa.s)	D11 (Pa.s)	D20 (Pa.s)
UND (A)	0.09 ± 0.02	0.41 ± 0.06	0.63 ± 0.04	0.9 ± 0.1	0.89 ± 0.05
USD (B)	0.067 ± 0.001	0.570 ± 0.001	0.95 ± 0.05	1.29 ± 0.02	1.4 ± 0.3

(ND: 1.4 Pa.s ± 0.1 at 5.62 s^{-1})

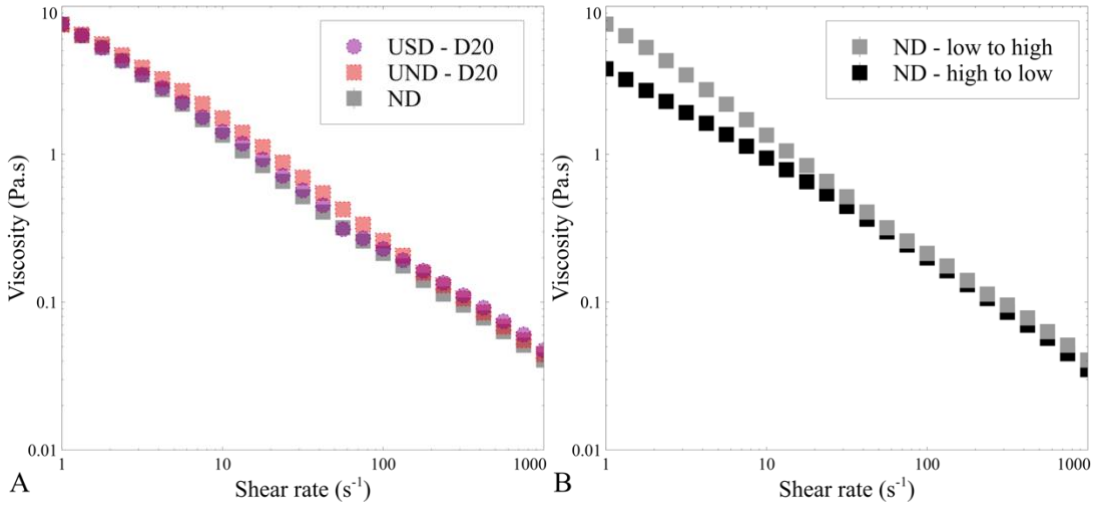

Figure 5.6: A: Sample viscosities of 6.4 wt% never-dried and spray-dried CNC ultrasonicated suspensions, respectively noted UND or USD (E = 167 $kJ.g^{-1}.L^{-1}$,V = 60 mL, P = 65 W) after 20 days (D20) compared with a 6.4 wt% never-dried CNC suspension, noted ND (no ultrasonication) as function of shear rate (low to high). B: Sample viscosities of a 6.4 wt% never-dried CNC suspension (ND) from low to high and high to low shear rate.

To conclude on the dispersion state of the USD and UND suspensions, the particle sizes were compared, and the results are reported on Figure 5.7 just after ultrasonication (D0) and after 1 day (D1). At D0, the USD suspension presents larger particles than the UND suspension - these differences are of the same range than the initial particle size measured by the supplier Celluforce. Thus, a well-dispersed state must have been reached for the USD. After one day, the particle sizes increase for both suspensions, with a higher increase for the USD suspension. This is consistent with the faster ageing over time that was observed in the rheology measurements. Particle size increase over time illustrates that a percolating network of particles is forming, as expected for a gel.

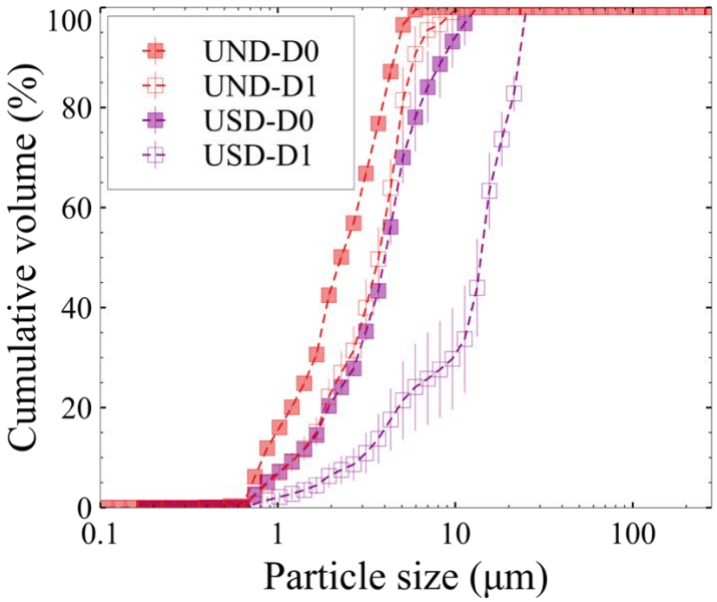

Figure 5.7: Cumulative volume distribution of 6.4 wt% never-dried and spray-dried CNC ultrasonicated suspensions, respectively noted UND or USD (E = 167 kJ.g^{-1}.L^{-1},V = 60 mL, P = 65 W) after 0 and 1 day (D0 and D1 respectively).

Compared to the study at 3.2 wt% CNC suspension (Section 5.3.3), the dispersion and distribution state of a 6.4 wt% CNC suspension cannot be determined as easily. Indeed, the method presented needs to be adapted as the concentrated suspension viscosity evolves quickly over time. The distribution state needs to be analyzed at the same time by comparing the behavior of similar suspensions. Figure 5.5 shows very small standard deviation with three samples of three different suspensions obtained with the same parameters, implying a good distribution state. In addition, as explained above, the dispersion is established by comparing the measurements with a never-dried suspension which had undergone the same ultrasonic energy level. The initial behavior (at D0) must be sufficient to conclude that the spray-dried CNC suspension is as well-dispersed as the never-dried CNC suspension.

5.4 Conclusion and further recommendations

Using ultrasonication to disperse nanoparticles can be challenging, especially when assessing the distribution and dispersion states. In this work, it has been demonstrated that rheology was a powerful tool for characterizing CNC suspensions at low concentration, if used properly. Studying the viscosity homogeneity in a suspension provides information on the

distribution state. However, the sample volume is an important limitation for further conclusions. The viscosity value itself can be used to assess the dispersion state as it decreases until a minimal value as the dispersion improves.

One must keep in mind the sampling volume influence when carrying analyses, such as density measurement or even microscopy observations. It could mask the true state of the suspension, leading the researcher to an incorrect interpretation.

The sampling volume issue also hints at greater issues when attempting to disperse larger volumes. The volume which can be handled is indeed a strong limitation for using sonication as a dispersion tool. One possible solution is to use a continuous setup that would gradually treat the suspension. The knowledge developed in the present work on ascertaining how both the dispersion and distribution states evolve during ultrasonication will facilitate implementation of an online measurement technique in larger-scale systems. This work is on-going in our team.

Finally, for higher CNC concentrations, the fast evolution of the microstructure (presence of tactoids) complicates its study. However, a comparison with a never-dried suspensions provides insight on the distribution and dispersion state. The rigorous protocol developed in our previous work was successfully applied to produce a 6.4 wt% suspension, and similar properties as never-dried CNC suspensions could be obtained from spray-dried CNCs.

Because other nanoparticles share the same issue related to their dispersion, this study could eventually be broadened to them as well.

CRediT authorship contribution statement

Mélanie Girard: Conceptualization, Methodology, Validation, Investigation, Writing – original draft, Visualization. **François Bertrand:** Writing - review & editing, Supervision. **Jason R. Tavares:** Writing - review & editing, Supervision. **Marie-Claude Heuzey:** Writing - review & editing, Supervision.

Declaration of Competing Interest

The authors declare that they have no known competing financial interests or personal relationships that could have appeared to influence the work reported in this paper.

Acknowledgments

The authors acknowledge the National Science and Engineering Research Council of Canada (NSERC), namely its CRD and CREATE programs, Prima Québec and FPInnovations for the financial support. The authors are also grateful to Celluforce for providing the cellulose nanocrystals. Additionally, we would like to thank CREPEC for the expertise and infrastructure access, as well as the Simulation-based Engineering Science (Génie Par la Simulation) group for scholarship support.

CHAPTER 6 ARTICLE 3: A TECHNIQUE FOR THE ULTRASONIC DISPERSION OF LARGER QUANTITIES OF CELLULOSE NANOCRYSTALS WITH IN-LINE VALIDATION

Mélanie Girard, François Bertrand, Jason R. Tavares, Marie-Claude Heuzey. A technique for the ultrasonic dispersion of larger quantities of cellulose nanocrystals with in-line validation. *Submitted in Chemical Engineering Journal*, February 2022.

Connecting statement

All the work presented in Chapter 4 and Chapter 5 was carried out using a continuous ultrasonication mode in a batch process. In this Chapter though, a pulse mode (8 s ON – 2 s OFF) is chosen to prevent damaging the probe as the process is much longer with the semi-continuous process. Despite this difference, the batch process is used as a reference here as its dispersion state has been deeply studied and is assumed to be optimal.

Abstract

Cellulose nanocrystals (CNCs) can be used in a wide range of applications due to their unique properties. However, the dispersion required to achieve these properties in various media may be quite challenging, especially at larger scales. Starting from an optimized protocol to prepare small volumes (60 mL) of aqueous suspensions, a semi-continuous setup is developed in this work to disperse larger quantities (200 mL). Using this technique, a higher efficiency is achieved, consuming only 35 % of the energy needed with a comparable batch method. To follow the dispersion state, an in-line process rheometry technique is adapted and validated through finite element simulation. While this allows for fast and easy validation, a deeper analysis may also be carried out to extract additional information such as the process viscosity. This setup is further exploited for the CNC surface modification using polyethylenimine. Although it has been designed for CNCs, it may be adapted for other nanoparticle dispersion.

Keywords: Ultrasonication, cellulose nanocrystals, suspension, dispersion, in-line measurement, semi-continuous setup

6.1 Introduction

Cellulose nanocrystals (CNCs) are bio-based material displaying several valuable properties attributed to their surface chemistry and their nano-rod morphology. They find applications in mechanical reinforcement, optical films, 3D printing and Pickering emulsions, to name only a few [93, 175, 208, 209].

CNCs are obtained from acid hydrolysis of cellulose fibers, removing the amorphous portion of the fibers. This may be carried out using hydrochloric or sulfuric acid (HCl or H_2SO_4). The choice of the acid will impact on the particle size [16, 185, 186], and the surface chemistry: H_2SO_4, compared to HCl, promotes dispersion in water by generating charged sulfate half-ester groups on the CNC surface [31, 39]. After hydrolysis, the CNCs may then be neutralized to improve stability or facilitate dispersion, depending on the counterion being used [38, 111]. Neutralization is generally followed by a drying phase, with typically spray-drying or freeze-drying methods. Spray-drying requires less energy and results in a more compact powder – this leads to higher crystallinity and better thermal stability [12, 41]. However, for both drying strategies, CNCs form aggregates or flakes. The bond strength within these may reach up to 10^9 Pa for the smallest particles (0.5 μm in diameter when spherical) [46]. Thus, a powerful technique is crucial to redisperse CNCs and benefit from all their properties. By providing an energy density up to 10^8 J/m^3 [188], ultrasonication is the most commonly used method at the lab scale, for efficient dispersion in low-viscosity media. High-pressure homogenization may alternatively be employed, but it requires a less ubiquitous and more expensive infrastructure.

For CNC dispersion, ultrasonication probes are favored compared to baths, offering a greater efficiency through direct contact [117]. The probes are made of a piezoelectric material, inducing pressure waves in the liquid via mechanical vibration at high frequencies. Vacuum bubbles are formed because of the alternating positive and negative pressures. Negative pressure leads to bubble growth whereas these are compressed at positive pressure. Cavitation takes place at high intensities once the bubbles are large enough (with a diameter of 170 μm for ultrasonication at 20 kHz in water). The cavities are thus able to absorb a very high amount of energy during the growing cycle, which is violently released by implosion of the bubble - local temperatures and pressures up to 5000 K and 100 bars are possible. Implosion leads to shock

waves that may erode or break the CNC agglomerates. Sometimes, a cavitation "microjet" (jet induced by a small bubble collapse) is also formed near a solid boundary but only particles smaller than 200 μm will be affected [120, 190].

Batch ultrasonication protocols have recently been optimized and better understood for CNCs dispersion in water [173, 174]. These works demonstrated that the most efficient probe position is off-centered, in the upper part of the tank. Moreover, CNC addition must be carried out carefully to avoid gelation on the surface or on the container walls (half the desired water is added before the CNC powder, followed by the remaining water content). However, sonicating larger suspension volumes leads to increasing dead zones, this process must be thus limited to small quantities (~60 mL maximum [173]). This dead zone problem is accentuated for more viscous media, as the size of active region below the probe is decreased. However, being able to work at a much larger scale is essential to tackle industrial applications. Increasing the probe size may not be efficient as higher power is needed to provide the same intensity in a larger probe [193]. Moreover, a higher power will lead to important mechanical, electrical and heat losses, impacting the efficiency of the process. Large probes are thus usually limited to smaller amplitudes. Industrial Sonomechanics (a firm specialized in ultrasonic technology) suggests a barbell horn to overcome this problem, able to treat volumes larger than 2 L, but remains around 5 times more expensive that the traditional probe [145, 146]. To the authors' knowledge, two other solutions are currently offered at a varying cost based on ultrasonication probe technology. In the first case, the suspension to be dispersed flows in a pipe and several sonication probes are set up in series or in parallel [145]. This process increases the residence time of the suspension in active dispersion zones without increasing the overall process time. The second case is a continuous flow ultrasonication: the fluid is recirculated using a pump between a tank and a flow cell in which ultrasonication is applied. This method has been proven to be more efficient than batch sonication, both in terms of energy and time [143, 144]. In all cases, however, an external validation procedure is required to confirm the dispersion state.

In-line measurements could thus be relevant. A useful technique has been patented to extract the properties of a power-law fluid under laminar flow (flow and consistency index n and m, process viscosity μ_{pr}) through two static mixers [210, 211]. This method is based on the Metzner-Otto concept that will be detailed in Section 6.2.8 [212].

Well dispersed CNCs may then be further used to prepare Pickering emulsions, achieve surface modification or solvent exchange. For example, Khandal et al. carried out polyethyleneimine (PEI) physical adsorption surface modification by adding PEI to CNC aqueous suspensions during ultrasonication. The PEI's charged amine groups were successfully electrostatically bounded to the charged sulfate groups of CNC after adequate dispersion of the particles in aqueous media [85].

Therefore, this work proposes a method to disperse larger volumes of CNCs using in-line validation. After presenting our setup composed of a semi-continuous system allowing for recirculation between a small ultrasonication vessel and a larger tank, in-line pressure measurements are used to determine the dispersion state. External conductivity and rheology are employed afterwards to validate our conclusions. Then, process viscosity is extracted from the pressure measurements, allowing confirmation of the dispersion state without external experiments. Finally, surface modification using PEI is performed to demonstrate the expanded potential of this work.

6.2 Methodology

6.2.1 Materials

CNCs, derived from sulfuric acid hydrolysis and neutralized by a sodium counterion, were supplied in a spray-dried form by Celluforce. Their density is around 1540 $kg.m^{-3}$ and their sulfur over carbon S/C atomic ratio is ~0.0057 [12] or 211 $mmol.kg^{-1}$.

Branched PEI was purchased from Sigma-Aldrich. It has an average molecular weight of 25,000 $g.mol^{-1}$, a polydispersity of 2.5 and a density of 1030 $kg.m^{-3}$ at 25 ˚C.

6.2.2 Semi-continuous setup

Figure 6.1 depicts the semi-continuous setup. A 250 mL beaker (beaker A) is plugged to a pump (Hffheer – 5 V water pump – 120L/h flow rate) and used to mix CNCs coarsely in water and help the particle wetting process. This pump recirculates a portion of the fluid back to beaker A. The other part goes to a small 100 mL beaker (beaker B) using a peristaltic pump (Cole Parmer Master Flex model no. 7520-35 with the head model no. 7016-20 and Masterflex 96400-

16 tubing) to control the flow rate. The ultrasonic probe (Cole-Parmer - CP505, 20 kHz with a 12.7 mm probe) is immersed in beaker B (process details may be found in Section 6.2.3). The sonicated fluid is sent back to beaker A using a second identical peristaltic head (mounted on the same pump to ensure an identical flow rate). This stream is monitored through two gauged pressure sensors (NPX - MPXV7002GP, calibrated as explained in Supplementary information C.2). A static mixer is installed between the two pressure sensors to increase the pressure drop. This static mixer is a 3D-printed model equivalent to a KM-Kenics mixer with helical elements, each rotating 90˚ from the previous one (Figure C.3). The pressure sensor data are acquired with an Arduino board and a LabView interface. The tubes (Tygon ND-100-65) present an internal diameter *D* of 4.8 mm (3/16").

A cooling system (blue area in Figure 6.1) was added around beaker B and before the first pressure sensor with 5 ˚C water circulation to prevent overheating. The temperature in the system was stable at 35 ˚C. Moreover, an air filtration system (Dri-Eaz DefendAir HEPA) is employed during CNC addition for safety issues.

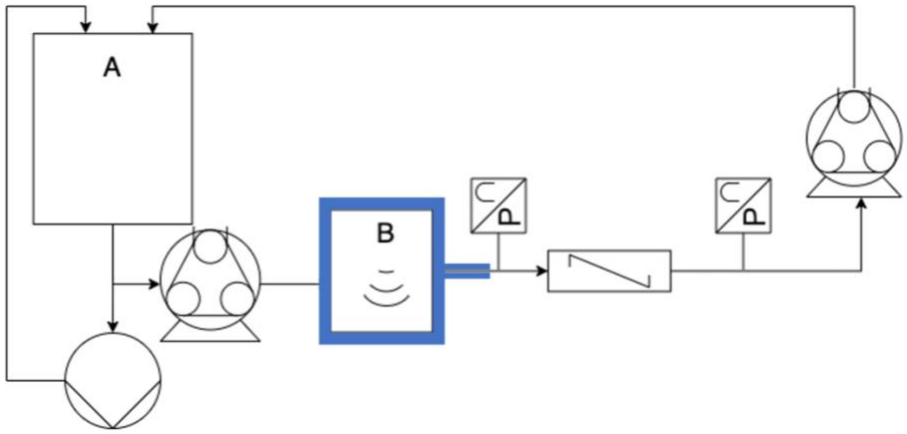

Figure 6.1: Semi-continuous setup schematic where A is a 250 mL beaker, B a 100 mL beaker and P the pressure sensors. Blue area corresponds to the cooling system.

6.2.3 CNC suspension preparation

In a previous article [173], we demonstrated that 167 $kJ.g^{-1}.L^{-1}$ (grams of CNC and liter of suspension) were necessary to achieve a well-dispersed CNC suspension in a 60 mL batch

process. This required the probe to be placed at 1/3 of the total volume height and off-centered such that r/R=0.3 (where r is the probe position and R the beaker radius). Moreover, the necessary power was set to 65 W, balancing ultrasonication efficiency with the time needed to complete dispersion. These guidelines (power and probe position) have been followed in this work for a total volume of 200 mL. Three concentrations (1.6 wt%, 3.2 wt% and 4.8 wt%) have been tested. They are named respectively CNC-1.6, CNC-3.2 and CNC-4.8 (Table 6.1). The CNC addition rate has been set around 30 mg/10 s to ensure time for wetting and avoid exaggerate agglomeration. Accordingly, the flow rate Q controlled by the peristaltic pump has been set such that the residence time t_R in beaker B is half the one required to disperse the same amount of CNC in a batch process t_{R*}. Indeed, if $t_R = 0.5t_{R*}$, and $Q = 3.8*10^{-7}$ $m^3.s^{-1}$, the concentration of CNC in beaker B will reach up to 0.725 wt% if no stagnant zone is assumed during one cycle (9 minutes, corresponding to the CNC addition time for CNC-1.6), which is half of the CNC-1.6 concentration. Further addition increases proportionally the concentration. Even if the CNC concentration gets higher by homogenization after the end of CNC addition, CNCs would have already been mostly de-agglomerated. The dispersion state is monitored with the pressure drop values – when it reaches a plateau, the suspension is considered well-dispersed.

It must be noted that ultrasonication was used in a pulse mode (8 s ON - 2 s OFF) to avoid excessive damage of the probe as the treatment is quite long.

Table 6.1: CNC suspension parameters.

Name	**Concentration (wt%)**	**Addition time (min)**
CNC-1.6	1.6	9
CNC-3.2	3.2	18
CNC-4.8	4.8	27

For comparison purpose, the same concentrations have been prepared using a batch process and are noted CNC-1.6*, CNC-3.2* and CNC-4.8*. All dispersion parameters were kept the same except the volume which was 60 mL in the batch process. The final dispersion state is achieved when applying 167 $kJ.g^{-1}.L^{-1}$, as per [173].

6.2.4 Newtonian and power-law fluids preparation

Newtonian and power-law fluids are prepared to validate the experimental setup's parameters as they have predictable behaviors. Thus, three glycerol-water solutions are made from Omnipur Glycerol (Calbiochem) at 65, 67 and 70 wt% (respectively Glyc-65, Glyc-67 and Glyc-70) to generate Newtonian fluids. In addition, the required amount of xanthan gum (Keltrol SF, CP Kelco) was stirred for 12 hours in water to prepare 0.09, 0.11 and 0.14 wt% solutions (respectively XTN-0.09, XTN-0.11, XTN-0.14). These solutions are known to present a power-law behavior. The glycerol and xanthan gum solution properties (Table 6.2) were characterized by the protocol described in Section 6.2.5. The corresponding rheological curves are presented in Figure C.1 and Figure C.2.

Table 6.2: Newtonian and power-law fluid properties

	ρ (kg.m^{-3})	**μ (mPa.s)**		**ρ (kg.m^{-3})**	**n**	**m (Pa.s^n)**
Glyc-65	1179.3 ± 0.1	17.41 ± 0.06	XTN-0.09	1000	0.548	0.101
Glyc-67	1183.3 ± 0.4	20.05 ± 0.07	XTN-0.11	1000	0.532	0.129
Glyc-70	1192.0 ± 0.4	24.19 ± 0.08	XTN-0.14	1000	0.512	0.165

6.2.5 Experimental validation of dispersion state

The dispersion state may be easily evaluated by measuring the electrical conductivity of the suspension. Indeed, the ionic charges, which are present on the CNC surface due to the sulfate half ester groups, are released during sonication as the CNCs are individualized [58]. The conductivity value will increase accordingly until a maximum is reached. A baseline has been defined for batch conditions in our previous work [173] and is reported in the following section as targeted value for the semi-continuous setup. The conductivity is measured using an Oakton device (CON 6+) after observing a plateau of the pressure drop values to confirm that the well-dispersed state for the given concentration has been obtained. These measurements are carried out in both beakers A and B to confirm the homogeneity of the dispersion.

All suspensions have been further analyzed using rheology to validate that the final dispersion state was the same as with a batch method. For this purpose, an Anton-Paar rheometer (MCR501) was used with a double Couette flow geometry. All tests were conducted at 25 ˚C

unless specified otherwise. A pre-shear was applied for 100 s at 10 $s^{-1,}$ followed by a 180 s rest time. Then the dynamic viscosity was measured with a shear rate sweep from 500 s^{-1} to 0.5 s^{-1}.

Finally, the densities of the glycerol solutions were measured using the Anton-Paar densimeter (DMA 4500M).

6.2.6 Numerical modeling

The fluid flow was modeled by the finite element COMSOL Multiphysics solver (version 5.5) to validate experiments and provide additional insight. The simulation considers a pipe diameter D, and a flow rate Q defined in Section 6.2.3. The static mixer has been modeled using the dimensions from Figure C.3 and is placed at the same position as in the actual continuous setup, 5 cm after the first sensor. The distance between both sensors is L = 25 cm. Finally, the relative pressure at the entrance of the pipe is set to 381 Pa referring to the actual hydrostatic pressure. The fluid employed for the simulation part correspond to the Newtonian fluid Glyc-65 and the three power-law fluids (XTN-0.09, XTN-0.11, XTN-0.14) defined in Section 6.2.4). The Reynolds number for the power-law fluid Re_{PL} is defined as:

$$Re_{PL} = \frac{\rho v^{2-n} D^n}{m} \tag{6.1}$$

with v the fluid velocity and D is the pipe diameter. Reynolds number calculations (Table 6.3) confirms a laminar regime (such as Re <10).

Table 6.3: Reynolds number

Fluid	Re
Glyc-65	6.9 ± 0.2
XTN-0.09	5.1 ± 0.2
XTN-0.11	4.2 ± 0.2
XTN-0.14	3.5 ± 0.2

Thus, using a laminar flow study in COMSOL, the Navier-Stokes equations are solved for an incompressible medium:

$$\rho(\boldsymbol{v} \cdot \nabla)\boldsymbol{v} = \nabla\left[-2pI + \mu\left((\nabla \boldsymbol{v}) + (\nabla \boldsymbol{v})^T\right)\right] \tag{6.2}$$

with p the fluid pressure and ρ and μ respectively the fluid density and Newtonian viscosity, assuming that the continuity equation is valid, defined by:

$$(\nabla \cdot \boldsymbol{v}) = 0 \tag{6.3}$$

In the case of non-Newtonian fluid following a power-law, μ is replaced by the dynamic viscosity η:

$$\eta = m\dot{\gamma}^{n-1} \tag{6.4}$$

in which $\dot{\gamma}$ is the shear rate.

6.2.7 Entry pressure estimation

The presence of a static mixer between the two sensors may imply an entry pressure ΔP_e that may be taken into using Bagley correction. To ease our calculations, we have kept the Newtonian model fluid (Glyc-65), with its corresponding viscosity and density. The flow rate is the same as for the CNC dispersion process, giving a laminar regime.

The wall stress τ_w may be determined by:

$$\tau_w = \mu\dot{\gamma}_e \tag{6.5}$$

with $\dot{\gamma}_e$ the effective shear rate. Then this wall stress is defined by:

$$\tau_w = D\left(\frac{\Delta P - \Delta P_e}{4L}\right) \tag{6.6}$$

where L is the pipe length and ΔP and ΔPe are respectively the pressure drop and the entry pressure.

6.2.8 Metzner and Otto concept

To calculate the in-line viscosity, it is possible to use the Metzner and Otto concept, which has been developed in the context of mechanical (impeller) stirring in the laminar regime, linking $\dot{\gamma}_e$ and the rotational speed N in the tank [210-212], using:

$$\dot{\gamma}_e = K_s N \tag{6.7}$$

where K_s is a geometry-dependent constant. This concept has been extended to static mixing, where the rotational speed is replaced by the characteristic fluid velocity in the pipe of characteristic dimension D:

$$\dot{\gamma}_e = K_s \frac{v}{D} \tag{6.8}$$

The constant K_s may then be calculated using the rheological properties of two power-law and Newtonian fluids, and the related pressure drops in the pipe $\Delta P_{(n)}$ and ΔP, respectively:

$$K_s = \frac{D}{v}\left[\frac{\Delta P_{(n)}}{\Delta P}\frac{\mu}{m}\right]^{\frac{1}{n-1}} \tag{6.9}$$

In this work, the constant K_s was determined for our system using the Newtonian and power-law fluids defined in Section 6.2.4, flowing in a laminar regime.

The power number, N_p, is known to be linked to the Reynolds numbers, Re and Re_{PL} (defined by equation (6.1)), for the Newtonian and power-law fluids, respectively, using the following relations:

$$K_p = N_p Re \tag{6.10}$$

$$K_{p(n)} = N_p Re_{PL} \tag{6.11}$$

where K_p and $K_{p(n)}$ are the so-called power constants, which depend on the static mixer geometry and power-law index n:

$$K_p = \frac{\Delta P D^2}{\mu L v} \tag{6.12}$$

$$K_{p(n)} = \frac{\Delta P_{(n)} D^{n+1}}{m L v^n} \tag{6.13}$$

Once they have been determined from experimental data, these constants can then be used to calculate K_s from equations (6.7), (6.11) and (6.12):

$$K_s = \left(\frac{K_{p(n)}}{K_p}\right)^{\frac{1}{n-1}} \tag{6.14}$$

This value for K_s can be compared with the one obtained for an empty tube (no static mixer) K_s' (calculations developed in Supplementary information C.1), defined by:

$$K_s' = \frac{6n+2}{n} \tag{6.15}$$

Finally, the so-called process viscosity μ_{pr} for a power-law fluid, which is related to the Metzner and Otto concept, may be obtained from:

$$\mu_{pr} = m\left(\frac{K_s Q}{D^3}\right)^{n-1} \quad (6.16)$$

6.2.9 Surface modification with PEI

To expand the range of application for the experimental setup, surface modification on dispersed CNCs has been carried out. PEI was used for this purpose following the guidelines from Khandal et al. [85]. They observed indeed that ultrasonication was mandatory during PEI addition to prevent phase separation. A 1 wt% PEI solution was prepared by stirring the required amount of PEI in water at 50 ˚C for 30 min. After obtaining a 3.2 wt% CNC suspension with the previous protocol (CNC-3.2), this PEI solution was added dropwise in beaker B while ultrasonication was running to obtain (CNC/PEI-3.2). Sonication was maintained until a stable pressure drop value was obtained. To ensure that this additional ultrasonication treatment did not alter the CNCs, a reference experiment was conducted the same way without any PEI (CNC/noPEI-3.2). All preparation parameters are reported in Table 6.4.

Table 6.4: PEI addition parameters.

Name	**CNC concentration (wt%)**	**PEI concentration (g/gCNC)**	**Additional ultrasonication treatment time (s)**
CNC-3.2	3.2	-	-
CNC/noPEI-3.2	3.2	-	968
CNC/PEI-3.2	3.2	0.01	920

X-ray photoelectron spectroscopy (XPS) was employed on freeze-dried unmodified and modified CNCs to identify the presence of nitrogen. The instrument (XPS Axis UltraDLD, Kratos) was used with a monochromatic anode (225 W) and a charge neutralizer. The analyzed surface was 700*300 μm with a depth < 10 μm.

6.3 Results and discussion

6.3.1 Pressure drop measurements

The pressure drop has been calculated from the values obtained for each sensor as explained in Supplementary information C.2. The raw data exhibited important oscillations resulting from several elements, namely the peristaltic pump. At the operating flow rate, the

periodicity of the pump is ~2.23 s. As data values are acquired each 0.1 s, it was possible to filter some of the noise by determining a moving average on 22 points. Therefore, the standard deviation presented in this paper only considers the setup sensitivity, neglecting pump variation. Other components of the setup, like the tubes which may be slightly flexible, as well as the sensor sensitivity indicated by the manufacturer, generate additional noise on the signal. It must also be noted that ultrasonication lead to bubble formation which, when transported into the tubes, induced measurable pressure fluctuations.

At t=0, the sensors only measure water and the values should be the same in all experiments. In our case, a slight variation has been observed which may be due to the sensitivity of the setup and the fact that water leads to a transitional-turbulent regime (Re = 102). Therefore, the pressure drop values have been normalized such as this initial value is around 0.

Figure 6.2 depicts the pressure drop measurements during the dispersion of the CNCs at 3 different concentrations. For each concentration, a plateau is observed after 13, 24 and 34 minutes respectively for 1.6, 3.2 and 4.8 wt% as reported in Table 6.5 (when the pressure drop oscillates around the same value ± 0.5 kPa for ~300 s). Additionally, whereas the pressure drop increases steadily for 1.6 and 3.2 wt% suspensions, an overshoot is seen with the highest concentration before reaching the plateau value. This may correspond to the dispersion homogenization time, more apparent at higher CNC loadings, with a higher local concentration.

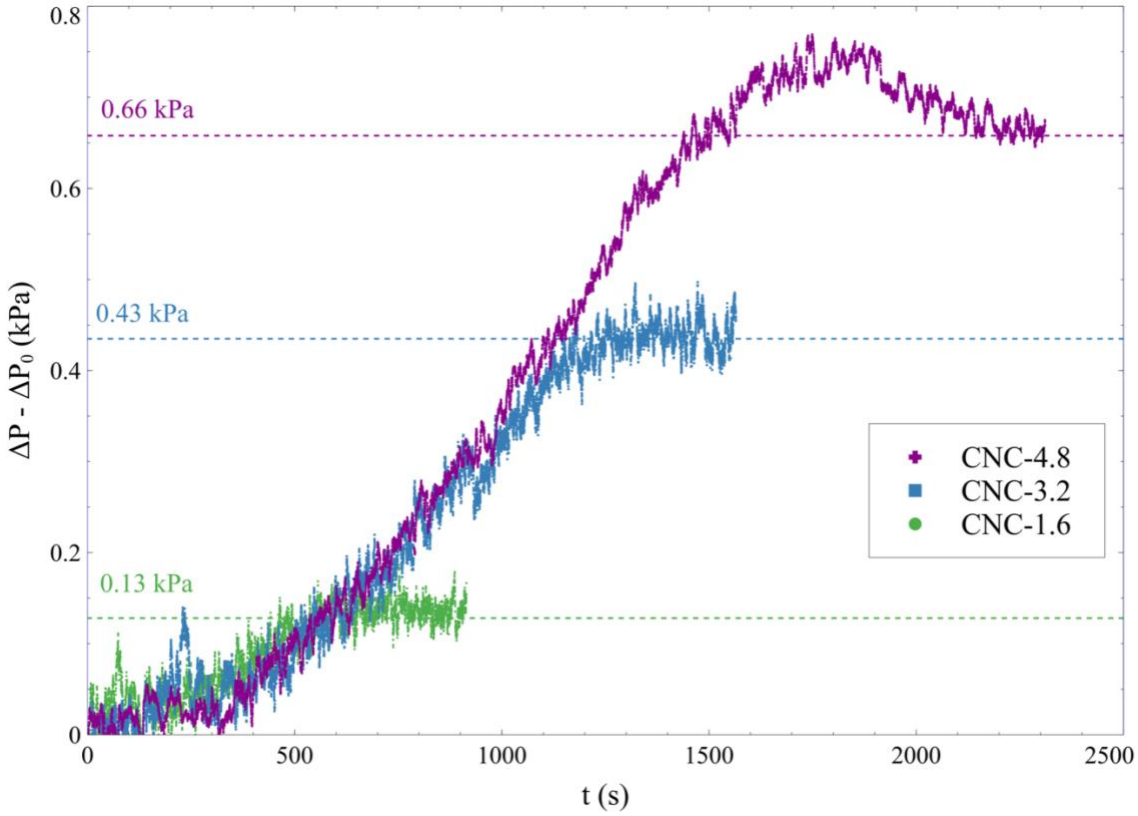

Figure 6.2: Pressure drop normalized by the initial value (water) of CNC suspensions as a function of process time. CNCs are added during the first minutes, and ultrasonication is initiated after 120 s.

Table 6.5 reports the overall energy applied to reach the final dispersion state. The ultrasonication energy is decreased by almost 2/3 compared to batch conditions (60 compared to 167 $kJ.g^{-1}.L^{-1}$). The energy brought by the pump is negligible in comparison, as it represents 10^{-5} times the ultrasonication energy. This gain in energy is mainly attributed to the gradual addition of CNCs in the beaker A, as the amount of CNCs to be dispersed at a given time becomes much lower than in batch. Moreover, the flow added by the peristaltic pump in beaker B provides additional beneficial mixing. Although the change from continuous sonication (reference scenario) to pulsed mode (current case) was considered in the calculations, it may slightly impact the efficiency as well.

Table 6.5: Dispersion parameters.

Name	Total dispersion time (min)	Ultrasonication energy ($kJ.g^{-1}.L^{-1}$)	Pump energy ($J.g^{-1}.L^{-1}$)
CNC-1.6	13	60	0.9
CNC-3.2	24	60	0.9
CNC-4.8	34	60	0.9

6.3.2 Dispersion state validation with external tools

Reaching a pressure drop plateau must imply that the best dispersion conditions have been reached, and this should be sufficient to monitor the dispersion state. However, additional validation experiments could confirm that there is no loss of CNCs in the setup, or that its efficiency is not limited. For this purpose, conductivity and rheology have been used (Figure 6.3).

Figure 6.3a) plots the measured conductivity at the three studied concentrations obtained for the final dispersion state with the semi-continuous setup. The batch measurements are reported as a comparison. The targeted values have been reached for all concentrations, implying that the CNCs have indeed been well dispersed.

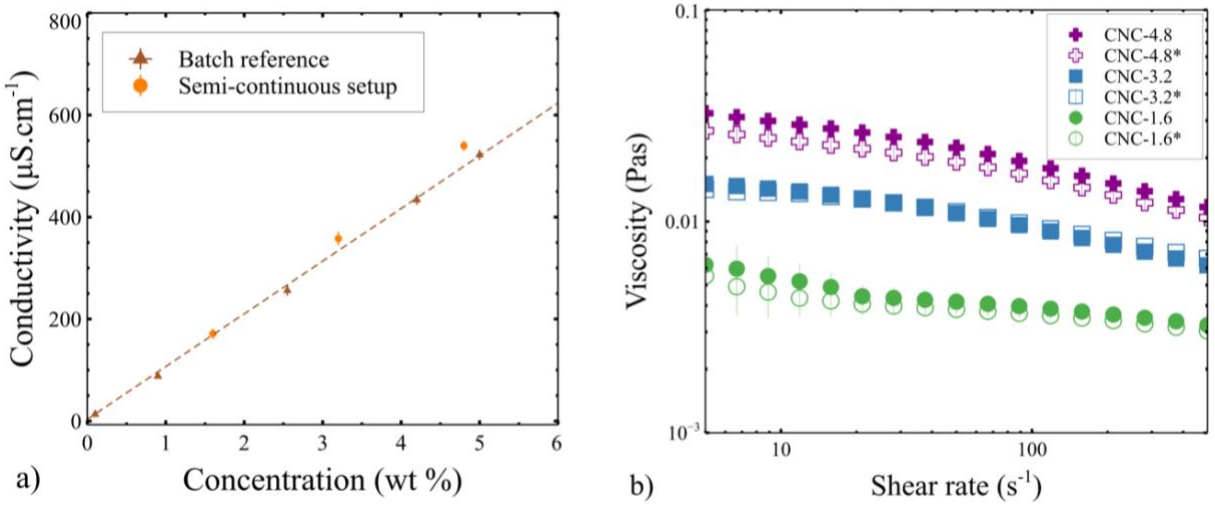

Figure 6.3: a) Conductivity as function of CNC concentration. Standard deviations are represented by vertical lines for the semi-continuous setup and is ± 10 µm for the batch reference. b) Viscosity of CNC ultrasonicated suspensions as function of shear rate (V = 60 mL, P = 65 W, E = 167 kJ.g-1.L-1) obtained either using a batch process (empty symbols) or the semi-continuous setup (full symbols). Standard deviations are represented by vertical lines.

Figure 6.3b) demonstrates that the viscosities as function of shear rate are the same for both dispersion methods. The highest concentration gives the largest difference between the batch and the semi-continuous path, while remaining within the standard deviation range. This may be explained because this concentration is close to the gel point (around 5 wt% [69]), where the viscosity is more time dependent. A slight delay between the preparation and the measurements may have impacted the results. Nevertheless, these measurements confirm that the desired dispersion state has been obtained.

6.3.3 Dispersion state validation using in-line measurements

While pressure drop measurements may give enough information to conclude on adequate dispersion state, additional analysis can provide more direct insight into the viscosity of the system, without the need for external validation.

6.3.3.1 Effective shear rate and entry pressure

The numerical modeling of the tube between the pressure sensors described in Section 6.2.6 provides an estimation of several flow parameters for a 65 wt% glycerol solution (Glyc-65). Accordingly, the effective shear rate obtained by modeling $\dot{\gamma}_e$ is 52.5 s^{-1}. In addition, it comes from the pressure profile (Figure C.5) that the pressure drop ΔPm between the two sensors is 0.915 kPa. We must note that this value is determined by point estimation (rather than surface average) as the sensors measure the pressure locally in our setup. The experimental value ΔPexp for the same fluid is 1.4 ± 0.1 kPa, which is higher than the prediction. It may be due to additional effects not considered in the simulation, such as the pulsing of the peristaltic pump.

In both cases, it is then possible to quantify the entry pressure using equations (6.5) and (6.6) (Table 6.6). For the purposes of these calculations, the $\dot{\gamma}_e$ value retained is extracted from the simulation – this value will be validated experimentally in Section 6.3.3.2. A higher total pressure drop value is measured experimentally (ΔP_{exp}) leading logically to a higher entry pressure, compared to the modeling value (ΔP_m).

Table 6.6 : Entry pressure estimation for Glyc-65.

	Modeling	**Experiment**
μ **(mPa.s)**	17.41 ± 0.06	-
$\dot{\gamma}_e$ **(s^{-1})**	52.5	-
τ_w **(Pa)**	0.914	-
ΔP_m **or** ΔP_{exp} **(kPa)**	0.915	1.4 ± 0.1
ΔP_e **(kPa)**	0.723	1.2 ± 0.1

Nevertheless, modeling and experiments lead to the same conclusion: the entry pressure is considerable ($\Delta P_e/\Delta P_{exp}$ = 86%). One solution that will diminish the impact of this entry pressure is to increase the distance between the two sensors. However, by doubling the distance, the result remains unacceptable (for L = 59.4 cm, $\Delta P_e/\Delta P_{exp}$ = 76%), and a longer tube will cause practical problems (i.e. increased volume in tubing). In addition, this effect is fluid dependent, so it is challenging to predict. For all these reasons, the pressure drop measured by the sensors cannot directly provide a viscosity value simply using capillary flow analysis.

6.3.3.2 Process viscosity

However, using equation (6.16) defined in Section 6.2.8, it is possible to determine the process viscosity depending only on the setup geometry. To do so, the Newtonian and power-law fluids stated in Section 6.2.4 are introduced in the semi-continuous setup, and the pressure drop is measured at different flow rates (Figure C.6).

Using equations (6.12) and (6.13), the constants K_p and $K_{p(n)}$ were calculated (Table 6.7). As expected, $K_{p(n)}$ depends on n whereas K_p is constant for all the Newtonian fluids considered. K_s was then deduced from these results using equation (6.14), with an average value of all glycerol solutions for K_p. For this system, $K_s = 12$. K_s' is also calculated for a comparison purpose: $K_s > K_s'$ as the static mixer implies additional shear in the pipe.

Table 6.7: Metzner and Otto analogy calculations using Newtonian and power-law fluids.

	n	K_p or $K_{p(n)}(10^1)$	K_s	K_s'
Glyc-65	1	33 ± 7	-	
Glyc-67	1	34 ± 6	-	8.0
Glyc-70	1	30 ± 4	-	
XTN-0.09	0.548	11 ± 3	11 ± 10	9.7
XTN-0.11	0.532	10 ± 3	12 ± 10	9.8
XTN-0.14	0.512	9 ± 2	13 ± 10	9.9

It is important to note that for the 65 wt% glycerol solution, this value of K_s gives an average effective shear rate of $\dot{\gamma_e} = 53 \pm 50\ s^{-1}$ with equation (6.8) and $Q = 3.8*10^{-7}$ m^3.s^{-1}. Therefore, even if the standard deviation is high due to the sensor sensitivity, the simulation gives a similar result (52.5 s^{-1}), confirming the reliability of the method. Moreover, the effective shear rate for the corresponding empty tube is 44 s^{-1}. This agrees with the fact that adding a static mixer in the pipe leads to additional obstruction and more shear.

An additional validation has been performed using the numerical modeling presented in Section 6.2.6 on each power law fluids and Glyc-65. The pressure drop was estimated and K_s was obtained with equation (6.9). For this system, $K_s = 18$ which confirms again the consistency of our results, being in the same order of magnitude as the experimental value.

Once our system parameters were clearly defined, the same method was applied for the CNC suspensions. The 3.2 wt% concentration is here chosen as an example. As a reference, the same concentration obtained in batch (CNC-3.2*) was characterized at 35 ˚C using rheology. The

CNC suspension does not display a power-flow behavior over the entire shear rate range. Thus, while the shear rate in the tube is not constant, the average value determined above (53 s^{-1}) is used to obtain the parameters *n* and *m* and the targeted viscosity reported in Table 6.8 (see Figure C.7 for the rheological data).

Table 6.8 : Rheological properties of the 3.2 wt% CNC suspension obtained in batch

	n	**m**	**η (mPa.s) at 53 s^{-1}**
CNC-3.2*	0.767	0.0212	8.4 ± 0.1

Then, $K_{p(n)}$ was calculated using the pressure drop that was obtained at the end of the dispersion using the semi-continuous setup for CNC-3.2 (ΔP-ΔP_0 = 0.43 kPa). Next, K_s was estimated, leading to the process viscosity (equation (6.16)). All results are presented in Table 6.9. We may note that the standard deviation is quite large, considering the pressure sensor sensitivity. However, the modeling comparison in this section has demonstrated the reliability of the method.

Table 6.9: Process viscosity calculation for the 3.2 wt% CNC suspension

Dispersion time	**ΔPn (kPa)**	**$K_{p(n)}$ (10^1)**	**K_s**	**μ_{pr} (mPa.s)**
24 min	0.7 ± 0.1	18 ± 5	11 ± 20	9 ± 70

At the same shear rate, the dynamic viscosity of CNC-3.2* obtained using rheology is close to the value determined experimentally, which confirms that the final dispersion state at 24 minutes is the desired one. Note that in case of a bad dispersion, it would have given a different value of K_s even if *m* and *n* from CNC-3.2*, considered as an optimal dispersion, are used It must be emphasized that this could be obtained without external validation. Such a process viscometry method can thus be transposed to a variety of fluids or concentrations with the same setup, provided initial in-line measurements on known fluids are conducted, as it is mainly dependent on geometry.

6.3.4 Surface modification

6.3.4.1 PEI addition

PEI addition was monitored via pressure measurements. Figure 6.4 illustrates the pressure drop values as function of dispersion time. Below 1570 s is the initial dispersion stage and the red

line in the figure separates it from the PEI addition step. As expected, the addition of PEI leads to a fast increase of the pressure drop (see CNC/PEI-3.2) due to the viscosity increase. The CNC dispersion undergoing the same sonication without PEI addition (CNC/noPEI-3.2) shows a pressure drop oscillating around the plateau value (0.43 kPa) reached after the final dispersion state. This confirms that no further change is made on the CNC dispersion with the additional ultrasonication time.

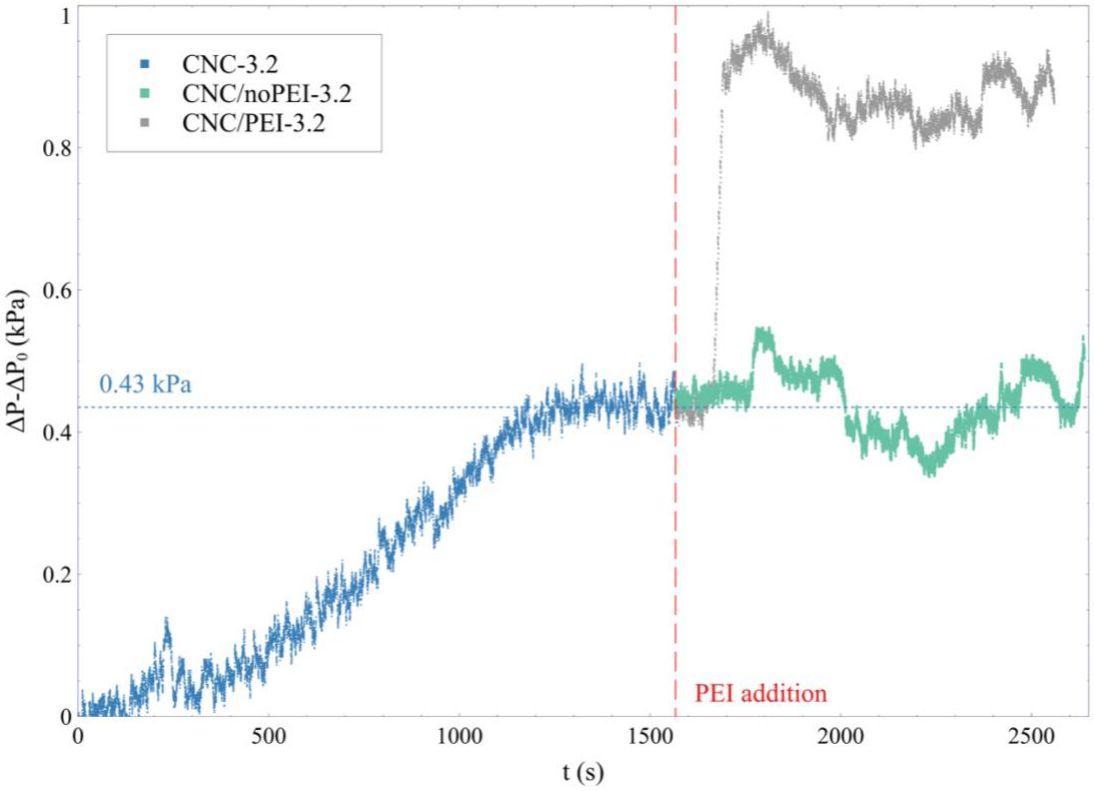

Figure 6.4: Pressure drop of CNC suspensions as function of process time. CNCs are added during the 60 s, and ultrasonication is started after 120 s. At t=1570 s, the CNC dispersions are further ultrasonicated with or without PEI addition.

The ultrasonication energy applied to complete the PEI addition was based on the work of Khandal et al. [85] who was working in a batch mode. Because the semi-continuous setup provides a gain of efficiency, only 36% of the suggested energy amount has been applied. Yet, no drastic change is observed on ΔP after the first five minutes following the addition. The purpose of this experiment was to prove that our setup could be used for CNC modification. However, an optimization study on the ultrasonication energy needed in this step may be relevant.

Figure 6.5 depicts the viscosity of the different suspensions as function of shear rate. The results confirmed what was observed in Figure 6.4: the CNC suspension with additional ultrasonic energy but no PEI (CNC/noPEI-3.2) presents the same viscosity as the initial CNC suspension (CNC-3.2). A slight increase in viscosity is noted for the modified CNC suspension (CNC/PEI-3.2 (fresh)) when analyzed just after the dispersion. After 13 days, this suspension demonstrates a shear thinning behavior, typical of a gel-like suspension. This rheopexy concurs with Khandal et al.'s observations [85], validating the success of the PEI physical adsorption on CNCs. Additionally, XPS analyses has been carried out to confirms nitrogen presence at 0.3%, close to the theorical value of 0.32% (Figure C.8).

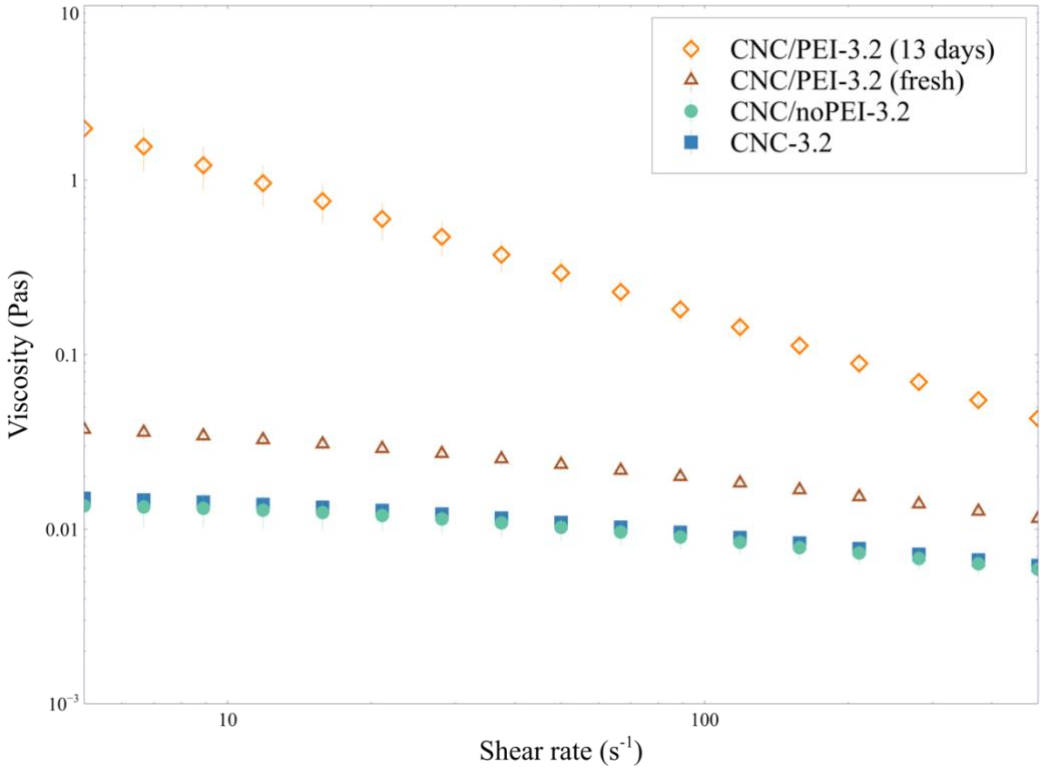

Figure 6.5: Viscosity of CNC ultrasonicated suspensions as function of shear rate (V = 60 mL, P = 15 (65) W, E = 167 kJ.g-1.L-1) after dispersion or with further ultrasonication with/without PEI addition.

6.4 Conclusion

The semi-continuous setup used in this work offers a successful method to adapt the optimized batch ultrasonication procedure to larger volumes using standard probe. By

maintaining the volume directly exposed to ultrasonication the same as what was suggested in a smaller batch (60 mL), continuously fed by a larger to-be-dispersed volume, it was possible to achieve a well-dispersed state with an excellent gain in energy efficiency (64% less energy than required in batch). This approach provides the additional asset of working with an ultrasonication probe without additional significant infrastructure costs. Pressure sensors provided direct information on the dispersion state with a simple in-line measurement read-out: a stable value implying the final state has been reached. However, through a more in-depth analysis, it is also possible to extract the process viscosity, confirming that the desired CNC dispersion has been reached without additional analyses validation or sampling. Thus, this ensures for example that no CNCs have remained stuck on the tank wall. This method may then be applied to different systems as long as the setup parameters are known. The dispersion state may also be quantified by conductivity, but contrary to the pressure measurements and viscosity estimation, this technique can only be used in case of charged particles (such as CNCs). We have further shown that this setup can be used for surface modification, using the example of PEI adsorption.

This work may be adapted at other scales, especially since the constant K_s used for process viscosity calculation remains the same. Indeed, once the so-called Metzner and Otto constant Ks is known, it is possible to estimate the parameters n and m of any power-law fluid using an additional static mixer. It was however not the scope of the present work. Nevertheless, it would be interesting to study the shear rate values for different system dimensions and evaluate the limits of the comparison made between the viscosity obtained in rheology and the process viscosity. In addition to surface modification, the semi-continuous setup could also be exploited for other applications after validating the dispersion state, such as Pickering emulsion preparation. Finally, as the method does not depend on CNC properties, it is realistic to suggest that it may be used for other nanoparticle dispersion.

Acknowledgments

The authors are grateful for the National Science and Engineering Research Council of Canada (NSERC), namely its CRD and CREATE programs, Prima Québec and FPInnovations for their financial support. The authors also acknowledge Celluforce for providing the cellulose nanocrystals. Additionally, we would like to thank CREPEC for the expertise and infrastructure

access, and the Simulation-based Engineering Science (Génie Par la Simulation) group for scholarship support. Moreover, we would like to thank S. Chenard and M. Beaudoin for their help on the flow setup and the data acquisition system.

CHAPTER 7 GENERAL DISCUSSION

The main objective of this project – obtaining reproducible and validated well-dispersed CNC suspension with ultrasonication at various scales – has been successfully addressed in this thesis. The first article [173] (Chapter 4) answered the objective 1 (ultrasonic dispersion understanding and optimization), defined in Section 3.2. It was published in 2021 in *Ultrasonics Sonochemistry* and several works have been published afterwards relying on our findings [213, 214]. The second article [174] (Chapter 5) addresses the objective 2 (CNC dispersion state evaluation). It was also published in 2021 in *Ultrasonics Sonochemistry*. Finally, the objective 3 (dispersion of larger volumes with inline validation) was tackled in the third article (Chapter 6). It has been submitted to *Chemical Engineering Journal* in February 2022 and is pending peer review.

In this work, the ultrasonication protocol has been optimized for CNC dispersion in aqueous media for small and larger volumes of suspension. Whereas the dispersion state was not confirmed by micrography due to the limitations presented in Section 2.5.4, the viscosity measurements obtained with the optimal conditions are in accordance with those obtained by Beuguel et al. at 3 wt% [12]. In their work, they validated the adequate dispersion state using TEM. This observation also helped to confirm that the CNCs were not broken with this process. This should also be true for the semi-continuous setup as a lower sonication energy is applied. For higher concentration (6.4 wt%), our conclusion is based on the comparison with the never-dried suspension. While the same dispersion state must have been obtained based on the same rheological behavior, it must be pointed out that a “truly” individualized state at this concentration may not be achievable. The nanoparticles should indeed be densely packed.

In Chapter 4, the cavitation zone was estimated as a 0.96 cm high cylinder located under the probe for a fluid with a viscosity of 10 mPa.s. However, prior to applying this assumption, experimental attempts were conducted to visualize the cavitation zone and better understand how the particles behave during ultrasonication. Tests either using colorimetry [215] or sonoluminescence [141] were carried out. It was possible to observe the viscosity influence on the process and the cone shape of the cavitation zone (introduced in Section 2.5.2), using colored oil in water (Figure 7.1a and b). However, the cavitation phenomenon was too brief and the fluid velocity too large to be able to capture any relevant information without a high-speed camera. An

alternate idea was also explored: a particle presenting a density similar to that of water was prepared using the appropriate ratio of low-density polyethylene and stainless steel. This experiment aimed to visualize the fluid flow induced by ultrasonication without adding a contribution from the particle's buoyancy (Figure 7.1c). The particle motion was then captured with a digital image correlation technique. The resulting video was nonetheless unsatisfactory. Again, the camera definition was the main limitation, along with the loss of information due to the 2D images. With appropriate equipment, these experiments would merit reproduction to obtain additional validation of the numerical models presented in Chapter 4.

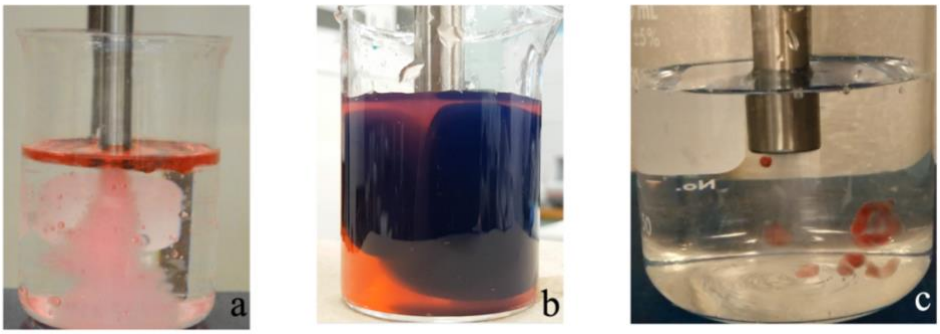

Figure 7.1: Visualization experiments: colorimetric method in a) a low viscosity or b) a highly viscous fluid. c) Particle tracking (images have been superimposed to observe the trajectory)

The optimal parameters obtained to disperse CNCs (off-centered probe placed near the surface in a small beaker (up to 60 mL), as determined in Chapter 4) are not the same as those reported by Son et al. for sonochemical reactions [141]. As introduced in Chapter 2, this may be explained by the differences underlying in the application. The requirement to obtain a "good" dispersion is to achieve a well-dispersed and a well-distributed state (see Chapter 5). For this purpose, it is necessary to minimize dead zones, which cannot be accomplished with a centered probe. In addition, Son et al. worked in a 500 mL vessel. Based on the conclusion that such a volume could not give optimal results, especially for more viscous fluid, we did not perform a study in a large beaker to confirm that our finding obtained for a 60 mL could be extrapolated. Rather, we opted for the coupled system described in Chapter 6. The probe manufacturer's guidelines for nanoparticle dispersion indicate to use the smallest beaker geometry possible, placing the probe halfway in the liquid. A magnetic stirrer should also be added for highly

concentrated suspension [216]. While it suggests that the efficiency issue is known, the protocol suggested in this thesis may increase the flexibility of the process.

We may note that only glass beakers were used for both the batch and semi-continuous setup. Thus, any vessel erosion was avoided. This should however be kept in mind for industrial scale-up.

Being able to observe CNCs at different stages of the dispersion without altering their positions would have been an asset for this project. Performing microscopy with a wet cell was considered, however no suitable device was found. Labeling CNCs with a fluorescent agent was deemed to not be the right approach, as the fluorescent tag could have modified their behavior (altering the surface charge of the particle, for example). Some preliminary experiments were carried out via small-angle light scattering (SALS) coupled with a rheometer (rheo-SALS). Though this technique was proven to give relevant information about CNC behavior in suspension, it would have required considerable time for a proper analysis, and it was beyond the project scope.

This PhD proposal was born from a joint project on the dispersion of CNCs in non-polar media, as explained in Chapter 1. While it does not explicitly address the original issue by focusing only on aqueous media, it answers several shortcomings highlighted in Chapter 2 that are necessary to work further with CNCs. A small study has been carried out on other polar solvents (DMF, DMSO) with a CNC concentration of 3.2 wt%. The objective was to find the optimal sonication energy based on rheology and conductivity, as described in Chapter 4 for water. Formamide and DMSO both resulted in stable suspensions. However, a higher energy than for water suspension seemed necessary (~300 $kJ.g^{-1}.L^{-1}$ for formamide instead of 167 $kJ.g^{-1}.L^{-1}$). Pure DMF lead to an unstable suspension, but this was overcome by adding 20 wt% water. All these behaviors were expected from the work of Bruel et al. [14]. Gelation occurred in the formamide suspension, its viscosity doubling over 100 min at 1 s^{-1}. DMSO should lead to the same phenomenon and a possible explanation is the desulfation of CNCs [13, 217]. However, during the ultrasonication process, a rapid increase in temperature was observed (to a greater degree than in aqueous suspension) with formamide. An exothermic reaction is suggested, which may be the hydrolysis of formamide into formic acid (which can induce desulfation [218]) and

ammonia [13, 219]. Due to the apparent complexity of the topic and lack of time, no further work has been done on this system.

Surface modification was briefly discussed in Chapter 6 using PEI. However, it would have been interesting to go further and obtain hydrophobic CNCs to be able to incorporate them in non-polar matrices.

Eventually, this whole study focuses on CNC dispersion but as mentioned several times in this thesis, it may certainly be applied to other nanoparticles. This would be interesting to demonstrate this idea, and study how this research may be adapted to them.

CHAPTER 8 CONCLUSION AND RECOMMANDATIONS

8.1 Original contribution

This thesis contributes important knowledge regarding the dispersion of CNC using sonication, knowledge that is necessary before considering further uses of these nanoparticles. While ultrasonication is commonly employed to handle the issue of particle agglomeration, this work proposes a more standardized method to ensure proper dispersion and distribution of CNCs in water. Optimal experimental parameters, determined by numerical modeling and validated by experimental analysis, allowed to maximize both mixing and dispersion efficiency. Namely, ultrasonication should be performed in a relatively small vessel (60 mL) and the probe must be placed off-centered at 1/3 in depth from the air/liquid interface. Conductivity (considering the case of sulfated CNC having ionic charges) and viscosity measurements helped to evaluate the optimal sonication energy needed to achieve a good dispersion. This value was estimated to E ~ 167 kJ per gram of CNC per liter of suspending media under batch conditions. An operating window is then proposed, displaying the influence of the probe depth and centering through a dispersion index related to the efficiency of the process. A value close to 1 is obtained with the suggested parameters (Article 1, Chapter 4).

These experimental guidelines lead to well-dispersed and well-distributed suspensions over a wide range of concentrations. Higher concentrations achieved by this method presented the same flow properties as never-dried suspensions. Furthermore, this targeted state has been properly defined and evaluated. Rheometry brought valuable information on the dispersion state as well as on the distribution. The CNC distribution (or homogeneity) may be obtained from the viscosity standard deviation, with appropriate precautions on the sampling volume being employed. The CNC dispersion (how well the particles are individualized) is characterized by the viscosity value. If the distribution is good, minimum viscosity values are expected for a complete dispersion, illustrating agglomeration breakage and electrostatic double layer thinning (Article 2, Chapter 5).

This understanding allows then to design a semi-continuous setup using the same sonication protocol while processing larger volumes. Different concentrations below the gelation limit were successfully prepared with 64% less energy than in batch mode. Moreover, inline

pressure measurements provide a direct evaluation of the dispersion state as stable values are anticipated when the final state is reached. An approach to determine the process viscosity from these pressure measurements is employed, confirming that the final state is the targeted one. The process viscosity may indeed be compared to the viscosity obtained in rheology at the same shear rate, which is the average of the "real" value in the setup. Though this was applied only to intermediate quantities (200 mL), higher scale may easily be achieved with the same approach. Finally, this setup can also be used for CNC surface modification, as was demonstrated using a polycationic surfactant, PEI (Article 3, Chapter 6).

8.2 Limits and recommendations

This thesis focuses on a specific application – ultrasonic dispersion of CNCs in water – and inhibits several effects that may occur when working under different conditions. First, changing the type of CNCs will affect the dispersion behavior that was observed in this study. A different cellulosic source, different extraction or drying conditions or different surface charge are known to alter the properties of the nanoparticles and their behavior in suspension. It would thus be interesting to test other kinds of CNCs and validate that the recommendations developed here may be easily adapted. Similarly, the findings herein could potentially be transposed to other nanoparticles, as agglomeration is a common issue when working with nanomaterials. The conductivity assessment is not relevant for neutral materials, but the rheological analysis should provide equivalent information. However, some modifications may be needed for a non-Newtonian fluid whose viscosity does not follow a power-law behavior. In any cases, a reference case with the desired dispersion state must be used to define the targeted viscosity and conductivity (if applicable) values. This desired dispersion state may not be when the CNCs are individualized as in this work. This objective should be adapted depending on the needed properties in the given application. In addition, it must be noted that working at a very low concentration (< 1.5 wt%) may be a limitation of the rheometry method to evaluate the dispersion and distribution state, as the rheometer demonstrated a weak accuracy at such concentration. This may skew any conclusion on the suspension homogeneity as the low sensitivity generates large standard deviation between samples. Nevertheless, this issue is easier to solve with the semi-continuous setup, choosing the appropriate pressure sensors (with the right sensitivity).

The suspending medium is also an important parameter. Water was chosen here as a basic and suitable solvent to disperse CNCs. Since the viscosity, density or sound velocity in the medium directly impacts the propagation of the acoustic waves, a different behavior must be expected in other media. Therefore, it could be relevant to test this approach with other solvents, as long as theory (such as Hansen solubility parameters) indicates that the retained solvents can disperse the nanoparticles selected. More specifically, the influence of viscosity on acoustic wave attenuation was underlined - this implies that all conclusions reported in this thesis are valid only up to a certain point. The viscosity could prove an even greater limitation in the semi-continuous configuration. Whereas a concentrated suspension giving a gel-like behavior was successfully obtained in batch, this is not recommended in the semi-continuous setup. Indeed, the local concentration may be much higher than the global targeted one, leading to pipe clogging. It would actually be relevant to determine the maximum achievable concentration for this system. Other dispersion techniques, such as high-pressure homogenization, should then be considered for highly viscous fluids.

The semi-continuous setup paves the way for dispersing large quantities of nanoparticles with a built-in validation approach. However, it has only been applied to 200 mL compared to 60 mL in batch. While this is still a considerable change, higher scales remain to be investigated. Treating larger quantities should be easily feasible as the volume subjected to ultrasonication can remain the same while the reservoir containing the undispersed nanoparticles may be larger. The volume limitation of this vessel should nonetheless be defined. For a too large volume, the pump will not be sufficiently efficient to convey the nanoparticles to the smaller beaker where ultrasonication is applied. A more powerful pump would then be needed, but its contribution in the dispersion process might be more significant (though it was demonstrated in Chapter 6 that the energy requirement for the pump was negligible compared to sonication). The tubing diameter may also have to be adjusted, with the appropriate flow rate. The Metzner and Otto concept can easily be adapted at any scale, so that the inline validation approach would still be relevant. Nevertheless, larger tubing implies a greater shear rate variability within - a second static mixer is then recommended to be able to determine the power-law parameters n and m of the unknown fluid. This would allow determining the apparent viscosity without external measurements as was done in this work. In addition, probe erosion may become an important

limitation for scale-up. While this problem was hindered in the semi-continuous setup by sonicating in pulsed mode, it would be relevant to look deeper at this issue to find suitable solutions.

In this work, the particle size measured are hydrodynamic diameters. These values could be refined by correlating with additional measurements (such as electron microscopy). In addition, while the sonication process should not break the CNCs based on previous work [12], additional characterization analyses such as X-Ray diffraction would help to confirm that the crystallinity remains unchanged.

Ultrasonication is the main technique used in most research labs. That is why it was employed in this study, beside the fact that its standardization was missing in the literature. However, high pressure homogenization is also an efficient method, especially for larger-scale applications. A comparison between both approaches may validate the advantages of one over the other. Assessments regarding their energy consumption and efficiency in terms of dispersion, at different scales, would be very valuable.

Dispersion is the first stage to benefit from CNC properties. Surface modification with PEI was achieved in Chapter 6, but a deeper study is needed. Using the semi-continuous setup developed here, it would be interesting to investigate its advantages regarding modification efficiency and homogeneity. Starting from a well-dispersed and distributed state should certainly lead to optimal conditions for the reaction to take place. This setup could also be employed to prepare Pickering emulsions, by suspending the nanoparticles in the first phase before progressively introducing the second phase while sonicating. Better control on the dispersion state may similarly be expected when producing a masterbatch or a suspension for solvent casting. Further experiments are required to confirm these assumptions.

REFERENCES

[1] B. E. C. Bogdanski, "The rise and fall of the Canadian pulp and paper sector," (in English), *Forestry Chronicle,* vol. 90, no. 6, pp. 785-793, Nov-Dec 2014, doi: DOI 10.5558/tfc2014-151.

[2] A. Dufresne, "Nanomatériaux cellulosiques," *Technique de l'ingénieur Bois et papiers,* vol. TIP590WEB, no. nm3490, 2015, doi: 10.51257/a-v1-nm3490.

[3] X. Qiu and S. Hu, ""Smart" Materials Based on Cellulose: A Review of the Preparations, Properties, and Applications," *Materials (Basel),* vol. 6, no. 3, pp. 738-781, Feb 28 2013, doi: 10.3390/ma6030738.

[4] H. Kargarzadeh, M. Mariano, D. Gopakumar, I. Ahmad, S. Thomas, A. Dufresne, J. Huang, and N. Lin, "Advances in cellulose nanomaterials," *Cellulose,* vol. 25, no. 4, pp. 2151-2189, 2018, doi: 10.1007/s10570-018-1723-5.

[5] A. Dufresne, "Cellulose nanomaterial reinforced polymer nanocomposites," *Current Opinion in Colloid & Interface Science,* vol. 29, pp. 1-8, 2017, doi: 10.1016/j.cocis.2017.01.004.

[6] C. Miao and W. Y. Hamad, "Critical insights into the reinforcement potential of cellulose nanocrystals in polymer nanocomposites," *Current Opinion in Solid State and Materials Science,* vol. 23, no. 4, 2019, doi: 10.1016/j.cossms.2019.06.005.

[7] S. A. Kedzior, V. A. Gabriel, M. A. Dube, and E. D. Cranston, "Nanocellulose in Emulsions and Heterogeneous Water-Based Polymer Systems: A Review," *Adv Mater,* vol. 33, no. 28, p. e2002404, Jul 2021, doi: 10.1002/adma.202002404.

[8] G. Delepierre, O. M. Vanderfleet, E. Niinivaara, B. Zakani, and E. D. Cranston, "Benchmarking Cellulose Nanocrystals Part II: New Industrially Produced Materials," *Langmuir,* vol. 37, no. 28, pp. 8393-8409, Jul 20 2021, doi: 10.1021/acs.langmuir.1c00550.

[9] "List of all the challenges." https://www.novacentris.com/nc/en/list-of-challenges-to-be-solved (accessed Februar 17, 2022).

[10] "The Nanocellulose Challenges Program a huge success." https://web.fpinnovations.ca/the-nanocellulose-challenges-program-a-huge-success/ (accessed Februar 19, 2022).

[11] "Dispersion of cellulose nanocrystals in non-polar matrices." https://www.novacentris.com/nc/en/fiche.php?todo=dl_defi&lang=en&def_id=1021164 (accessed Februar 17, 2022).

[12] Q. Beuguel, J. R. Tavares, P. J. Carreau, and M. C. Heuzey, "Ultrasonication of spray- and freeze-dried cellulose nanocrystals in water," *J Colloid Interface Sci,* vol. 516, pp. 23-33, Apr 15 2018, doi: 10.1016/j.jcis.2018.01.035.

[13] C. Bruel, T. S. Davies, P. J. Carreau, J. R. Tavares, and M. C. Heuzey, "Self-assembly behaviors of colloidal cellulose nanocrystals: A tale of stabilization mechanisms," *J Colloid Interface Sci,* vol. 574, pp. 399-409, Aug 15 2020, doi: 10.1016/j.jcis.2020.04.049.

[14] C. Bruel, J. R. Tavares, P. J. Carreau, and M.-C. Heuzey, "The structural amphiphilicity of cellulose nanocrystals characterized from their cohesion parameters," *Carbohydrate Polymers,* vol. 205, pp. 184-191, 2019, doi: 10.1016/j.carbpol.2018.10.026.

[15] C. Bruel, S. Queffeulou, P. J. Carreau, J. R. Tavares, and M. C. Heuzey, "Orienting Cellulose Nanocrystal Functionalities Tunes the Wettability of Water-Cast Films," *Langmuir,* vol. 36, no. 41, pp. 12179-12189, Oct 20 2020, doi: 10.1021/acs.langmuir.0c01799.

[16] R. J. Moon, A. Martini, J. Nairn, J. Simonsen, and J. Youngblood, "Cellulose nanomaterials review: structure, properties and nanocomposites," *Chem Soc Rev,* vol. 40, no. 7, pp. 3941-94, Jul 2011, doi: 10.1039/c0cs00108b.

[17] A. D. French, "Glucose, not cellobiose, is the repeating unit of cellulose and why that is important," *Cellulose,* vol. 24, no. 11, pp. 4605-4609, 2017, doi: 10.1007/s10570-017-1450-3.

[18] A. Dufresne, *Nanocellulose: From Nature to High Performance Tailored Materials*. De Gruyter, 2017.

[19] Y. Nishiyama, "Structure and properties of the cellulose microfibril," *Journal of Wood Science,* vol. 55, no. 4, pp. 241-249, 2009, doi: 10.1007/s10086-009-1029-1.

[20] K. J. Nagarajan, N. R. Ramanujam, M. R. Sanjay, S. Siengchin, B. Surya Rajan, K. Sathick Basha, P. Madhu, and G. R. Raghav, "A comprehensive review on cellulose

nanocrystals and cellulose nanofibers: Pretreatment, preparation, and characterization," *Polymer Composites,* vol. 42, no. 4, pp. 1588-1630, 2021, doi: 10.1002/pc.25929.

[21] R. H. Marchessault and P. R. Sundararajan, "Cellulose," in *The Polysaccharides*, 1983, pp. 11-95.

[22] A. C. O'Sullivan, "Cellulose: the structure slowly unravels.," *Cellulose,* vol. 4, no. 3, pp. 173-207, 1997, doi: 10.1023/a:1018431705579.

[23] D. Klemm, B. Heublein, H.-P. Fink, and A. Bohn, "Cellulose: Fascinating Biopolymer and Sustainable Raw Material," *Angewandte Chemie International Edition,* vol. 44, no. 22, pp. 3358-3393, 2005, doi: 10.1002/anie.200460587.

[24] M. A. Hubbe, O. J. Rojas, L. A. Lucia, and M. Sain, "Cellulosic Nanocomposites: A Review," (in English), *Bioresources,* vol. 3, no. 3, pp. 929-980, 2008. [Online]. Available: <Go to ISI>://WOS:000209653700009.

[25] I. Siró and D. Plackett, "Microfibrillated cellulose and new nanocomposite materials: a review," *Cellulose,* vol. 17, no. 3, pp. 459-494, 2010, doi: 10.1007/s10570-010-9405-y.

[26] S. Iwamoto, A. N. Nakagaito, and H. Yano, "Nano-fibrillation of pulp fibers for the processing of transparent nanocomposites," *Applied Physics A,* vol. 89, no. 2, pp. 461-466, 2007, doi: 10.1007/s00339-007-4175-6.

[27] R. K. Johnson, A. Zink-Sharp, S. H. Renneckar, and W. G. Glasser, "A new bio-based nanocomposite: fibrillated TEMPO-oxidized celluloses in hydroxypropylcellulose matrix," *Cellulose,* vol. 16, no. 2, pp. 227-238, 2008, doi: 10.1007/s10570-008-9269-6.

[28] D. Klemm, F. Kramer, S. Moritz, T. Lindstrom, M. Ankerfors, D. Gray, and A. Dorris, "Nanocelluloses: a new family of nature-based materials," *Angew Chem Int Ed Engl,* vol. 50, no. 24, pp. 5438-66, Jun 6 2011, doi: 10.1002/anie.201001273.

[29] O. M. Vanderfleet and E. D. Cranston, "Production routes to tailor the performance of cellulose nanocrystals," *Nature Reviews Materials,* vol. 6, no. 2, pp. 124-144, 2020, doi: 10.1038/s41578-020-00239-y.

[30] S. Beck-Candanedo, M. Roman, and D. G. Gray, "Effect of reaction conditions on the properties and behavior of wood cellulose nanocrystal suspensions," *Biomacromolecules,* vol. 6, no. 2, pp. 1048-54, Mar-Apr 2005, doi: 10.1021/bm049300p.

[31] J. Araki, M. Wada, S. Kuga, and T. Okano, "Flow properties of microcrystalline cellulose suspension prepared by acid treatment of native cellulose," *Colloids and Surfaces A: Physicochemical and Engineering Aspects*, vol. 142, no. 1, pp. 75-82, 1998, doi: 10.1016/s0927-7757(98)00404-x.

[32] Y. Habibi, L. A. Lucia, and O. J. Rojas, "Cellulose nanocrystals: chemistry, self-assembly, and applications," *Chem Rev*, vol. 110, no. 6, pp. 3479-500, Jun 9 2010, doi: 10.1021/cr900339w.

[33] W. Y. Hamad, *Cellulose Nanocrystals: Properties, Production, and Applications*. Wiley, 2017.

[34] M. Roman and W. T. Winter, "Effect of sulfate groups from sulfuric acid hydrolysis on the thermal degradation behavior of bacterial cellulose," *Biomacromolecules*, vol. 5, no. 5, pp. 1671-7, Sep-Oct 2004, doi: 10.1021/bm034519+.

[35] F. D'Acierno, W. Y. Hamad, C. A. Michal, and M. J. MacLachlan, "Thermal Degradation of Cellulose Filaments and Nanocrystals," *Biomacromolecules*, vol. 21, no. 8, pp. 3374-3386, Aug 10 2020, doi: 10.1021/acs.biomac.0c00805.

[36] P. Dhar, S. M. Bhasney, A. Kumar, and V. Katiyar, "Acid functionalized cellulose nanocrystals and its effect on mechanical, thermal, crystallization and surfaces properties of poly (lactic acid) bionanocomposites films: A comprehensive study," *Polymer*, vol. 101, pp. 75-92, 2016, doi: 10.1016/j.polymer.2016.08.028.

[37] A. Dufresne, "Current Challenges in Melt Extrusion of Cellulose-Based Nanocomposites," in *Biomass Extrusion and Reaction Technologies: Principles to Practices and Future Potential*, (ACS Symposium Series, 2018, pp. 105-116.

[38] X. M. Dong and D. G. Gray, "Effect of Counterions on Ordered Phase Formation in Suspensions of Charged Rodlike Cellulose Crystallites," *Langmuir*, vol. 13, no. 8, pp. 2404-2409, 1997, doi: 10.1021/la960724h.

[39] N. Wang, E. Y. Ding, and R. S. Cheng, "Thermal degradation behaviors of spherical cellulose nanocrystals with sulfate groups," (in English), *Polymer*, vol. 48, no. 12, pp. 3486-3493, Jun 4 2007, doi: 10.1016/j.polymer.2007.03.062.

[40] N. Wang, E. Ding, and R. Cheng, "Preparation and liquid crystalline properties of spherical cellulose nanocrystals," *Langmuir*, vol. 24, no. 1, pp. 5-8, Jan 1 2008, doi: 10.1021/la702923w.

[41] Y. C. Peng, D. J. Gardner, Y. Han, A. Kiziltas, Z. Y. Cai, and M. A. Tshabalala, "Influence of drying method on the material properties of nanocellulose I: thermostability and crystallinity," (in English), *Cellulose*, vol. 20, no. 5, pp. 2379-2392, Oct 2013, doi: 10.1007/s10570-013-0019-z.

[42] Y. Peng, D. J. Gardner, and Y. Han, "Drying cellulose nanofibrils: in search of a suitable method," *Cellulose*, vol. 19, no. 1, pp. 91-102, 2011, doi: 10.1007/s10570-011-9630-z.

[43] S. Beck, J. Bouchard, and R. Berry, "Dispersibility in water of dried nanocrystalline cellulose," *Biomacromolecules*, vol. 13, no. 5, pp. 1486-94, May 14 2012, doi: 10.1021/bm300191k.

[44] H. Hatakeyama and T. Hatakeyama, "Structural change of amorphous cellulose by water- and heat-treatment," *Die Makromolekulare Chemie,* vol. 182, no. 6, pp. 1655-1668, 1981, doi: 10.1002/macp.1981.021820606.

[45] S. Yildiz and E. Gümüşkaya, "The effects of thermal modification on crystalline structure of cellulose in soft and hardwood," *Building and Environment,* vol. 42, no. 1, pp. 62-67, 2007, doi: 10.1016/j.buildenv.2005.07.009.

[46] V. Khoshkava and M. R. Kamal, "Effect of drying conditions on cellulose nanocrystal (CNC) agglomerate porosity and dispersibility in polymer nanocomposites," (in English), *Powder Technology*, vol. 261, pp. 288-298, Jul 2014, doi: 10.1016/j.powtec.2014.04.016.

[47] M. I. Voronova, A. G. Zakharov, O. Y. Kuznetsov, and O. V. Surov, "The effect of drying technique of nanocellulose dispersions on properties of dried materials," *Materials Letters*, vol. 68, pp. 164-167, 2012, doi: 10.1016/j.matlet.2011.09.115.

[48] C. M. Hansen, C. Press, Ed. *Hansen Solubility Parameters: A User's Handbook*, 2nd ed. Taylor&Francis Group, 2007.

[49] D. Viet, S. Beck-Candanedo, and D. G. Gray, "Dispersion of cellulose nanocrystals in polar organic solvents," *Cellulose*, vol. 14, no. 2, pp. 109-113, 2006, doi: 10.1007/s10570-006-9093-9.

[50] M. Mariano, N. El Kissi, and A. Dufresne, "Cellulose nanocrystals and related nanocomposites: Review of some properties and challenges," *Journal of Polymer Science Part B: Polymer Physics*, vol. 52, no. 12, pp. 791-806, 2014, doi: 10.1002/polb.23490.

[51] C. Goussé, H. Chanzy, G. Excoffier, L. Soubeyrand, and E. Fleury, "Stable suspensions of partially silylated cellulose whiskers dispersed in organic solvents," *Polymer*, vol. 43, no. 9, pp. 2645-2651, 2002, doi: 10.1016/s0032-3861(02)00051-4.

[52] M. Salajkova, L. A. Berglund, and Q. Zhou, "Hydrophobic cellulose nanocrystals modified with quaternary ammonium salts," (in English), *Journal of Materials Chemistry*, vol. 22, no. 37, pp. 19798-19805, 2012, doi: 10.1039/c2jm34355j.

[53] J. Araki, M. Wada, and S. Kuga, "Steric Stabilization of a Cellulose Microcrystal Suspension by Poly(ethylene glycol) Grafting," *Langmuir*, vol. 17, no. 1, pp. 21-27, 2000, doi: 10.1021/la001070m.

[54] L. Heux, G. Chauve, and C. Bonini, "Nonflocculating and Chiral-Nematic Self-ordering of Cellulose Microcrystals Suspensions in Nonpolar Solvents," *Langmuir*, vol. 16, no. 21, pp. 8210-8212, 2000, doi: 10.1021/la9913957.

[55] M. M. de Souza Lima and R. Borsali, "Rodlike Cellulose Microcrystals: Structure, Properties, and Applications," *Macromolecular Rapid Communications*, vol. 25, no. 7, pp. 771-787, 2004, doi: 10.1002/marc.200300268.

[56] S. Shafeiei-Sabet, W. Y. Hamad, and S. G. Hatzikiriakos, "Influence of degree of sulfation on the rheology of cellulose nanocrystal suspensions," *Rheologica Acta*, vol. 52, no. 8-9, pp. 741-751, 2013, doi: 10.1007/s00397-013-0722-6.

[57] R. H. Marchessault, F. F. Morehead, and N. M. Walter, "Liquid Crystal Systems from Fibrillar Polysaccharides," *Nature*, vol. 184, no. 4686, pp. 632-633, 1959, doi: 10.1038/184632a0.

[58] S. Beck, J. Bouchard, and R. Berry, "Controlling the reflection wavelength of iridescent solid films of nanocrystalline cellulose," *Biomacromolecules*, vol. 12, no. 1, pp. 167-72, Jan 10 2011, doi: 10.1021/bm1010905.

[59] R. M. Parker, G. Guidetti, C. A. Williams, T. Zhao, A. Narkevicius, S. Vignolini, and B. Frka-Petesic, "The Self-Assembly of Cellulose Nanocrystals: Hierarchical Design of

Visual Appearance," *Advanced Materials,* vol. 30, no. 19, 2018, doi: 10.1002/adma.201704477.

[60] S. Beck, J. Bouchard, G. Chauve, and R. Berry, "Controlled production of patterns in iridescent solid films of cellulose nanocrystals," *Cellulose,* vol. 20, no. 3, pp. 1401-1411, 2013, doi: 10.1007/s10570-013-9888-4.

[61] T. Abitbol, D. Kam, Y. Levi-Kalisman, D. G. Gray, and O. Shoseyov, "Surface Charge Influence on the Phase Separation and Viscosity of Cellulose Nanocrystals," *Langmuir,* vol. 34, no. 13, pp. 3925-3933, Apr 3 2018, doi: 10.1021/acs.langmuir.7b04127.

[62] G. Lenfant, M.-C. Heuzey, T. G. M. van de Ven, and P. J. Carreau, "A comparative study of ECNC and CNC suspensions: effect of salt on rheological properties," *Rheologica Acta,* vol. 56, no. 1, pp. 51-62, 2016, doi: 10.1007/s00397-016-0979-7.

[63] J. Araki, M. Wada, S. Kuga, and T. Okano, "Influence of surface charge on viscosity behavior of cellulose microcrystal suspension," *Journal of Wood Science,* vol. 45, no. 3, pp. 258-261, 1999, doi: 10.1007/bf01177736.

[64] S. Shafiei-Sabet, W. Y. Hamad, and S. G. Hatzikiriakos, "Rheology of nanocrystalline cellulose aqueous suspensions," *Langmuir,* vol. 28, no. 49, pp. 17124-33, Dec 11 2012, doi: 10.1021/la303380v.

[65] F. Pignon, M. Challamel, A. De Geyer, M. Elchamaa, E. F. Semeraro, N. Hengl, B. Jean, J. L. Putaux, E. Gicquel, J. Bras, S. Prevost, M. Sztucki, T. Narayanan, and H. Djeridi, "Breakdown and buildup mechanisms of cellulose nanocrystal suspensions under shear and upon relaxation probed by SAXS and SALS," *Carbohydr Polym,* vol. 260, p. 117751, May 15 2021, doi: 10.1016/j.carbpol.2021.117751.

[66] Y. Xu, A. D. Atrens, and J. R. Stokes, "Rheology and microstructure of aqueous suspensions of nanocrystalline cellulose rods," *J Colloid Interface Sci,* vol. 496, pp. 130-140, Jun 15 2017, doi: 10.1016/j.jcis.2017.02.020.

[67] Y. Xu, A. Atrens, and J. R. Stokes, "A review of nanocrystalline cellulose suspensions: Rheology, liquid crystal ordering and colloidal phase behaviour," *Adv Colloid Interface Sci,* vol. 275, p. 102076, Jan 2020, doi: 10.1016/j.cis.2019.102076.

[68] H. Tanaka, J. Meunier, and D. Bonn, "Nonergodic states of charged colloidal suspensions: repulsive and attractive glasses and gels," *Phys Rev E Stat Nonlin Soft Matter Phys,* vol. 69, no. 3 Pt 1, p. 031404, Mar 2004, doi: 10.1103/PhysRevE.69.031404.

[69] Y. Xu, A. D. Atrens, and J. R. Stokes, "“Liquid, gel and soft glass” phase transitions and rheology of nanocrystalline cellulose suspensions as a function of concentration and salinity," *Soft Matter,* vol. 14, no. 10, pp. 1953-1963, 2018, doi: 10.1039/c7sm02470c.

[70] R. F. Fedors, "An equation suitable for describing the viscosity of dilute to moderately concentrated polymer solutions," *Polymer,* vol. 20, no. 2, pp. 225-228, 1979, doi: 10.1016/0032-3861(79)90226-x.

[71] L. Jowkarderis and T. G. M. van de Ven, "Intrinsic viscosity of aqueous suspensions of cellulose nanofibrils," *Cellulose,* vol. 21, no. 4, pp. 2511-2517, 2014, doi: 10.1007/s10570-014-0292-5.

[72] R. Simha, "The Influence of Brownian Movement on the Viscosity of Solutions," *The Journal of Physical Chemistry,* vol. 44, no. 1, pp. 25-34, 2002, doi: 10.1021/j150397a004.

[73] Y. Boluk, R. Lahiji, L. Zhao, and M. T. McDermott, "Suspension viscosities and shape parameter of cellulose nanocrystals (CNC)," *Colloids and Surfaces A: Physicochemical and Engineering Aspects,* vol. 377, no. 1-3, pp. 297-303, 2011, doi: 10.1016/j.colsurfa.2011.01.003.

[74] A. Bismarck, S. Mishra, and T. Lampke, "Plant fibers as Reinforcement for green composites," in *Natural fibers, biopolymers, and biocomposites,* A. K. Mohanty, M. Misra, and L. T. Drzal Eds., 2005, pp. 37-108.

[75] C. M. Walters, C. E. Boott, T. D. Nguyen, W. Y. Hamad, and M. J. MacLachlan, "Iridescent Cellulose Nanocrystal Films Modified with Hydroxypropyl Cellulose," *Biomacromolecules,* vol. 21, no. 3, pp. 1295-1302, Mar 9 2020, doi: 10.1021/acs.biomac.0c00056.

[76] C. Aulin, S. Ahola, P. Josefsson, T. Nishino, Y. Hirose, M. Osterberg, and L. Wagberg, "Nanoscale cellulose films with different crystallinities and mesostructures--their surface properties and interaction with water," *Langmuir,* vol. 25, no. 13, pp. 7675-85, Jul 7 2009, doi: 10.1021/la900323n.

[77] E. Niinivaara, M. Faustini, T. Tammelin, and E. Kontturi, "Water Vapor Uptake of Ultrathin Films of Biologically Derived Nanocrystals: Quantitative Assessment with Quartz Crystal Microbalance and Spectroscopic Ellipsometry," *Langmuir,* vol. 31, no. 44, pp. 12170-6, Nov 10 2015, doi: 10.1021/acs.langmuir.5b01763.

[78] S. Belbekhouche, J. Bras, G. Siqueira, C. Chappey, L. Lebrun, B. Khelifi, S. Marais, and A. Dufresne, "Water sorption behavior and gas barrier properties of cellulose whiskers and microfibrils films," (in English), *Carbohydrate Polymers,* vol. 83, no. 4, pp. 1740-1748, Feb 1 2011, doi: 10.1016/j.carbpol.2010.10.036.

[79] W. Thielemans, C. R. Warbey, and D. A. Walsh, "Permselective nanostructured membranes based on cellulose nanowhiskers," (in English), *Green Chemistry,* vol. 11, no. 4, pp. 531-537, 2009, doi: 10.1039/b818056c.

[80] Y. Habibi, H. Chanzy, and M. R. Vignon, "TEMPO-mediated surface oxidation of cellulose whiskers," *Cellulose,* vol. 13, no. 6, pp. 679-687, 2006, doi: 10.1007/s10570-006-9075-y.

[81] N. Lin, J. Huang, and A. Dufresne, "Preparation, properties and applications of polysaccharide nanocrystals in advanced functional nanomaterials: a review," *Nanoscale,* vol. 4, no. 11, pp. 3274-94, Jun 7 2012, doi: 10.1039/c2nr30260h.

[82] W. Wan, H. Ouyang, W. Long, W. Yan, M. He, H. Huang, S. Yang, X. Zhang, Y. Feng, and Y. Wei, "Direct Surface Functionalization of Cellulose Nanocrystals with Hyperbranched Polymers through the Anionic Polymerization for pH-Responsive Intracellular Drug Delivery," *ACS Sustainable Chemistry & Engineering,* vol. 7, no. 23, pp. 19202-19212, 2019, doi: 10.1021/acssuschemeng.9b05231.

[83] B. Braun and J. R. Dorgan, "Single-step method for the isolation and surface functionalization of cellulosic nanowhiskers," *Biomacromolecules,* vol. 10, no. 2, pp. 334-41, Feb 9 2009, doi: 10.1021/bm8011117.

[84] S. Spinella, A. Maiorana, Q. Qian, N. J. Dawson, V. Hepworth, S. A. McCallum, M. Ganesh, K. D. Singer, and R. A. Gross, "Concurrent Cellulose Hydrolysis and Esterification to Prepare a Surface-Modified Cellulose Nanocrystal Decorated with Carboxylic Acid Moieties," *ACS Sustainable Chemistry & Engineering,* vol. 4, no. 3, pp. 1538-1550, 2016, doi: 10.1021/acssuschemeng.5b01489.

[85] D. Khandal, B. Riedl, J. R. Tavares, P. J. Carreau, and M.-C. Heuzey, "Tailoring cellulose nanocrystals rheological behavior in aqueous suspensions through surface functionalization with polyethyleneimine," *Physics of Fluids,* vol. 31, no. 2, 2019, doi: 10.1063/1.5046669.

[86] M. Ly and T. H. Mekonnen, "Cationic surfactant modified cellulose nanocrystals for corrosion protective nanocomposite surface coatings," *Journal of Industrial and Engineering Chemistry,* vol. 83, pp. 409-420, 2020, doi: 10.1016/j.jiec.2019.12.014.

[87] A. Kaboorani and B. Riedl, "Surface modification of cellulose nanocrystals (CNC) by a cationic surfactant," (in English), *Industrial Crops and Products,* vol. 65, pp. 45-55, Mar 2015, doi: 10.1016/j.indcrop.2014.11:027.

[88] B. L. Tardy, S. Yokota, M. Ago, W. Xiang, T. Kondo, R. Bordes, and O. J. Rojas, "Nanocellulose–surfactant interactions," *Current Opinion in Colloid & Interface Science,* vol. 29, pp. 57-67, 2017, doi: 10.1016/j.cocis.2017.02.004.

[89] R. R. Lahiji, X. Xu, R. Reifenberger, A. Raman, A. Rudie, and R. J. Moon, "Atomic Force Microscopy Characterization of Cellulose Nanocrystals," *Langmuir,* vol. 26, no. 6, pp. 4480-4488, 2010, doi: 10.1021/la903111j.

[90] Nishino, Takano, and Nakamae, "Elastic Modulus of the Crystalline Regions of Cellulose Polymorphs," *Journal of Polymer Science: Part B: Polymer Physics,* vol. 33, pp. 1647-1651, 1995.

[91] M. Matos Ruiz, J. Y. Cavaillé, A. Dufresne, J. F. Gérard, and C. Graillat, "Processing and characterization of new thermoset nanocomposites based on cellulose whiskers," *Composite Interfaces,* vol. 7, no. 2, pp. 117-131, 2012, doi: 10.1163/156855400300184271.

[92] V. Favier, H. Chanzy, and J. Y. Cavaille, "Polymer Nanocomposites Reinforced by Cellulose Whiskers," *Macromolecules,* vol. 28, no. 18, pp. 6365-6367, 2002, doi: 10.1021/ma00122a053.

[93] N. B. Palaganas, J. D. Mangadlao, A. C. C. de Leon, J. O. Palaganas, K. D. Pangilinan, Y. J. Lee, and R. C. Advincula, "3D Printing of Photocurable Cellulose Nanocrystal Composite for Fabrication of Complex Architectures via Stereolithography," *ACS Appl*

Mater Interfaces, vol. 9, no. 39, pp. 34314-34324, Oct 4 2017, doi: 10.1021/acsami.7b09223.

[94] Q. Q. Wang, J. Z. Sun, Q. Yao, C. C. Ji, J. Liu, and Q. Q. Zhu, "3D printing with cellulose materials," (in English), *Cellulose,* vol. 25, no. 8, pp. 4275-4301, Aug 2018, doi: 10.1007/s10570-018-1888-y.

[95] C. Miao, L. Reid, and W. Y. Hamad, "Moisture-tunable, ionic strength-controlled piezoelectric effect in cellulose nanocrystal films," *Applied Materials Today,* vol. 24, 2021, doi: 10.1016/j.apmt.2021.101082.

[96] H. Fashandi, M. M. Abolhasani, P. Sandoghdar, N. Zohdi, Q. Li, and M. Naebe, "Morphological changes towards enhancing piezoelectric properties of PVDF electrical generators using cellulose nanocrystals," *Cellulose,* vol. 23, no. 6, pp. 3625-3637, 2016, doi: 10.1007/s10570-016-1070-3.

[97] J. Wang, C. Carlos, Z. Zhang, J. Li, Y. Long, F. Yang, Y. Dong, X. Qiu, Y. Qian, and X. Wang, "Piezoelectric Nanocellulose Thin Film with Large-Scale Vertical Crystal Alignment," *ACS Appl Mater Interfaces,* vol. 12, no. 23, pp. 26399-26404, Jun 10 2020, doi: 10.1021/acsami.0c05680.

[98] D. Ponnamma, H. Parangusan, A. Tanvir, and M. A. A. AlMa'adeed, "Smart and robust electrospun fabrics of piezoelectric polymer nanocomposite for self-powering electronic textiles," *Materials & Design,* vol. 184, 2019, doi: 10.1016/j.matdes.2019.108176.

[99] J. P. F. Lagerwall, C. Schutz, M. Salajkova, J. Noh, J. H. Park, G. Scalia, and L. Bergstrom, "Cellulose nanocrystal-based materials: from liquid crystal self-assembly and glass formation to multifunctional thin films," (in English), *Npg Asia Materials,* vol. 6, Jan 2014, doi: ARTN e80

10.1038/am.2013.69.

[100] M. K. Khan, M. Giese, M. Yu, J. A. Kelly, W. Y. Hamad, and M. J. MacLachlan, "Flexible Mesoporous Photonic Resins with Tunable Chiral Nematic Structures," *Angewandte Chemie,* vol. 125, no. 34, pp. 9089-9092, 2013, doi: 10.1002/ange.201303829.

[101] M. K. Khan, W. Y. Hamad, and M. J. Maclachlan, "Tunable mesoporous bilayer photonic resins with chiral nematic structures and actuator properties," *Adv Mater,* vol. 26, no. 15, pp. 2323-8, Apr 16 2014, doi: 10.1002/adma.201304966.

[102] M. Mohammadi, M. C. Heuzey, and P. J. Carreau, "Morphological, thermal, and mechanical properties of cellulose nanocrystal reinforced poly(lactic acid) and poly(butylene adipate-co-terephthalate): A comparative study on common and novel solvent casting methods," (in English), *Polymer Composites,* vol. 42, no. 12, pp. 6688-6703, Dec 2021, doi: 10.1002/pc.26332.

[103] D. Bagheriasl, F. Safdari, P. J. Carreau, C. Dubois, and B. Riedl, "Development of cellulose nanocrystal-reinforced polylactide: A comparative study on different preparation methods," *Polymer Composites,* vol. 40, no. S1, 2017, doi: 10.1002/pc.24676.

[104] A. P. Mathew, G. Gong, N. Bjorngrim, D. Wixe, and K. Oksman, "Moisture Absorption Behavior and Its Impact on the Mechanical Properties of Cellulose Whiskers-Based Polyvinylacetate Nanocomposites," (in English), *Polymer Engineering and Science,* vol. 51, no. 11, pp. 2136-2142, Nov 2011, doi: 10.1002/pen.22063.

[105] F. Safdari, P. J. Carreau, M. C. Heuzey, and M. R. Kamal, "Effects of poly(ethylene glycol) on the morphology and properties of biocomposites based on polylactide and cellulose nanofibers," (in English), *Cellulose,* vol. 24, no. 7, pp. 2877-2893, Jul 2017, doi: 10.1007/s10570-017-1327-5.

[106] F. V. Ferreira, A. Dufresne, I. F. Pinheiro, D. H. S. Souza, R. F. Gouveia, L. H. I. Mei, and L. M. F. Lona, "How do cellulose nanocrystals affect the overall properties of biodegradable polymer nanocomposites: A comprehensive review," *European Polymer Journal,* vol. 108, pp. 274-285, 2018, doi: 10.1016/j.eurpolymj.2018.08.045.

[107] I. M. Mahbubul, E. B. Elcioglu, R. Saidur, and M. A. Amalina, "Optimization of ultrasonication period for better dispersion and stability of TiO2-water nanofluid," *Ultrason Sonochem,* vol. 37, pp. 360-367, Jul 2017, doi: 10.1016/j.ultsonch.2017.01.024.

[108] M. Kamalgharibi, F. Hormozi, S. A. H. Zamzamian, and M. M. Sarafraz, "Experimental studies on the stability of CuO nanoparticles dispersed in different base fluids: influence of stirring, sonication and surface active agents," *Heat and Mass Transfer,* vol. 52, no. 1, pp. 55-62, 2015, doi: 10.1007/s00231-015-1618-z.

[109] A. Asadi and I. M. Alarifi, "Effects of ultrasonication time on stability, dynamic viscosity, and pumping power management of MWCNT-water nanofluid: an experimental study," *Sci Rep,* vol. 10, no. 1, p. 15182, Sep 16 2020, doi: 10.1038/s41598-020-71978-9.

[110] J. Jiang, G. Oberdörster, and P. Biswas, "Characterization of size, surface charge, and agglomeration state of nanoparticle dispersions for toxicological studies," *Journal of Nanoparticle Research,* vol. 11, no. 1, pp. 77-89, 2008, doi: 10.1007/s11051-008-9446-4.

[111] E. J. Foster, R. J. Moon, U. P. Agarwal, M. J. Bortner, J. Bras, S. Camarero-Espinosa, K. J. Chan, M. J. D. Clift, E. D. Cranston, S. J. Eichhorn, D. M. Fox, W. Y. Hamad, L. Heux, B. Jean, M. Korey, W. Nieh, K. J. Ong, M. S. Reid, S. Renneckar, R. Roberts, J. A. Shatkin, J. Simonsen, K. Stinson-Bagby, N. Wanasekara, and J. Youngblood, "Current characterization methods for cellulose nanomaterials," *Chem Soc Rev,* vol. 47, no. 8, pp. 2609-2679, Apr 23 2018, doi: 10.1039/c6cs00895j.

[112] S. Bhattacharjee, "DLS and zeta potential - What they are and what they are not?," *J Control Release,* vol. 235, pp. 337-351, Aug 10 2016, doi: 10.1016/j.jconrel.2016.06.017.

[113] C. Schulze Isfort and M. Rochnia, "Production and physico-chemical characterisation of nanoparticles," *Toxicol Lett,* vol. 186, no. 3, pp. 148-51, May 8 2009, doi: 10.1016/j.toxlet.2008.11.021.

[114] T. Stepisnik Perdih, M. Zupanc, and M. Dular, "Revision of the mechanisms behind oil-water (O/W) emulsion preparation by ultrasound and cavitation," *Ultrason Sonochem,* vol. 51, pp. 298-304, Mar 2019, doi: 10.1016/j.ultsonch.2018.10.003.

[115] J. A. Fuentes-Garcia, J. Santoyo-Salzar, E. Rangel-Cortes, G. F. Goya, V. Cardozo-Mata, and J. A. Pescador-Rojas, "Effect of ultrasonic irradiation power on sonochemical synthesis of gold nanoparticles," *Ultrason Sonochem,* vol. 70, p. 105274, Jan 2021, doi: 10.1016/j.ultsonch.2020.105274.

[116] Y. Z. Cao, P. Zavattieri, J. Youngblood, R. Moon, and J. Weiss, "The relationship between cellulose nanocrystal dispersion and strength," (in English), *Construction and Building Materials,* vol. 119, pp. 71-79, Aug 30 2016, doi: 10.1016/j.conbuildmat.2016.03.077.

[117] J. S. Taurozzi, V. A. Hackley, and M. R. Wiesner, "Ultrasonic dispersion of nanoparticles for environmental, health and safety assessment--issues and recommendations,"

Nanotoxicology, vol. 5, no. 4, pp. 711-29, Dec 2011, doi: 10.3109/17435390.2010.528846.

[118] A. Asadi, F. Pourfattah, I. Miklos Szilagyi, M. Afrand, G. Zyla, H. Seon Ahn, S. Wongwises, H. Minh Nguyen, A. Arabkoohsar, and O. Mahian, "Effect of sonication characteristics on stability, thermophysical properties, and heat transfer of nanofluids: A comprehensive review," *Ultrason Sonochem*, vol. 58, p. 104701, Nov 2019, doi: 10.1016/j.ultsonch.2019.104701.

[119] K. S. Suslick, "The Chemical Effects of Ultrasound," *Scientific American*, pp. 80-86, 1989.

[120] K. S. Suslick, "Sonochemistry," in *Kirk-Othmer Encyclopedia of Chemical Technology*, vol. 26, I. John Wiley & Sons Ed., Fourth ed. New-York, 1998, pp. 516-541.

[121] W. Lauterborn and R. Mettin, "Acoustic cavitation: bubble dynamics in high-power ultrasonic fields," in *Power Ultrasonics*, 2015, pp. 37-78.

[122] S. Merouani, H. Ferkous, O. Hamdaoui, Y. Rezgui, and M. Guemini, "A method for predicting the number of active bubbles in sonochemical reactors," *Ultrasonics Sonochemistry*, vol. 22, pp. 51-58, 2015, doi: 10.1016/j.ultsonch.2014.07.015.

[123] P. Riesz, D. Berdahl, and C. L. Christman, "Free radical generation by ultrasound in aqueous and nonaqueous solutions," *Environ Health Perspect*, vol. 64, pp. 233-52, Dec 1985, doi: 10.1289/ehp.8564233.

[124] I. Tzanakis, G. S. Lebon, D. G. Eskin, and K. A. Pericleous, "Characterizing the cavitation development and acoustic spectrum in various liquids," *Ultrason Sonochem*, vol. 34, pp. 651-662, Jan 2017, doi: 10.1016/j.ultsonch.2016.06.034.

[125] A. Moussatov, C. Granger, and B. Dubus, "Cone-like bubble formation in ultrasonic cavitation field," *Ultrason Sonochem*, vol. 10, no. 4-5, pp. 191-5, Jul 2003, doi: 10.1016/S1350-4177(02)00152-9.

[126] O. Louisnard, "A simple model of ultrasound propagation in a cavitating liquid. Part I: Theory, nonlinear attenuation and traveling wave generation," *Ultrason Sonochem*, vol. 19, no. 1, pp. 56-65, Jan 2012, doi: 10.1016/j.ultsonch.2011.06.007.

[127] O. Louisnard, "A simple model of ultrasound propagation in a cavitating liquid. Part II: Primary Bjerknes force and bubble structures," *Ultrason Sonochem,* vol. 19, no. 1, pp. 66-76, Jan 2012, doi: 10.1016/j.ultsonch.2011.06.008.

[128] D. Schanz, B. Metten, T. Kurz, and W. Lauterborn, "Molecular dynamics simulations of cavitation bubble collapse and sonoluminescence," *New Journal of Physics,* vol. 14, no. 11, 2012, doi: 10.1088/1367-2630/14/11/113019.

[129] D. Rubinetti and D. A. Weiss, "Ultrasound-Driven Fluid Motion - Modelling Approach," (in English), *International Journal of Multiphysics,* vol. 12, no. 1, pp. 1-8, 2018, doi: 10.21152/1750-9548.12.1.1.

[130] D. Rubinetti, D. A. Weiss, J. Müller, and A. Wahlen, "Numerical Modeling and Validation Concept for Acoustic Streaming Induced by Ultrasonic Treatment," presented at the COMSOL Conference, Munich, 2016.

[131] V. S. Ayar, H. K. Parmar, and M. P. Sutaria, "Computational Analysis of Ultrasonic Treatment of Melt for Effective Dispersion of Reinforcement Particles," presented at the International Conference on Re-search and Innovations in Science, Engineering &Technology., 2017.

[132] C. Guo, J. Liu, X. Li, and S. Yang, "Effect of cavitation bubble on the dispersion of magnetorheological polishing fluid under ultrasonic preparation," *Ultrason Sonochem,* vol. 79, p. 105782, Nov 2021, doi: 10.1016/j.ultsonch.2021.105782.

[133] K. A. Kusters, S. E. Pratsinis, S. G. Thoma, and D. M. Smith, "Energy—size reduction laws for ultrasonic fragmentation," *Powder Technology,* vol. 80, no. 3, pp. 253-263, 1994, doi: 10.1016/0032-5910(94)02852-4.

[134] B. S. Park, D. M. Smith, and S. G. Thoma, "Determination of agglomerate strength distributions, Part 4. Analysis of multimodal particle size distributions," *Powder Technology,* vol. 76, no. 2, pp. 125-133, 1993, doi: 10.1016/s0032-5910(05)80019-1.

[135] L. H. Thompson and L. K. Doraiswamy, "Sonochemistry: Science and Engineering," *Industrial & Engineering Chemistry Research,* vol. 38, no. 4, pp. 1215-1249, 1999, doi: 10.1021/ie9804172.

[136] F. Li, L. Li, G. Zhong, Y. Zhai, and Z. Li, "Effects of ultrasonic time, size of aggregates and temperature on the stability and viscosity of Cu-ethylene glycol (EG) nanofluids,"

International Journal of Heat and Mass Transfer, vol. 129, pp. 278-286, 2019, doi: 10.1016/j.ijheatmasstransfer.2018.09.104.

[137] N. Mandzy, E. Grulke, and T. Druffel, "Breakage of TiO2 agglomerates in electrostatically stabilized aqueous dispersions," *Powder Technology,* vol. 160, no. 2, pp. 121-126, 2005, doi: 10.1016/j.powtec.2005.08.020.

[138] L. Dumee, K. Sears, J. Schutz, N. Finn, M. Duke, and S. Gray, "Influence of the Sonication Temperature on the Debundling Kinetics of Carbon Nanotubes in Propan-2-ol," *Nanomaterials (Basel),* vol. 3, no. 1, pp. 70-85, Jan 31 2013, doi: 10.3390/nano3010070.

[139] V. S. Nguyen, D. Rouxel, R. Hadji, B. Vincent, and Y. Fort, "Effect of ultrasonication and dispersion stability on the cluster size of alumina nanoscale particles in aqueous solutions," *Ultrason Sonochem,* vol. 18, no. 1, pp. 382-8, Jan 2011, doi: 10.1016/j.ultsonch.2010.07.003.

[140] B. Brown and J. E. Goodman, "Propagation and absorption of ultrasonics," in *High-Intensity Ultrasonics*: Iliffe Books LTD, 1965, ch. 1, pp. 1-29.

[141] Y. Son, Y. No, and J. Kim, "Geometric and operational optimization of 20-kHz probe-type sonoreactor for enhancing sonochemical activity," *Ultrason Sonochem,* vol. 65, p. 105065, Jul 2020, doi: 10.1016/j.ultsonch.2020.105065.

[142] H. Ge, Y. Li, and H. Chen, "Ultrasonic cavitation noise in suspensions with ethyl cellulose nanoparticles," *Journal of Applied Physics,* vol. 125, no. 22, 2019, doi: 10.1063/1.5099937.

[143] J. Carpenter, S. George, and V. K. Saharan, "A comparative study of batch and recirculating flow ultrasonication system for preparation of multilayer olive oil in water emulsion stabilized with whey protein isolate and sodium alginate," *Chemical Engineering and Processing - Process Intensification,* vol. 125, pp. 139-149, 2018, doi: 10.1016/j.cep.2018.01.006.

[144] U. C. Lohani and K. Muthukumarappan, "Study of continuous flow ultrasonication to improve total phenolic content and antioxidant activity in sorghum flour and its comparison with batch ultrasonication," *Ultrasonics Sonochemistry,* vol. 71, 2021, doi: 10.1016/j.ultsonch.2020.105402.

[145] A. Peshkovsky, "From Research to Production: Overcoming Scale-Up Limitations of Ultrasonic Processing," in *Ultrasound: Advances for Food Processing and Preservation*, 2017, ch. 17, pp. 409-423.

[146] S. L. Peshkovsky and A. S. Peshkovsky, "High capacity ultrasonic reactor system," United States Patent US8651230B2, 2008.

[147] P. R. Gogate, S. Mujumdar, and A. B. Pandit, "Sonochemical reactors for waste water treatment: comparison using formic acid degradation as a model reaction," *Advances in Environmental Research,* vol. 7, no. 2, pp. 283-299, 2003, doi: 10.1016/s1093-0191(01)00133-2.

[148] H.-J. Lee, H.-S. Lee, J. Seo, Y.-H. Kang, W. Kim, and T. Kang, "State-of-the-Art of Cellulose Nanocrystals and Optimal Method for their Dispersion for Construction-Related Applications," *Applied Sciences,* vol. 9, no. 3, 2019, doi: 10.3390/app9030426.

[149] M. Paakko, M. Ankerfors, H. Kosonen, A. Nykanen, S. Ahola, M. Osterberg, J. Ruokolainen, J. Laine, P. T. Larsson, O. Ikkala, and T. Lindstrom, "Enzymatic hydrolysis combined with mechanical shearing and high-pressure homogenization for nanoscale cellulose fibrils and strong gels," *Biomacromolecules,* vol. 8, no. 6, pp. 1934-41, Jun 2007, doi: 10.1021/bm061215p.

[150] H. Wang, J. Li, X. Zeng, X. Tang, Y. Sun, T. Lei, and L. Lin, "Extraction of cellulose nanocrystals using a recyclable deep eutectic solvent," *Cellulose,* vol. 27, no. 3, pp. 1301-1314, 2019, doi: 10.1007/s10570-019-02867-2.

[151] Y. Wang, X. Wei, J. Li, F. Wang, Q. Wang, Y. Zhang, and L. Kong, "Homogeneous isolation of nanocellulose from eucalyptus pulp by high pressure homogenization," *Industrial Crops and Products,* vol. 104, pp. 237-241, 2017, doi: 10.1016/j.indcrop.2017.04.032.

[152] S. Schultz, G. Wagner, K. Urban, and J. Ulrich, "High-Pressure Homogenization as a Process for Emulsion Formation," *Chemical Engineering & Technology,* vol. 27, no. 4, pp. 361-368, 2004, doi: 10.1002/ceat.200406111.

[153] V. Heshmati, M. R. Kamal, and B. D. Favis, "Tuning the localization of finely dispersed cellulose nanocrystal in poly (lactic acid)/bio-polyamide11 blends," *Journal of Polymer*

Science Part B: Polymer Physics, vol. 56, no. 7, pp. 576-587, 2018, doi: 10.1002/polb.24563.

[154] Y. Li and X. Huang, "Dispersion evaluation, processing and tensile properties of carbon nanotubes-modified epoxy composites prepared by high pressure homogenization," *Composites Part A: Applied Science and Manufacturing,* vol. 78, pp. 166-173, 2015, doi: 10.1016/j.compositesa.2015.08.013.

[155] X.-L. Jia, Q. Zhang, J.-Q. Huang, C. Zheng, W.-Z. Qian, and F. Wei, "The direct dispersion of granular agglomerated carbon nanotubes in bismaleimide by high pressure homogenization for the production of strong composites," *Powder Technology,* vol. 217, pp. 477-481, 2012, doi: 10.1016/j.powtec.2011.11.004.

[156] S. M. Jafari, Y. He, and B. Bhandari, "Production of sub-micron emulsions by ultrasound and microfluidization techniques," *Journal of Food Engineering,* vol. 82, no. 4, pp. 478-488, 2007, doi: 10.1016/j.jfoodeng.2007.03.007.

[157] S. Bystryak, R. Santockyte, and A. S. Peshkovsky, "Cell disruption of S. cerevisiae by scalable high-intensity ultrasound," *Biochemical Engineering Journal,* vol. 99, pp. 99-106, 2015, doi: 10.1016/j.bej.2015.03.014.

[158] S. Azoubel and S. Magdassi, "The formation of carbon nanotube dispersions by high pressure homogenization and their rapid characterization by analytical centrifuge," *Carbon,* vol. 48, no. 12, pp. 3346-3352, 2010, doi: 10.1016/j.carbon.2010.05.024.

[159] Y. Mao, K. Liu, C. Zhan, L. Geng, B. Chu, and B. S. Hsiao, "Characterization of Nanocellulose Using Small-Angle Neutron, X-ray, and Dynamic Light Scattering Techniques," *J Phys Chem B,* vol. 121, no. 6, pp. 1340-1351, Feb 16 2017, doi: 10.1021/acs.jpcb.6b11425.

[160] C. Fraschini, G. Chauve, J.-F. Le Berre, S. Ellis, M. Méthot, B. O'Connor, and J. Bouchard, "Critical discussion of light scattering and microscopy techniques for CNC particle sizing," *Nordic Pulp & Paper Research Journal,* vol. 29, no. 1, pp. 31-40, 2014, doi: 10.3183/npprj-2014-29-01-p031-040.

[161] C. Campano, P. Lopez-Exposito, L. Gonzalez-Aguilera, A. Blanco, and C. Negro, "In-depth characterization of the aggregation state of cellulose nanocrystals through analysis

of transmission electron microscopy images," *Carbohydr Polym*, vol. 254, p. 117271, Feb 15 2021, doi: 10.1016/j.carbpol.2020.117271.

[162] C. Metzger, R. Drexel, F. Meier, and H. Briesen, "Effect of ultrasonication on the size distribution and stability of cellulose nanocrystals in suspension: an asymmetrical flow field-flow fractionation study," *Cellulose*, vol. 28, no. 16, pp. 10221-10238, 2021, doi: 10.1007/s10570-021-04172-3.

[163] X. Guan, R. Cueto, P. Russo, Y. Qi, and Q. Wu, "Asymmetric flow field-flow fractionation with multiangle light scattering detection for characterization of cellulose nanocrystals," *Biomacromolecules*, vol. 13, no. 9, pp. 2671-9, Sep 10 2012, doi: 10.1021/bm300595a.

[164] R. Franks, S. Morefield, J. Wen, D. Liao, J. Alvarado, M. Strano, and C. Marsh, "A study of nanomaterial dispersion in solution by wet-cell transmission electron microscopy," *J Nanosci Nanotechnol*, vol. 8, no. 9, pp. 4404-7, Sep 2008, doi: 10.1166/jnn.2008.306.

[165] C. Metzger, D. Auber, S. Dahnhardt-Pfeiffer, and H. Briesen, "Agglomeration of cellulose nanocrystals: the effect of secondary sulfates and their use in product separation," (in English), *Cellulose*, vol. 27, no. 17, pp. 9839-9851, Nov 2020, doi: 10.1007/s10570-020-03476-0.

[166] M. Shimizu, T. Saito, Y. Nishiyama, S. Iwamoto, H. Yano, A. Isogai, and T. Endo, "Fast and Robust Nanocellulose Width Estimation Using Turbidimetry," *Macromol Rapid Commun*, vol. 37, no. 19, pp. 1581-1586, Oct 2016, doi: 10.1002/marc.201600357.

[167] S. Parveen, S. Rana, S. Ferreira, A. Filho, and R. Fangueiro, "Ultrasonic dispersion of micro crystalline cellulose for developing cementitious composites with excellent strength and stiffness," *Industrial Crops and Products*, vol. 122, pp. 156-165, 2018, doi: 10.1016/j.indcrop.2018.05.060.

[168] V. Raman and A. Abbas, "Experimental investigations on ultrasound mediated particle breakage," *Ultrason Sonochem*, vol. 15, no. 1, pp. 55-64, Jan 2008, doi: 10.1016/j.ultsonch.2006.11.009.

[169] E. J. W. Wynn, "Relationship between particle-size and chord-length distributions in focused beam reflectance measurement: stability of direct inversion and weighting,"

Powder Technology, vol. 133, no. 1-3, pp. 125-133, 2003, doi: 10.1016/s0032-5910(03)00084-6.

[170] P. Kovalsky and G. Bushell, "In situ measurement of fractal dimension using focussed beam reflectance measurement," *Chemical Engineering Journal,* vol. 111, no. 2-3, pp. 181-188, 2005, doi: 10.1016/j.cej.2005.02.020.

[171] R. H. Marchessault, F. F. Morehead, and M. J. Koch, "Some hydrodynamic properties of neutral suspensions of cellulose crystallites as related to size and shape," *Journal of Colloid Science,* vol. 16, no. 4, pp. 327-344, 1961, doi: 10.1016/0095-8522(61)90033-2.

[172] E. Gicquel, J. Bras, C. Rey, J. L. Putaux, F. Pignon, B. Jean, and C. Martin, "Impact of sonication on the rheological and colloidal properties of highly concentrated cellulose nanocrystal suspensions," (in English), *Cellulose,* vol. 26, no. 13-14, pp. 7619-7634, Sep 2019, doi: 10.1007/s10570-019-02622-7.

[173] M. Girard, D. Vidal, F. Bertrand, J. R. Tavares, and M. C. Heuzey, "Evidence-based guidelines for the ultrasonic dispersion of cellulose nanocrystals," *Ultrason Sonochem,* vol. 71, p. 105378, Mar 2021, doi: 10.1016/j.ultsonch.2020.105378.

[174] M. Girard, F. Bertrand, J. R. Tavares, and M. C. Heuzey, "Rheological insights on the evolution of sonicated cellulose nanocrystal dispersions," *Ultrason Sonochem,* vol. 78, p. 105747, Oct 2021, doi: 10.1016/j.ultsonch.2021.105747.

[175] R. Moon, S. Beck, and A. Rudie, "Cellulose Nanocrystals – A Material with Unique Properties and Many Potential Applications," in *Production and Applications of Cellulose Nanomaterials*: TAPPI Press, 2013, ch. 1.

[176] A. Dufresne, "Nanocellulose: a new ageless bionanomaterial," (in English), *Materials Today,* vol. 16, no. 6, pp. 220-227, Jun 2013, doi: 10.1016/j.mattod.2013.06.004.

[177] Y. Chen, L. Gan, J. Huang, and A. Dufresne, "Reinforcing Mechanism of Cellulose Nanocrystals in Nanocomposites," in *Nanocellulose*, J. Huang, A. Dufresne, and N. Lin Eds., First Edition ed.: Wiley-VCH Verlag GmbH & Co. KGaA, 2019, ch. 7, pp. 201-249.

[178] J. Bras, D. Viet, C. Bruzzese, and A. Dufresne, "Correlation between stiffness of sheets prepared from cellulose whiskers and nanoparticles dimensions," *Carbohydrate Polymers,* vol. 84, no. 1, pp. 211-215, 2011, doi: 10.1016/j.carbpol.2010.11.022.

[179] Y. Nishiyama, "Molecular interactions in nanocellulose assembly," *Philos Trans A Math Phys Eng Sci,* vol. 376, no. 2112, Feb 13 2018, doi: 10.1098/rsta.2017.0047.

[180] M. S. Reid, M. Villalobos, and E. D. Cranston, "Cellulose nanocrystal interactions probed by thin film swelling to predict dispersibility," *Nanoscale,* vol. 8, no. 24, pp. 12247-57, Jun 16 2016, doi: 10.1039/c6nr01737a.

[181] H. Y. Yu, Z. Y. Qin, B. L. Liang, N. Liu, Z. Zhou, and L. Chen, "Facile extraction of thermally stable cellulose nanocrystals with a high yield of 93% through hydrochloric acid hydrolysis under hydrothermal conditions," (in English), *Journal of Materials Chemistry A,* vol. 1, no. 12, pp. 3938-3944, 2013, doi: 10.1039/c3ta01150j.

[182] L. Zhong, S. Fu, X. Peng, H. Zhan, and R. Sun, "Colloidal stability of negatively charged cellulose nanocrystalline in aqueous systems," *Carbohydr Polym,* vol. 90, no. 1, pp. 644-9, Sep 1 2012, doi: 10.1016/j.carbpol.2012.05.091.

[183] A. Kumar and C. K. Dixit, "Methods for characterization of nanoparticles," in *Advances in Nanomedicine for the Delivery of Therapeutic Nucleic Acids*, 2017, pp. 43-58.

[184] K.-H. Lin, D. Hu, T. Sugimoto, F.-C. Chang, M. Kobayashi, and T. Enomae, "An analysis on the electrophoretic mobility of cellulose nanocrystals as thin cylinders: relaxation and end effect," *RSC Advances*, vol. 9, no. 58, pp. 34032-34038, 2019, doi: 10.1039/c9ra05156b.

[185] J. Huang, A. Dufresne, and N. Lin, Eds. *Nanocellulose: From Fundamentals to Advanced Materials, First Edition*. John Wiley & Sons Inc., 2019.

[186] W. Y. Hamad and T. Q. Hu, "Structure-process-yield interrelations in nanocrystalline cellulose extraction," *The Canadian Journal of Chemical Engineering,* pp. n/a-n/a, 2010, doi: 10.1002/cjce.20298.

[187] Y. Min, M. Akbulut, K. Kristiansen, Y. Golan, and J. Israelachvili, "The role of interparticle and external forces in nanoparticle assembly," *Nature Materials,* vol. 7, no. 7, pp. 527-38, Jul 2008, doi: 10.1038/nmat2206.

[188] Y. Y. Huang and E. M. Terentjev, "Dispersion of Carbon Nanotubes: Mixing, Sonication, Stabilization, and Composite Properties," (in English), *Polymers,* vol. 4, no. 1, pp. 275-295, Mar 2012, doi: 10.3390/polym4010275.

[189] J. Shojaeiarani, D. Bajwa, and G. Holt, "Sonication amplitude and processing time influence the cellulose nanocrystals morphology and dispersion," *Nanocomposites,* vol. 6, no. 1, pp. 41-46, 2020, doi: 10.1080/20550324.2019.1710974.

[190] S. K. Bhangu and M. Ashokkumar, "Theory of Sonochemistry," *Top Curr Chem (Cham),* vol. 374, no. 4, p. 56, Aug 2016, doi: 10.1007/s41061-016-0054-y.

[191] J. G. Gwon, H. J. Cho, S. J. Chun, S. Lee, Q. Wu, M. C. Li, and S. Y. Lee, "Mechanical and thermal properties of toluene diisocyanate-modified cellulose nanocrystal nanocomposites using semi-crystalline poly(lactic acid) as a base matrix," (in English), *Rsc Advances,* vol. 6, no. 77, pp. 73879-73886, 2016, doi: 10.1039/c6ra10993d.

[192] E. Abraham, D. Kam, Y. Nevo, R. Slattegard, A. Rivkin, S. Lapidot, and O. Shoseyov, "Highly Modified Cellulose Nanocrystals and Formation of Epoxy-Nanocrystalline Cellulose (CNC) Nanocomposites," *ACS Appl Mater Interfaces,* vol. 8, no. 41, pp. 28086-28095, Oct 19 2016, doi: 10.1021/acsami.6b09852.

[193] R. F. Contamine, A. M. Wilhelm, J. Berlan, and H. Delmas, "Power Measurement in Sonochemistry," (in English), *Ultrasonics Sonochemistry,* vol. 2, no. 1, pp. S43-S47, May 1995, doi: Doi 10.1016/1350-4177(94)00010-P.

[194] Y. Boluk and C. Danumah, "Analysis of cellulose nanocrystal rod lengths by dynamic light scattering and electron microscopy," *Journal of Nanoparticle Research,* vol. 16, no. 1, 2013, doi: 10.1007/s11051-013-2174-4.

[195] B. S. B. Jean, "Auto-catalyzed acidic desulfation of cellulose nanocrystals," *Nordic Pulp & Paper Research Journal,* vol. 29, pp. 6-14, 2014.

[196] J. M. Schurr and K. S. Schmitz, "Dynamic Light Scattering Studies of Bioplymers: Effects of Charge, Shape, and Flexibility," *Annual Review Of Physical Chemistry,* vol. 37, no. 1, pp. 271-305, 1986, doi: 10.1146/annurev.pc.37.100186.001415.

[197] M. M. Alvarez, P. E. Arratia, and F. J. Muzzio, "Laminar Mixing in Eccentric Stirred Tank Systems," *The Canadian Journal of Chemical Engineering,* vol. 80, no. 4, pp. 546-557, 2008, doi: 10.1002/cjce.5450800418.

[198] N. Lin and A. Dufresne, "Nanocellulose in biomedicine: Current status and future prospect," *European Polymer Journal,* vol. 59, pp. 302-325, 2014, doi: 10.1016/j.eurpolymj.2014.07.025.

[199] E. Gicquel, C. Martin, J. Garrido Yanez, and J. Bras, "Cellulose nanocrystals as new bio-based coating layer for improving fiber-based mechanical and barrier properties," *Journal of Materials Science,* vol. 52, no. 6, pp. 3048-3061, 2016, doi: 10.1007/s10853-016-0589-x.

[200] Z. Berk, "Mixing," in *Food Process Engineering and Technology*, 2009, pp. 175-194.

[201] E. E. Ureña-Benavides, G. Ao, V. A. Davis, and C. L. Kitchens, "Rheology and Phase Behavior of Lyotropic Cellulose Nanocrystal Suspensions," *Macromolecules,* vol. 44, no. 22, pp. 8990-8998, 2011, doi: 10.1021/ma201649f.

[202] A. Lu, U. Hemraz, Z. Khalili, and Y. Boluk, "Unique viscoelastic behaviors of colloidal nanocrystalline cellulose aqueous suspensions," *Cellulose,* vol. 21, no. 3, pp. 1239-1250, 2014, doi: 10.1007/s10570-014-0173-y.

[203] B. Zakani and D. Grecov, "Yield stress analysis of cellulose nanocrystalline gels," *Cellulose,* vol. 27, no. 16, pp. 9337-9353, 2020, doi: 10.1007/s10570-020-03429-7.

[204] B. Derakhshandeh, G. Petekidis, S. Shafiei Sabet, W. Y. Hamad, and S. G. Hatzikiriakos, "Ageing, yielding, and rheology of nanocrystalline cellulose suspensions," *Journal of Rheology,* vol. 57, no. 1, pp. 131-148, 2013, doi: 10.1122/1.4764080.

[205] N. Willenbacher and K. Georgieva, "Rheology of Disperse Systems," in *Product Design and Engineering*, U. Bröckel, W. Meier, and G. Wagner Eds.: Wiley-VCH Verlab GmbH, 2013, ch. 1, pp. 7-49.

[206] L. Heymann and N. Aksel, "Transition pathways between solid and liquid state in suspensions," *Phys Rev E Stat Nonlin Soft Matter Phys,* vol. 75, no. 2 Pt 1, p. 021505, Feb 2007, doi: 10.1103/PhysRevE.75.021505.

[207] X. M. Dong, J.-F. Revol, and D. G. Gray, " Effect of microcrystallite preparation conditions on the formation of colloid crystals of cellulose," *Cellulose,* vol. 5, no. 1, pp. 19-32, 1998, doi: 10.1023/a:1009260511939.

[208] X. Feng, Z. Yang, S. Chmely, Q. Wang, S. Wang, and Y. Xie, "Lignin-coated cellulose nanocrystal filled methacrylate composites prepared via 3D stereolithography printing: Mechanical reinforcement and thermal stabilization," *Carbohydr Polym,* vol. 169, pp. 272-281, Aug 1 2017, doi: 10.1016/j.carbpol.2017.04.001.

[209] Z. Zhang, M. Cheng, M. S. Gabriel, A. A. Teixeira Neto, J. da Silva Bernardes, R. Berry, and K. C. Tam, "Polymeric hollow microcapsules (PHM) via cellulose nanocrystal stabilized Pickering emulsion polymerization," *J Colloid Interface Sci,* vol. 555, pp. 489-497, Nov 1 2019, doi: 10.1016/j.jcis.2019.07.107.

[210] A. Arzate, F. Bertrand, O. Reglat, and P. Tanguy, "Apparatus and method for measuring the rheological properties of a power law fluid," Patent Appl. 09/493,414, 2002.

[211] A. Arzate, "Détermination de la viscosité en ligne des sauces de couchage de papier," Master, Chemical Engineering, Polytechnique Montreal, Quebec, Canada, 1999.

[212] A. B. Metzner and R. E. Otto, "Agitation of non-Newtonian fluids," *AIChE Journal,* vol. 3, no. 1, pp. 3-10, 1957, doi: 10.1002/aic.690030103.

[213] B. Zakani, S. Entezami, D. Grecov, H. Salem, and A. Sedaghat, "Effect of ultrasonication on lubrication performance of cellulose nano-crystalline (CNC) suspensions as green lubricants," *Carbohydr Polym,* vol. 282, p. 119084, Apr 15 2022, doi: 10.1016/j.carbpol.2021.119084.

[214] F. Hajiali, S. Tajbakhsh, and M. Maric, "Epoxidized Block and Statistical Copolymers Reinforced by Organophosphorus-Titanium-Silicon Hybrid Nanoparticles: Morphology and Thermal and Mechanical Properties," *ACS Omega,* vol. 6, no. 17, pp. 11679-11692, May 4 2021, doi: 10.1021/acsomega.1c00993.

[215] F. Cabaret, S. Bonnot, L. Fradette, and P. A. Tanguy, "Mixing Time Analysis Using Colorimetric Methods and Image Processing," *Industrial & Engineering Chemistry Research,* vol. 46, no. 14, pp. 5032-5042, 2007, doi: 10.1021/ie0613265.

[216] "General Ultrasonic Processing Information and Techniques for Disrupting Cells," Sonics & Materials, 2019.

[217] H. Sojoudiasli, M.-C. Heuzey, P. J. Carreau, and B. Riedl, "Rheological behavior of suspensions of modified and unmodified cellulose nanocrystals in dimethyl sulfoxide," *Rheologica Acta,* vol. 56, no. 7-8, pp. 673-682, 2017, doi: 10.1007/s00397-017-1022-3.

[218] L. Lewis, M. Derakhshandeh, S. G. Hatzikiriakos, W. Y. Hamad, and M. J. MacLachlan, "Hydrothermal Gelation of Aqueous Cellulose Nanocrystal Suspensions," *Biomacromolecules,* vol. 17, no. 8, pp. 2747-54, Aug 8 2016, doi: 10.1021/acs.biomac.6b00906.

[219] L. Gorb, A. Asensio, I. Tunon, and M. F. Ruiz-Lopez, "The mechanism of formamide hydrolysis in water from ab initio calculations and simulations," *Chemistry,* vol. 11, no. 22, pp. 6743-53, Nov 4 2005, doi: 10.1002/chem.200500346.

APPENDIX A SUPPLEMENTARY INFORMATION TO ARTICLE 1: EVIDENCE-BASE GUIDELINES FOR THE ULTRASONIC DISPERSION OF CELLULOSE NANOCRYSTALS

Mélanie Girard, David Vidal, François Bertrand, Jason R. Tavares, Marie-Claude Heuzey. Evidence-base guidelines for the ultrasonic dispersion of cellulose nanocrystals. *Ultrasonics Sonochemistry*, 71 (2021), 105378.

Table A.1: Effective power P and amplitude *A* determination using a calorimetric method.

Set point power P_s **(W)**	**Effective power** P **(W)**	**Amplitude** A **(m)**
90	33	5.10^{-6}
75	25	4.10^{-6}
65	15	3.10^{-6}
15	5	2.10^{-6}

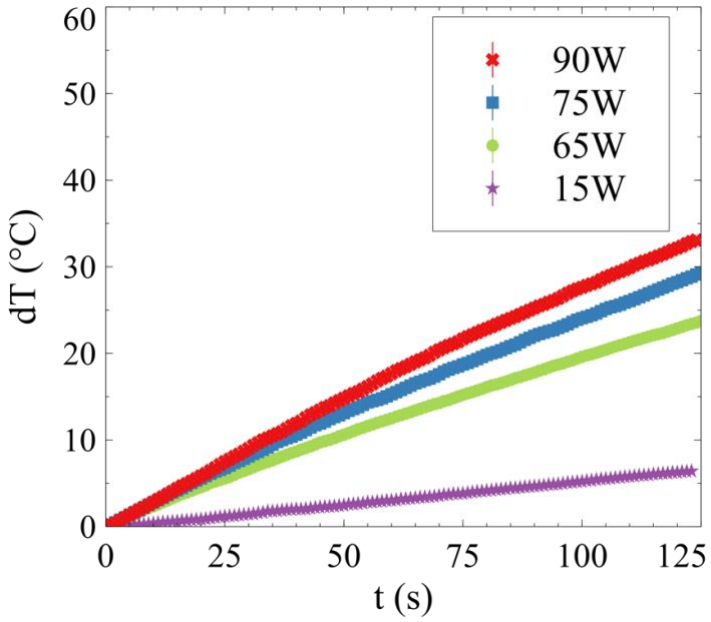

Figure A.1: Heat loss during ultrasonication using a calorimetric method for different set point powers ($V_{container}$ = 25 mL, $V_{adiabatic\ beaker}$ = 40 mL).

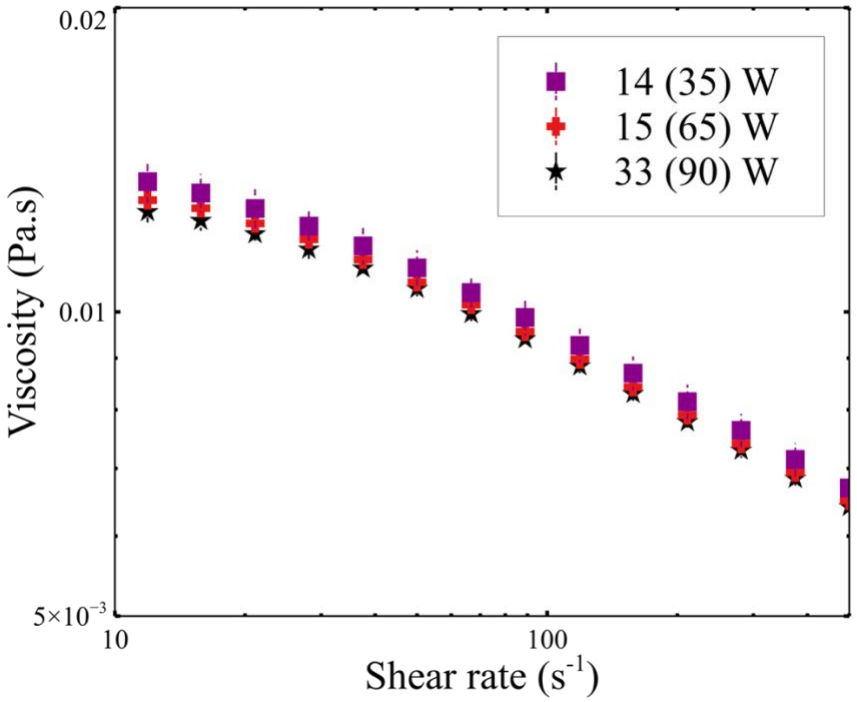

Figure A.2: Viscosity of 3 wt% CNC ultrasonicated suspensions as function of shear rate obtained with an off-centered probe high in the beaker (SOC, V = 60 mL, E = 167 kJ.g-1.L-1) for different powers (the effective value is specified along with the set point value in brackets).The vertical lines correspond to the standard deviation.

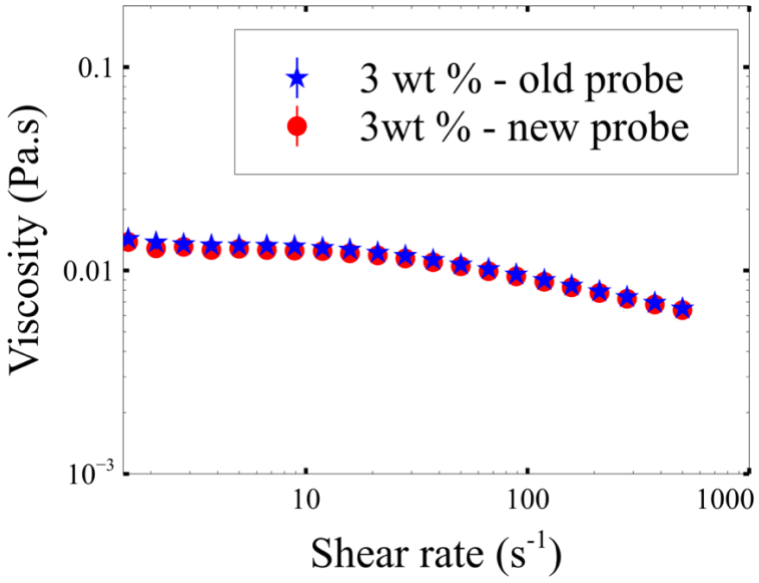

Figure A.3: Viscosity of 3 wt% CNC ultrasonicated suspensions as function of shear rate obtained with an off-centered probe high in the beaker (SOC, V = 60 mL, E = 167 $kJ.g^{-1}.L^{-1}$) with either a new probe or an old one. The vertical lines correspond to the standard deviation.

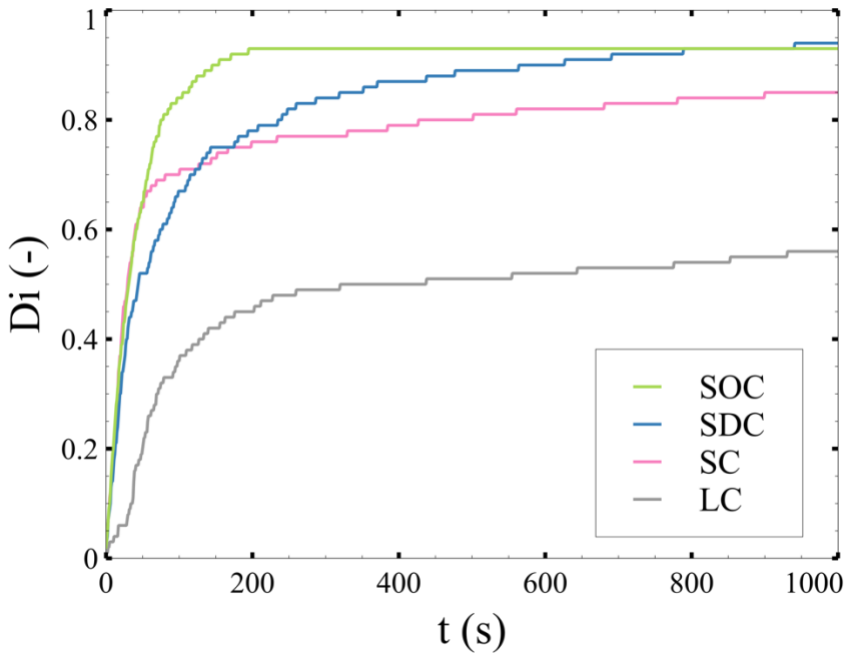

Figure A.4: Dispersion index vs. mixing time (final simulation time t = 1000 s) obtained by simulation either in a small beaker respectively with an off-centered probe high in the beaker (SOC), a deep centered probe (SDC), a centered probe (SC) or a large beaker with a centered probe (LC).

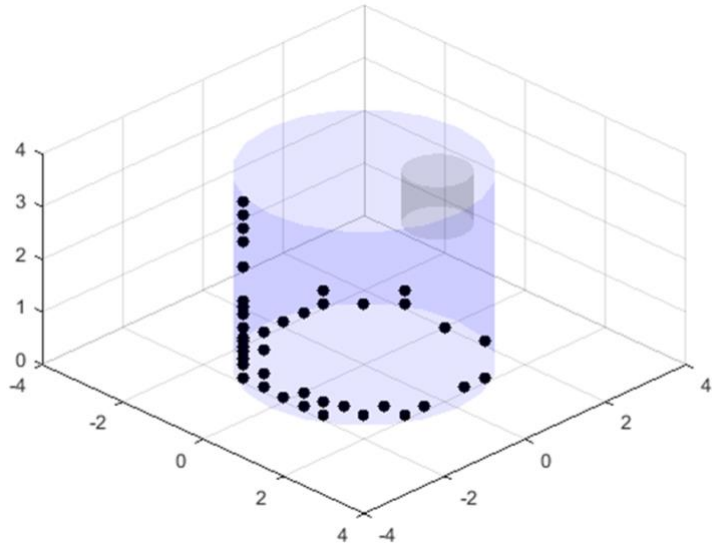

Figure A.5: Visualization of the initial position of the particles that do not go in the cavitation zone during the simulation time (up to t = 200 s) for the off-centered probe case (SOC).

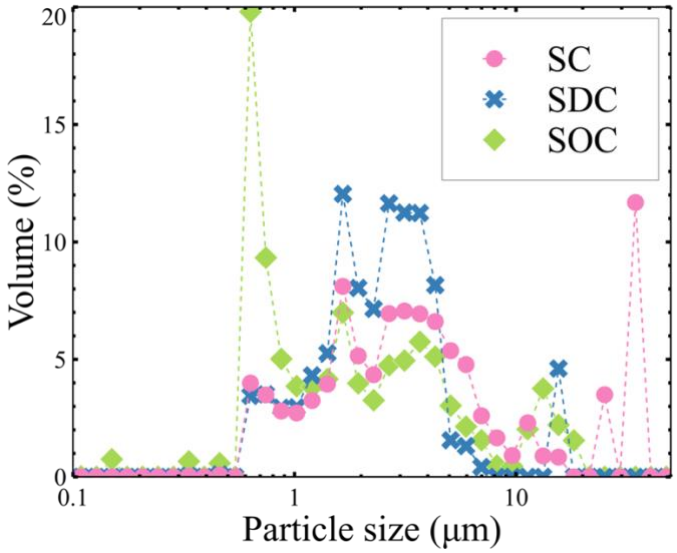

Figure A.6: Particle size in volume of 3 wt% CNC ultrasonicated suspensions (V = 60 mL, P = 15 (65) W, E = 167 kJ.g^{-1}.L^{-1}) obtained either with an off-centered probe high in the beaker (SOC), a centered probe (SC) or a deep centered probe (SDC)

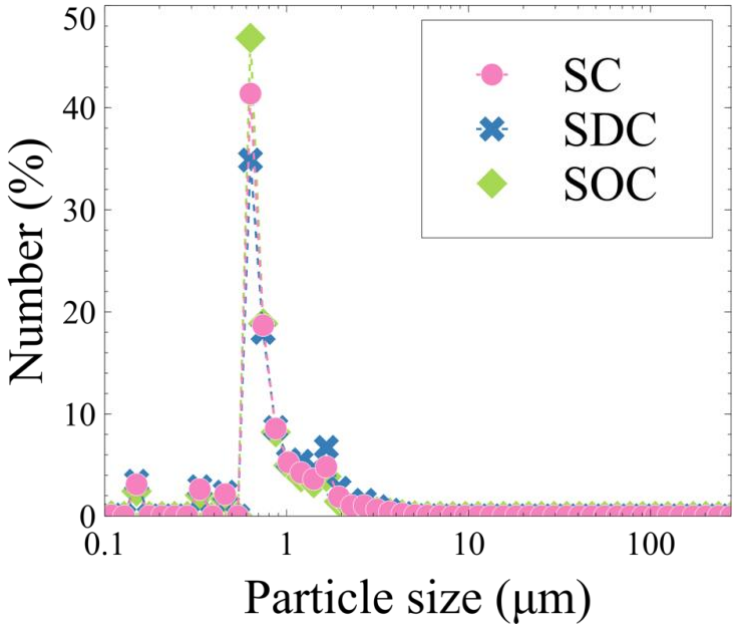

Figure A.7: Particle size in number of 3 wt% CNC ultrasonicated suspensions (V = 60 mL, P = 15 (65) W, E = 167 kJ.g^{-1}.L^{-1}) obtained either with an off-centered probe high in the beaker (SOC), a centered probe (SC) or a deep centered probe (SDC).

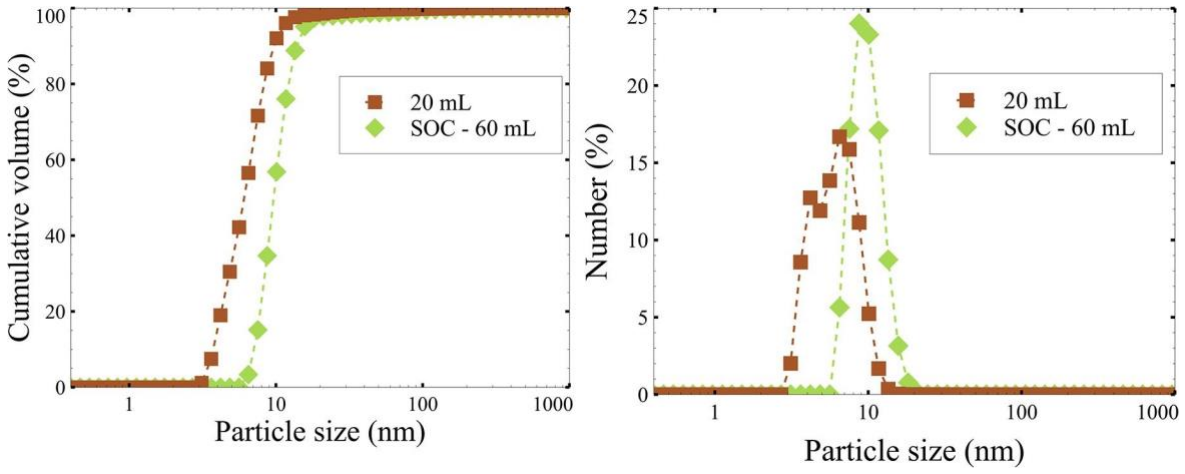

Figure A.8: Particle size in cumulative volume and in number obtained by DLS of 3 wt % ultrasonicated CNC suspensions CNC concentration obtained either with an off-centered probe high in the beaker (SOC, V = 60 mL, E = 167 $kJ.g^{-1}.L^{-1}$) or with the reference case presented in Section 4.3.3.1 (V = 20 mL, P = 33 (90) W, h/H = 0.3, (R-r)/R = 1, E = 500 $kJ.g^{-1}.L^{-1}$).

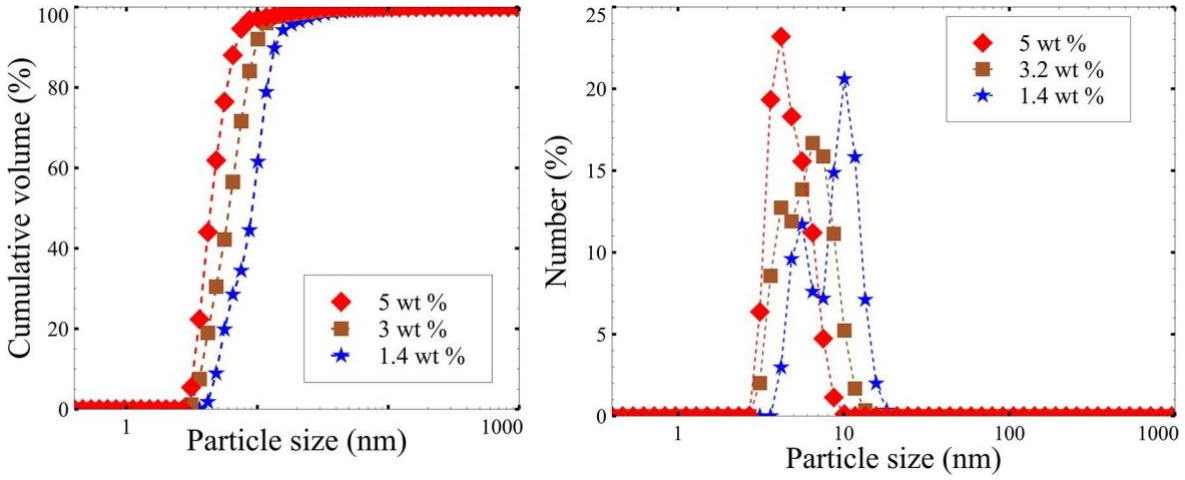

Figure A.9: Particle size in cumulative volume and in number obtained by DLS of ultrasonicated suspensions at various CNC concentration as a function of shear rate (V = 20 mL, P = 33 (90) W, h/H = 0.3, (R-r)/R = 1, E = 500 $kJ.g^{-1}.L^{-1}$).

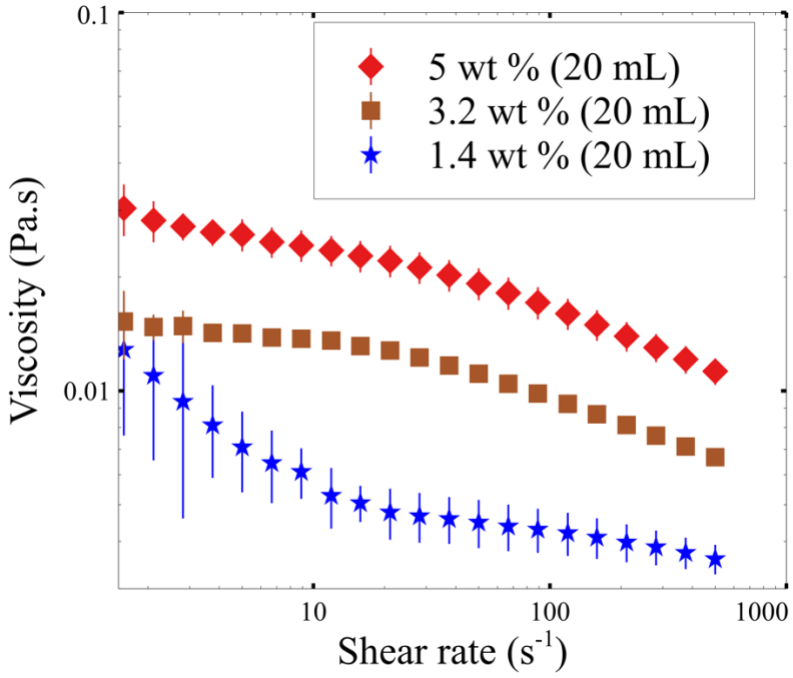

Figure A.10: Viscosity of ultrasonicated suspensions at various CNC concentration as a function of shear rate (V = 20 mL, P = 33 (90) W, h/H = 0.3, (R-r)/R = 1, E = 500 $kJ.g^{-1}.L^{-1}$). The vertical lines correspond to the standard deviation.

APPENDIX B SUPPLEMENTARY INFORMATION TO ARTICLE 2: RHEOLOGICAL INSIGHTS ON THE EVOLUTION OF SONICATED CELLULOSE NANOCRYSTAL DISPERSIONS

Mélanie Girard, François Bertrand, Jason R. Tavares, Marie-Claude Heuzey. Rheological insights on the evolution of sonicated cellulose nanocrystal dispersions. *Ultrasonics Sonochemistry*. 78 (2021), 105747.

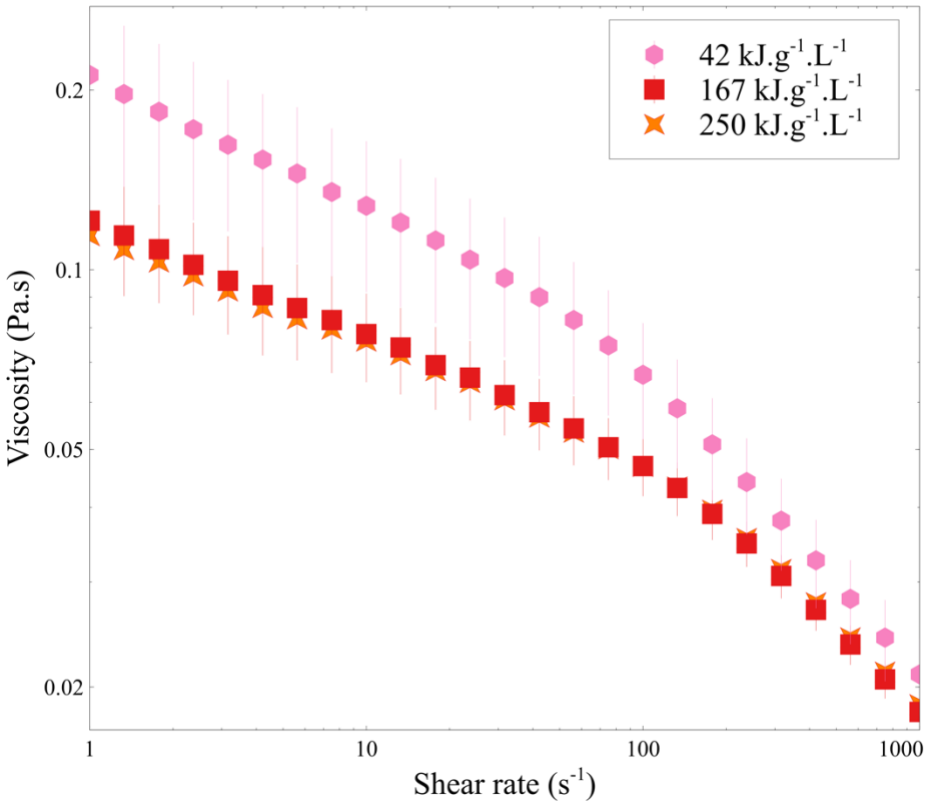

Figure B.1: Sample viscosities of 6.4 wt% spray-dried CNC ultrasonicated suspensions obtained either at E = 42, 167 or 250 $kJ.g^{-1}.L^{-1}$(V = 60 mL, P = 65 W) as function of shear rate

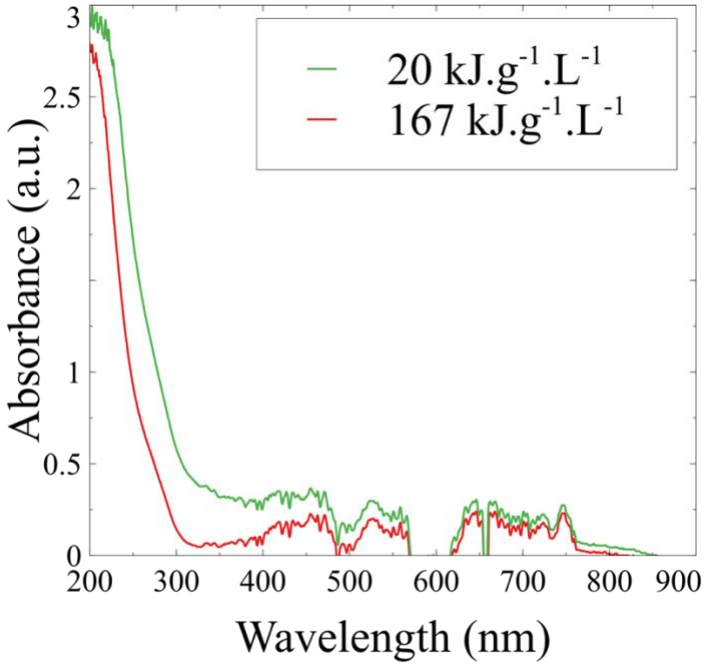

Figure B.2: Absorbance of 3.2 wt% spray-dried CNC ultrasonicated suspensions obtained either at E = 20 or 167 $kJ.g^{-1}.L^{-1}$(V = 60 mL, P = 65 W) as function of wavelength

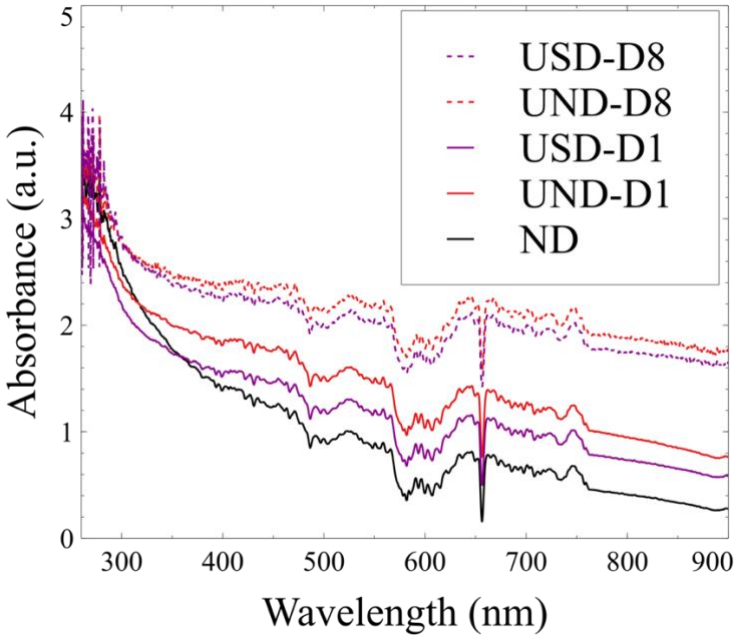

Figure B.3: Absorbance of 6.4 wt% spray-dried or never-dried CNC ultrasonicated suspensions (respectively USD and UND) obtained either at E = 20 or 167 $kJ.g^{-1}.L^{-1}$(V = 60 mL, P = 65 W) 1 day (D1) or 8 days (D8) after ultrasonication, compared with a 6.4wt.% never-dried CNC never sonicated suspension (ND) as function of wavelength

APPENDIX C SUPPLEMENTARY INFORMATION TO ARTICLE 3: A TECHNIQUE FOR THE ULTRASONIC DISPERSION OF LARGER QUANTITIES OF CELLULOSE NANOCRYSTALS WITH IN-LINE VALIDATION

Mélanie Girard, François Bertrand, Jason R. Tavares, Marie-Claude Heuzey. A technique for the ultrasonic dispersion of larger quantities of cellulose nanocrystals with in-line validation.

Submitted in Chemical Engineering Journal

Supplementary information C.1: Determination of K_s for an empty tube

For a power-law fluid in a pipe, Poiseuille law is defined such as:

$$Q = \frac{\pi R^3}{\frac{1}{n}+3}\left[\frac{R\Delta P}{2nL}\right]^{\frac{1}{n}} \quad \text{(C.1)}$$

According to this equation, $K_{p(n)}$ may be calculated from equation (6.11) giving:

$$K_{p(n)} = A^n \frac{2^{n+2}R^n}{V^n} \quad \text{(C.2)}$$

with A defined by:

$$A = \frac{\left(\frac{1}{n}+3\right)Q}{\pi R^3} \quad \text{(C.3)}$$

Then, using the same notation, K_p may be estimated from equation (6.12) such as:

$$K_{p(n)} = \frac{2^3 AR}{v} \quad \text{(C.4)}$$

Ks formula is thus obtained from equations (6.14), (C.2) and (C.4):

$$K_s = 6 + \frac{2}{n} \quad \text{(C.5)}$$

Supplementary information C.2: Pressure sensors calibration

The pressure sensors provide an output signal proportional to the measured pressure. The pressure value P (in kPa) and the output signal V_{out} (in V) are correlated by the manufacturer with the following formula:

$$V_{out} = V_s(0.2P + 0.5) \quad \text{(C.6)}$$

where $V_s = 5.0 \pm 0.25$ V is the supply voltage This equation has been validated with hydrostatic pressure measurements using a water column. For both sensors, there is a slight deviation between the two methods (Figure C.4), so the equation (C.6) was modified as follows:

$$V_{out} = 0.84P + 2.67 \quad \text{(C.7)}$$

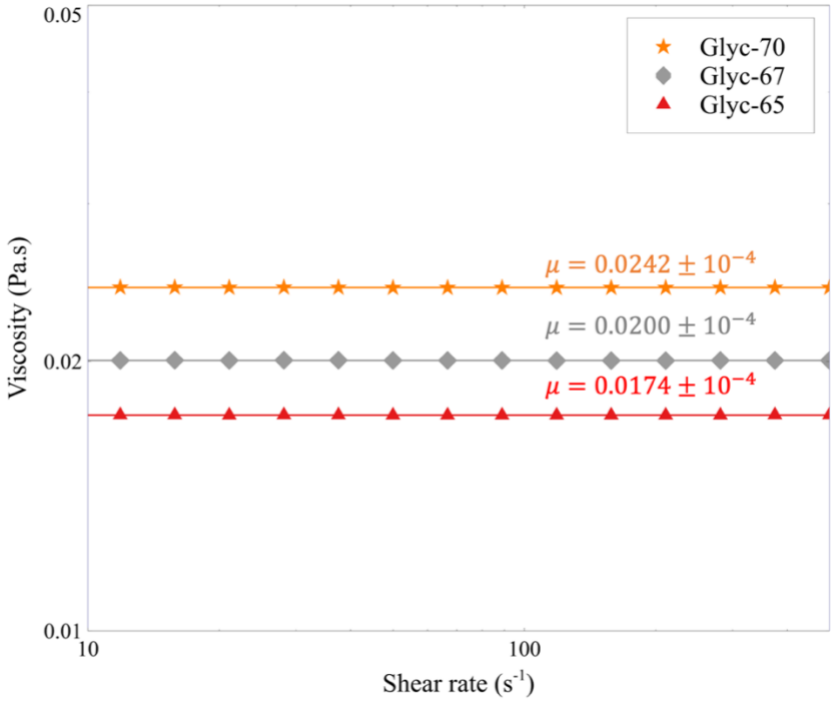

Figure C.1: Viscosity of glycerol water-based solutions at 65, 67 and 70 wt% as function of shear rate

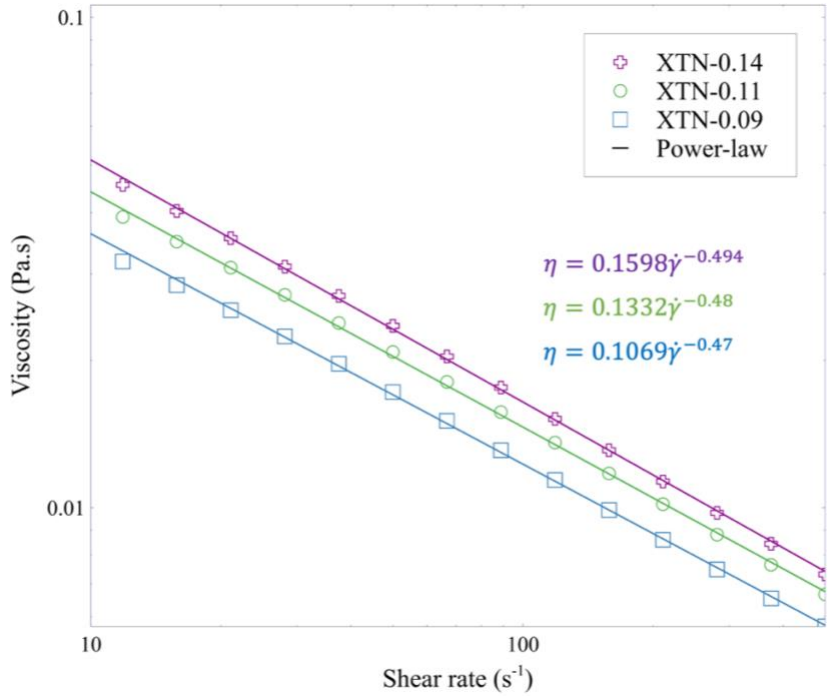

Figure C.2: Viscosity of xanthan water-based solutions at 0.09, 0.11 and 0.14 wt% as function of shear rate with a power-law fitting

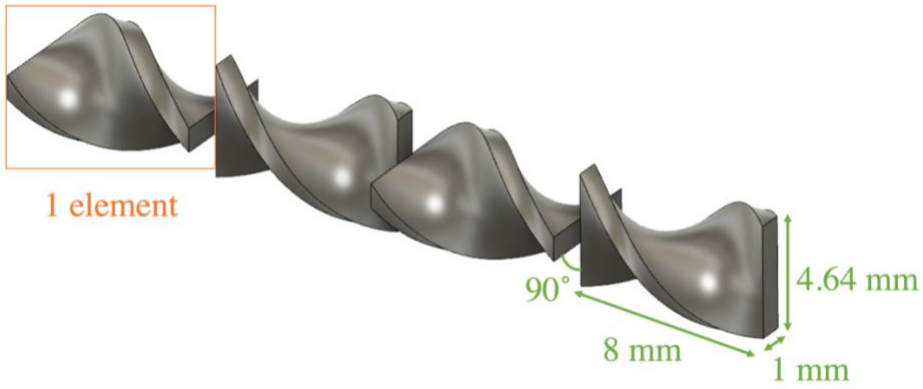

Figure C.3: Static mixer dimensions. Four elements out of 23 are represented for clarity purpose.

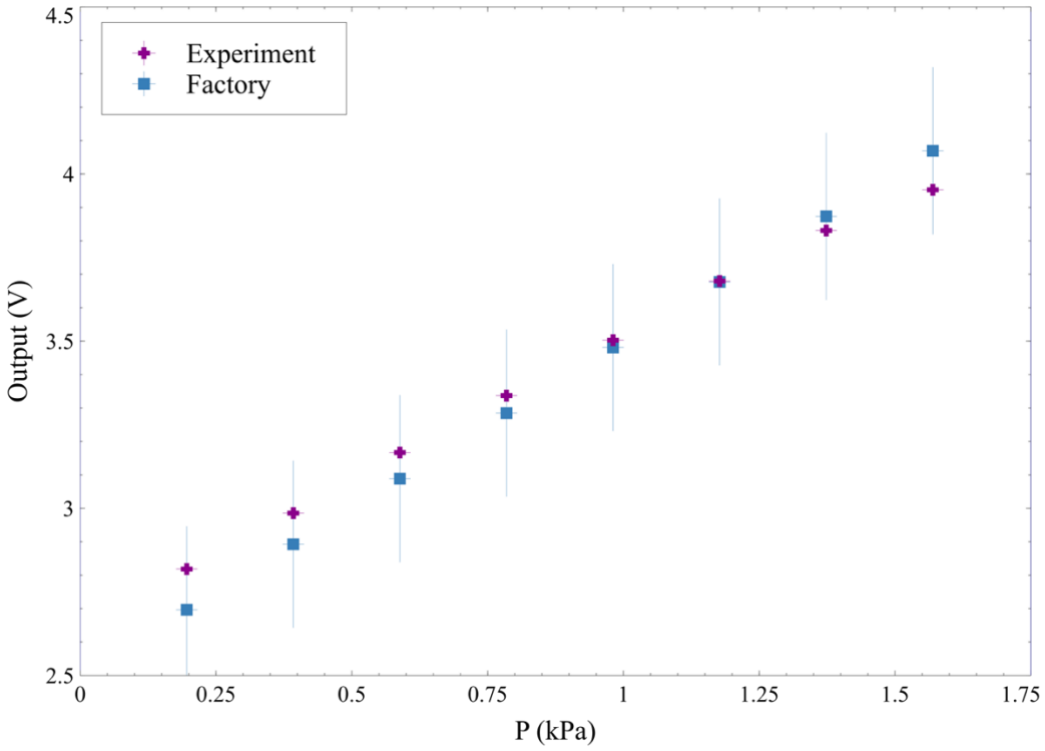

Figure C.4: Calibration of the pressure sensors. Both sensors were experimentally giving the same behavior, and the obtained values are compared with the factory calibration

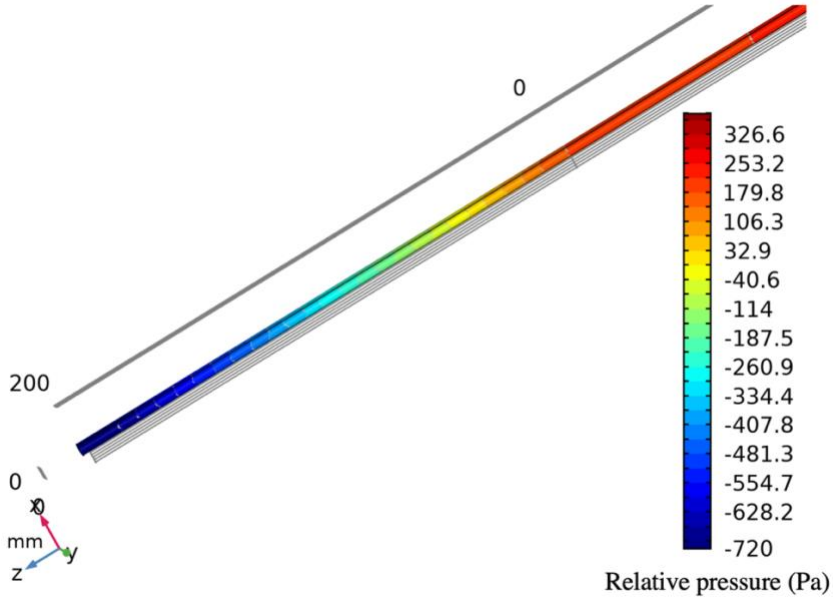

Figure C.5: Relative pressure field related to the 65 wt% glycerol solution flow in the semi-continuous setup modeling: (flow direction in positive z-direction, pressure sensors placed at z = - 50 mm and z = 200 mm, static mixer placed at z = 0 mm)

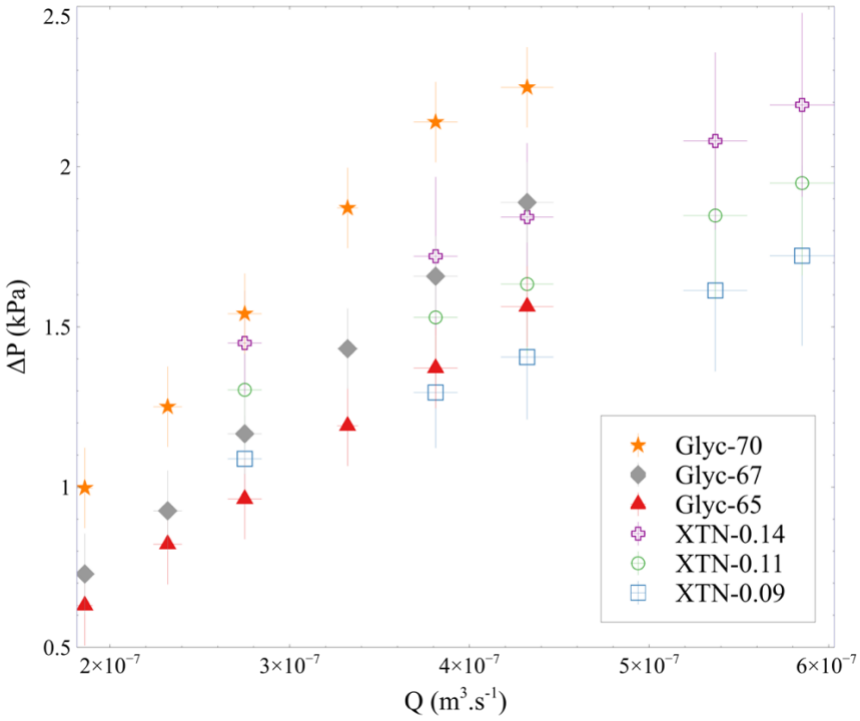

Figure C.6: Pressure drop as function of flow rate measured in the semi-continuous setup

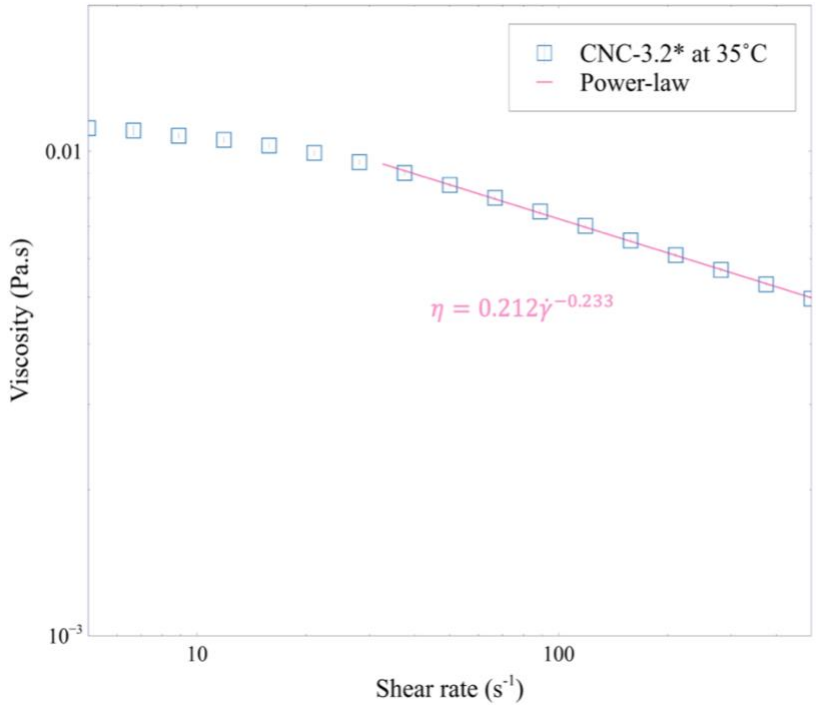

Figure C.7: Viscosity of a 3.2 wt% CNC ultrasonicated batch suspension (V = 60 mL, P = 15 (65) W, E = 167 kJ.g-1.L-1) as function of shear rate at 35˚C with a power-law fitting at high shear rate

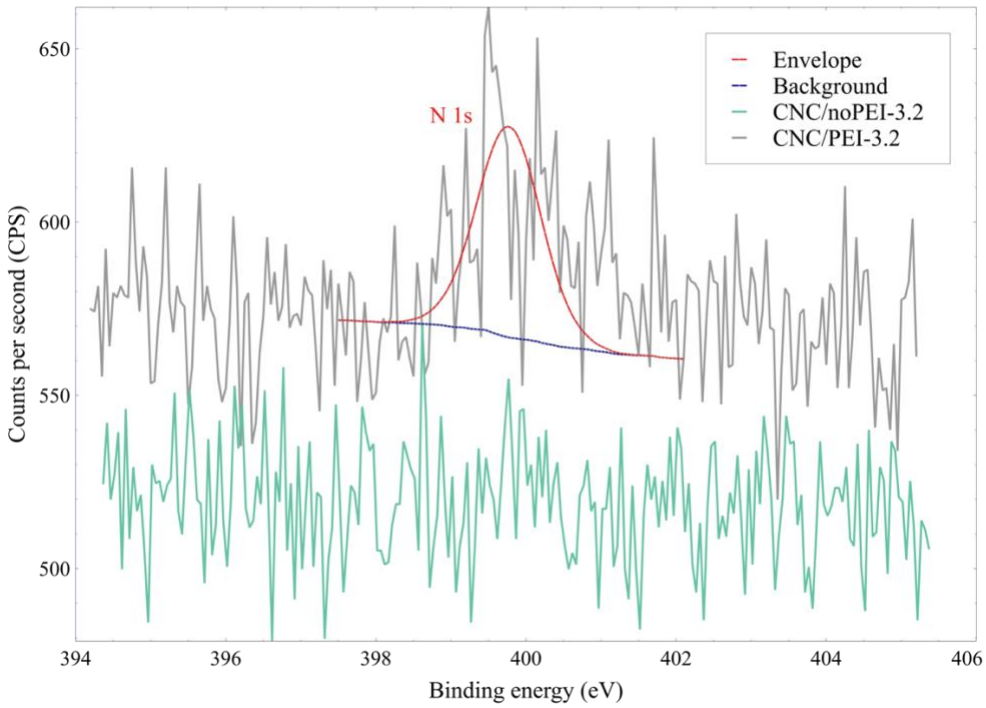

Figure C.8: XPS graph of freeze-dried CNC/noPEI-3.2 and CNC/PEI-3.2. The high signal-to-noise ratio is attributed to the low content of nitrogen for the modified CNC (~ 0.3%)

APPENDIX D LIST OF CONTRIBUTIONS

This annex lists the contributions made over this PhD project.

D.1. List of publications

Publications in peer-reviewed journals

M. Girard, F. Bertrand, J. R. Tavares, and M. C. Heuzey, "Rheological insights on the evolution of sonicated cellulose nanocrystal dispersions," *Ultrasonic Sonochemistry,* vol. 78, p. 105747, October 2021.

M. Girard, D. Vidal, F. Bertrand, J. R. Tavares, and M. C. Heuzey, "Evidence-based guidelines for the ultrasonic dispersion of cellulose nanocrystals," *Ultrasonic Sonochemistry,* vol. 71, p. 105378, March 2021.

Manuscripts submitted to peer-reviewed journals

M. Girard, F. Bertrand, J. R. Tavares, and M. C. Heuzey, " A technique for the ultrasonic dispersion of larger quantities of cellulose nanocrystals with in-line validation," *submitted in Chemical Engineering Journal*, February 2022.

D.2. List of presentations

Oral presentations

M. Girard, F. Bertrand, J. R. Tavares, and M. C. Heuzey. Ultrasonic dispersion and time evolution of concentrated cellulose nanocrystal suspensions characterized by rheology. Society of Rheology Conference, Bangor, Maine, United States, October 2021

M. Girard, F. Bertrand, J. R. Tavares, and M. C. Heuzey. Nanoparticle agglomeration problem approach: example of cellulose nanocrystals. 36th International Conference of the Polymer Processing Society, Montreal, Canada, September 2021

M. Girard, F. Bertrand, J. R. Tavares, and M. C. Heuzey. Influence of ultrasonication process parameter on the rheological behavior of cellulose nanocrystal dispersions. Young Rheologists Days, Giron, France, July 2021

M. Girard, F. Bertrand, J. R. Tavares, and M. C. Heuzey. Troubleshooting cellulose nanocrystal ultrasonic dispersion using rheology. Annual European Rheology Conference (AERC), April 2021

M. Girard, D. Vidal. F. Bertrand, J. R. Tavares, and M. C. Heuzey. Rheological behavior of cellulose nanocrystal dispersions obtained by ultrasonication. 18th International Congress on Rheology, December 2020

M. Girard, D. Vidal. F. Bertrand, J. R. Tavares, and M. C. Heuzey. Preparation and Processing of Cellulose Nanocrystal Dispersions. 70th Canadian Chemical Engineering Conference, October 2020

M. Girard, D. Vidal. F. Bertrand, J. R. Tavares, and M. C. Heuzey. How to efficiently disperse nanoparticles in suspension using ultrasonication?. IEEE Nano, July 2020

M. Girard, **J. R. Tavares**, and M. C. Heuzey. Ultrasonication-assisted dispersion of cellulose nanocrystals: a comprehensive study. 69th Canadian Chemical Engineering Conference, Halifax, Canada, October 2019

M. Girard, J. R. Tavares, and M. C. Heuzey. Ultrasonication-assisted dispersion of cellulose nanocrystals: a comprehensive study. 91st Annual Meeting of The Society of Rheology, Raleigh, United States, October 2019

M. Girard, J. R. Tavares, and M. C. Heuzey. Ultrasonication-assisted dispersion of cellulose nanocrystals. Chemical Engineering Research Day, Montreal, Canada, March 2019

M.C. Heuzey, J. R. Tavares, C. Bruel, M. Girard, W. Nakhle. Dispersion of CNCs in polar and nonpolar media: dictated by surface properties, improved by sonication and quantified by rheology. PaperWeek, Nanocellulose Challenge Symposium, Montreal, Canada, February 2019

Poster presentations

M. Girard, F. Bertrand, J. R. Tavares, and M. C. Heuzey. Guidelines to disperse nanoparticles using ultrasonication. Colloque annuel du CREPEC, Québec, Canada, December 2019. (Outstanding contribution, 2nd prize)

M. Girard, J. R. Tavares, and M. C. Heuzey. Ultrasonication-assisted dispersion of cellulose nanocrystals: a comprehensive study. TechConnect World Innovation Conference-Nanotech, Boston, United States, June 2019

M. Girard, J. R. Tavares, and M. C. Heuzey. Ultrasonication-assisted dispersion of cellulose nanocrystals: a comprehensive study. GDRI Nanomatériaux Multifonctionnels Contrôlés, 6e atelier, Jouvence, Canada, May 2019

M. Girard, J. R. Tavares, and M. C. Heuzey. Ultrasonication-assisted dispersion of cellulose nanocrystals: a comprehensive study. Paperweek, Montreal, Canada, February 2019